STUDIES ON BUOYANCY DRIVEN FLOWS THROUGH LARGE OPENINGS

By

BHUVANESHWAR GERA

ENGG01201204022

Bhabha Atomic Research Centre, Mumbai

A thesis submitted to the

Board of Studies in Engineering Sciences

In partial fulfillment of requirements
for the Degree of

DOCTOR OF PHILOSOPHY

of

HOMI BHABHA NATIONAL INSTITUTE

December 2020

Homi Bhabha National Institute

Recommendations of the Viva Voce Committee

As members of the Viva Voce Committee, we certify that we have read the dissertation prepared by *Bhuvaneshwar Gera*entitled *Studies on Buoyancy Driven Flows through Large Openings* and recommend that it may be accepted as fulfilling the thesis requirement for the award of Degree of Doctor of Philosophy.

Chairman - Prof. P. K. Vijayan		**Date:** 21/12/20
Guide / Convener - Prof. A. K. Nayak		**Date:** 21/12/2020
Co-guide - Prof. M. Alam		**Date:**
Examiner - Prof. Arun K. Saha		**Date:** 31/01/2021
Member 1-Prof. A.W. Patwardhan		**Date:** 21/12/2020
Member 2- Prof. A. M. Vaidya	Abhijit Vaidya	**Date:** 21/12/2020
Member 3- Prof. A. K. Nayak		**Date:** 21/12/2020
Member 4:		**Date:**
Technical Adviser-		**Date:**

Final approval and acceptance of this thesis is contingent upon the candidate's submission of the final copies of the thesis to HBNI.

I/We hereby certify that I/we have read this thesis prepared under my/our direction and recommend that it may be accepted as fulfilling the thesis requirement.

Date: 21-12-2020

Place: Mumbai

Prof. M. Alam
(Co- guide)

Prof. A. K. Nayak
(Guide)

STATEMENT BY AUTHOR

This dissertation has been submitted in partial fulfilment of requirements for an advanced degree at Homi Bhabha National Institute (HBNI) and is deposited in the Library to be made available to borrowers under rules of the HBNI.

Brief quotations from this dissertation are allowable without special permission, provided that accurate acknowledgement of source is made. Requests for permission for extended quotation from or reproduction of this manuscript in whole or in part may be granted by the Competent Authority of HBNI when in his or her judgment the proposed use of the material is in the interests of scholarship. In all other instances, however, permission must be obtained from the author.

Bhuvaneshwar Gera

BHUVANESHWAR GERA

DECLARATION

I, hereby declare that the investigation presented in the thesis has been carried out by me. The work is original and has not been submitted earlier as a whole or in part for a degree / diploma at this or any other Institution / University.

Bhuvaneshwar Gera

BHUVANESHWAR GERA

LIST OF PUBLICATIONS ARISING FROM THE THESIS

Journals:

1. **B. Gera**, A.K. Nayak, M. Alam, R.K. Singh, "Numerical Investigation of Effect of Density and Aspect Ratio on Buoyant Oscillatory Exchange Flow through Circular Opening in Horizontal Partition using Salt Water Analogy", **International Journal of Fluid Mechanics Research, 47 (2020) 229-245.**

   https://DOI: 10.1615/InterJFluidMechRes.2020029647

2. **B. Gera**, P.K. Sharma and R.K. Singh, "CFD analysis of flow through horizontal ceiling opening due to buoyancy and pressure difference", **International Journal of Modern Physics C**, 25 (2014) 1340022**.**

   https://doi.org/10.1142/S0129183113400226

3. **B. Gera**, P.K. Sharma and R.K. Singh, "Effect of the opening aspect ratio on a buoyant pulsating exchange flow through a circular ceiling opening in a horizontal partition", **Heat Transfer-Asian Research,** 41 (2012), 666-680.

   https://doi.org/10.1002/htj.21023

Conferences:

1. **B. Gera,** A. K. Nayak, M. Alam, "DES of Gravity Currents Related to Backdraft for various Compartment Aspect Ratios using Salt Water Analogy", 46th National Conference on Fluid Mechanics and Fluid Power **(FMFP 2019)** December 9-11, 2019, PSG College of Technology, Coimbatore, India.

2. **B. Gera**, A.K. Nayak, A.P. John, M. Alam, "Study of Hot Gas Flow in a Compartment having Large Opening using Salt Water Analogy", 7th International and 45th National Conference on Fluid Mechanics and Fluid Power **(FMFP 2018)** December 10-12, 2018, IIT Bombay, Mumbai, India.

3. **B. Gera**, R. K. Singh, M. Alam, "Numerical Study of Effect of Density and Aspect Ratio on Oscillatory Exchange Flow through a Circular Opening in Horizontal Partition", 6th International Congress on Computational Mechanics and Simulation **(ICCMS 2016)**, June 27- July 01, 2016, IIT Bombay, India.

4. **B. Gera**, R. K. Singh, M. Alam, "CFD Simulation of Combined Buoyancy and Pressure Driven Hot Gas Flows through Square Opening using Salt Water Analogy", 6th International Congress on Computational Mechanics and Simulation **(ICCMS 2016)**, June 27- July 01, 2016, IIT Bombay, India.

Bhuvaneshwar Gera

BHUVANESHWAR GERA

Dedicated to my family and teachers

ACKNOWLEDGEMENTS

I would like to express my deepest gratitude to my supervisors **Prof. A. K. Nayak, Prof. Meheboob Alam and Prof. R. K. Singh**, for their valuable guidance, patience, encouragement and the freedom given to me in carrying out research. Apart from the technical knowledge, the discipline, which I learned from my supervisors, is indispensable to my growth as an engineer and as a person. I considered myself to be honoured and fortunate to be associated with them.

Besides my guide, I would like to thank the rest of my thesis committee: Chairman of the committee, Prof. P. K. Vijayan, Prof. A. Vaidya, Prof. A. Patwardhan for their insightful comments and encouragement, but also for the hard questions, which incented me to widen my research from various perspectives.

I would like to express thanks to my colleagues Mr. Sunil Ganju, Mr. Pavan K. Sharma, Mr. Nandan Saha and Mr. Shubham Mishra for their valuable inputs during my work. They were being there for a technical guidance and subjective inputs whenever I needed them. My sincere thanks to Mr. Sunil V. Bhardwaj, post doc fellow, EMU, JNCASR for his help during salt water experiments.

I would like to thank my friends Mr. Tarvinder Singh, Mr. R. M. Parmar, Dr. Mukesh Kumar for the many fruitful discussions and merry memories.

I would also like to thank all Homi Bhabha National Institute Dean, Academic Dean, Registrar, administration and staff members for their constant cooperation in all administrative activities related to my PhD.

Last but not the least, my family, whosoever I am today, it is because of them only. It was my parents who first instilled in me the motivation for learning and their hard work made me have the chance for higher education. Special thank goes to my wife Dr. Poonam Gera. It is impossible for me to finish this thesis without her support, encouragement and sacrifice. Thanks to my son Mr. Darshil Gera for his support and love. I would like to thank my entire family for supporting me spiritually and emotionally throughout this journey and my life in general.

Thanks for all your encouragement and motivation. This journey would not have been completed without each and every one of you.

TABLE OF CONTENTS

NOMENCLATURE

Abbreviations:

AR	Aspect Ratio
CFD	Computation Fluid Dynamics
FVM	Finite Volume Method
GGDH	Generalized Gradient Diffusion Hypothesis
LES	Large Eddy Simulation
PIV	Particle Image Velocimetry
PLIF	Planar Laser Induced Florescence
QUICK	Quadratic Unwinding Interpolation of Convection Kinetics
RI	Refractive Index
SGDH	Simplified Gradient Diffusion Hypothesis
SGS	Sub-Grid Scale
SIMPLE	Semi-Implicit Method for Pressure Linked Equations

Nomenclatures:

$C_{1\varepsilon}, C_{1\varepsilon}^{*}, C_{2\varepsilon}, C_3, C_\mu$	Empirical constants used in RNG k- ε model
D	Diameter of the opening (m)
D_{ab}	Diffusion Coefficient, (m^2/s)
f	Frequency
g	Acceleration due to gravity (m^2/s)
G_k	Generation term for turbulent kinetic energy due to mean shear
G_B	Generation term for turbulent kinetic energy because of buoyancy
H	Height of the compartment (m)
k	Turbulent Kinetic Energy, (m^2/s^2)
L	Length of the partition (m)
L_C	Length of the compartment (m)
Δp	Pressure difference
p, P	Pressure (Pa)
$\Pr_k$	Turbulent Prandtl number for kinetic energy
$\Pr_\varepsilon$	Turbulent Prandtl number for dissipation
$\Pr_t$	Turbulent Prandtl number
$Q(t)$	Volumetric flow rate from upper to lower compartment (m^3/s)
$Q_s(t)$	Theoretical volumetric flow rate due to density difference (m^3/s)
Q^*	Dimensionless Froude number, Flow coefficient

q	Flooding flow rate (m^3/s)
r	Radial coordinate direction
S_{ij}	Rate of deformation (s^{-1})
Sc_t	Turbulent Schmidt Number
t	Time
u	Axial component of velocity (m/s)
$\vec{U}$	Velocity Vector
v	Radial component of velocity (m/s)
v^*	Dimensionless velocity, Froude number
V_H	Volume of upper compartment (m^3)
V_L	Volume of lower compartment (m^3)
Y	Mass fraction of species
z	Axial coordinate direction

Subscripts:

0	Initial Value
∞	Ambient condition
SW	Salt-water
FW	Fresh water
s	Salt
c	Characteristic/compartment
in	inlet
k	species

Superscripts:

"-"	Spatial filter
"~"	Favre filter
*	Non-dimensionalised

Greek Symbols:

β_{SW}	volumetric expansion coefficient for salt water = 0.76
β	Normalised density difference ($(\rho_H - \rho_L) / \rho_L$)
Δ	Filter width
ε	Turbulent Dissipation Rate, (m^2/s^3)
$\alpha_k, \alpha_\varepsilon,$ η_0, β_{RNG}	Empirical constants used in RNG k- ε model
μ	Dynamic viscosity, (Ns/m^2)
μ_t	Turbulent viscosity, (Ns/m^2)
μ_{eff}	Effective viscosity, (Ns/m^2)
$\overline{\Omega}_{ij}$	Mean rate of rotation tensor
ω_k	Angular velocity (rad/s)
ρ	density (kg/m^3)
ρ_H	Density of heavier fluid (kg/m^3)
ρ_L	Density of lighter fluid (kg/m^3)
$\Delta\rho(t)$, $\Delta\rho$	Instantaneous density difference between higher and lower density fluid (kg/m^3)
$\rho(t)$, ρ	Mixture instantaneous density (kg/m^3)
τ_{ij}	Reynolds stresses (N/m^2)

Dimensionless Numbers used:

Fr	Froude Number	$Fr = \frac{u}{\sqrt{\beta g H}}$
Pr	Prandtl Number	$\mathrm{Pr} = \frac{\mu Cp}{k}$
Re	Reynolds Number	$\mathrm{Re} = \frac{\rho U d}{\mu}$
St	Strouhal Number	$St = \frac{fL}{U}$
Sc	Schmidt Number	$Sc = \frac{\mu}{\rho\, D_{ab}}$

LIST OF FIGURES

LIST OF TABLES

CHAPTER 1: INTRODUCTION

1.1. Overview of flow through opening in horizontal and vertical partition

The buoyancy driven exchange flow through large openings in horizontal and vertical partitions occurs in many practical situations such as in nuclear reactor containments during blow-down, hydrogen distribution and accidental fire studies. The buoyant force is created due to density difference between compartments connected through large openings. The temperature or/and concentration variation between compartments causes this density difference. Various openings are present in multiple compartments and containment building and are impartment for fluid flow from one compartment to another compartment. Opening are provided in horizontal partition at staircases, stairwells, chimneys and shafts used for ventilation and services and study of fluid flow and heat and mass transfer through these openings is important for human comfort, pollutant and germs removal and control of fire and smoke.

Openings in horizontal and vertical partition are provided in domestic and commercial buildings; if fire occurs in a building these openings serve as outlet to smoke and inlet to fresh air. Accurate prediction of the movement of smoke within an enclosed space is essential information for the design and use of these buildings. Like many natural phenomena, the flow of smoke is complex and measurements in smoky environments can be very difficult and expensive due to the soot build-up within the enclosure and on equipment, as well as the high temperatures involved. Due to generation of heat, the medium inside the enclosure is lighter compare to ambient fluid, thus, an unstable interface is created at the opening in horizontal partition and a pulsating exchange flow occurs through the opening in horizontal partition from one compartment to another (Fig. 1.1). If the intensity of fire is high, the pressure generated inside the room will also govern the flow through the opening in horizontal partition. In this case, fire induced smoke flows are driven through the outlet vent by both, pressure and buoyancy forces, the first due to the finite volume flux of the source, and the second due to the unstable stratification across the outlet vent. Thus the nature of flow through opening whether unidirectional or bidirectional, is governed by both pressure and density difference across the opening. Zone based fire model calculates the smoke transport using standard vent models based on pressure difference using flow coefficient that do not accurately take in to account the buoyancy component of the flow. Openings in horizontal partitions are also widely used in ceiling for natural ventilation and to produce flow, which is unstable with irregular oscillatory behaviour even when the temperature difference is low.

Doors and windows are most common openings in vertical partition, which provides passage for smoke to escape from the room in case of fire. The fresh air enters from these openings in case of ventilated fire. During fire in an enclosure having opening in vertical partition, the smoke and hot gases get stratified in the top region of enclosure and leave from the upper portion (approximately half) of the opening while fresh air being heavier enters from the lower portion of the opening as shown in Fig. 1.2. During this process, some heat exchange also takes place. The flow through opening in vertical partition is stable and bi-directional.

In case of under ventilated fire in a room having large combustible, some of the combustibles may remain un-burnt at high temperature due to lack of oxygen. If openings like doors or windows are suddenly pushed open, fresh air enters and rapid deflagration may occur. The deflagration moving through the building and out of the opening is a backdraft. Backdraft continues to be a hazard that can kill people and cause the building to collapse. The consideration of air/smoke movement during fire through doors, windows requires an understanding of buoyancy driven fluid motion through vertical vents connecting rooms in a building.

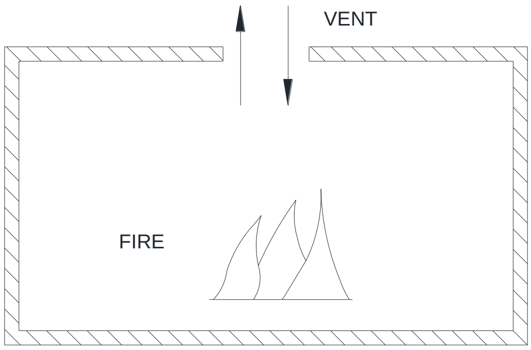

Figure 1.1: Bi-directional flow across an opening in horizontal partition during fire (Jaluria et al., 1998).

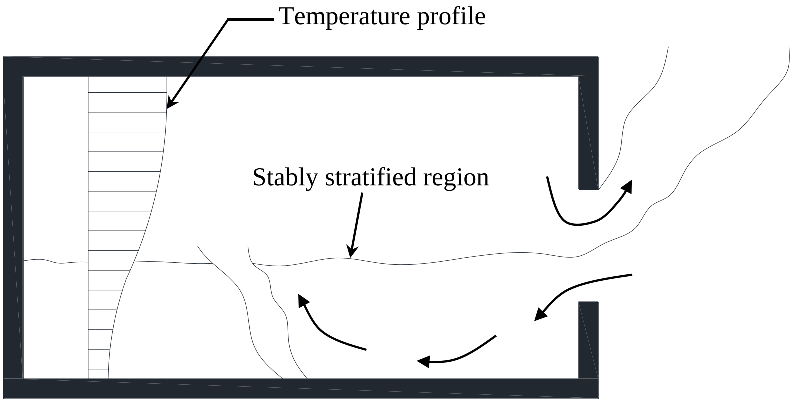

Figure 1.2: Bi-directional flow across an opening in vertical partition during fire (Quintiere et al., 1981).

During backdraft, flow through opening occurs only due to density difference and in case of ventilated fires, flow through opening occurs due to both the pressure and density difference. A turbulent bi-directional fluid flow occurs through opening between compartments, which is unstable in case of opening in horizontal partition while it stable for opening in vertical partition. The flows in such openings are difficult to model mathematically because the counter current flows often occur simultaneously in opposite directions through different parts of the opening. Apart from these, buoyancy plays a major role on turbulence, during unstable stratification, i.e., in case of buoyant jet, flow through ceiling opening buoyancy creates the turbulence while during stable stratification, i.e., in case of ceiling jet, flow through vertical opening buoyancy suppresses the turbulence. Initially a turbulent plume is developed in case of accidental hydrogen release or accidental fire. The plume spread during its movement and touches the ceiling and converts into ceiling jet which is expanding in radial direction. The turbulent structures are more complex as compared to linearly expanding plume. Due to stable stratification buoyancy suppresses the turbulence and turbulent mixing is reduced near the ceiling as compared to initial plume (Fig. 1.3).

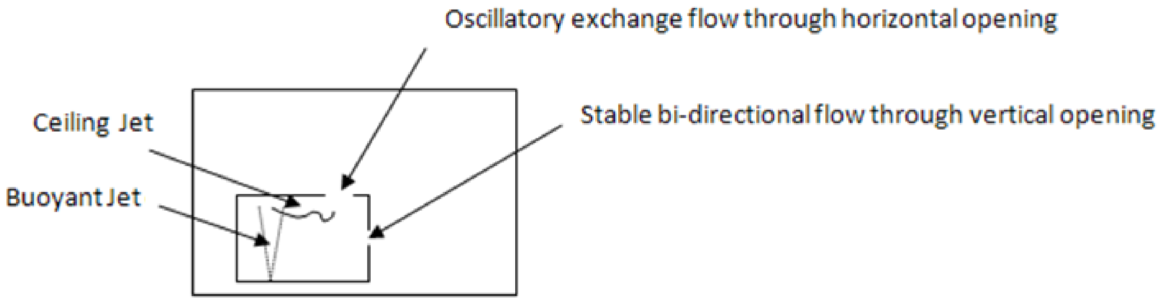

Figure 1.3: Smoke flows in multiple compartments.

Presently there are three main methods that can be used to investigate the fire-induced flow behaviour of openings in vertical and horizontal partitions; full or small-scale experiments, CFD models and salt water/fresh water modelling. The main advantages of the salt water modelling experiments are that they are clean and relatively inexpensive compared to the conventional fire test and CFD modelling.

1.2. Salt-water/fresh water system

Salt water modelling technique is a useful tool to simulate fire induced flows, which takes into account most of the flow characteristics and allows for good flow visualization (Clement, 2000; Conover et al., 1995; Epstein, 1988; Fleischmann and McGrattan, 1999; Jaluria et al., 1998; Jankiewicz, 2004; Lequesne, 2010; Siang, 2010; Steckler et al., 1986; Tan and Jaluria, 2001; Yao, 2006; Yao and Marshall, 2006). In salt-water modelling, turbulent buoyant salt water moving in fresh water is used to substitute for turbulent buoyant hot gas moving in cold gas. To perform experiments in full scale test facilities is challenging and also uneconomical in some cases, however experiments with salt water fresh water analogy are cheaper and very effective. In salt water fresh water analogy, flow visualisation is simple and straight-forward; the buoyant flow is at constant temperature so there is no heat transfer to outside and no need to protect the experimentalist by insulating the teat setup. The salt-water flows have features consistent with fire-induced flows and provide an excellent test-bed for CFD turbulence models used in such applications. Due to transparent set up, non-intrusive techniques such as Planar Laser Induced Fluorescence (PLIF) can easily be used and can provide concentration data at all points in a plane throughout the flow (Jankiewicz et al., 2014; Shan, 2004; Siang, 2010; Yao and Marshall, 2005; Yii, 1998). A schematic of salt water system is shown in Fig. 1.4, where salt water is injected in an enclosure filled with fresh water. The enclosure is connected to a large enclosure with an opening in horizontal or vertical partition. The PIV/PLIF system is used to measure velocity and concentration during the experiments.

The PLIF technique achieves good flow visualization by illuminating the salt-water plume with dye. To properly illuminate the plume of interest, a laser source and a special dye are required. A fixed amount of dye is mixed with the spilling saline solution that generates the spill plume flow. Illumination is achieved when the laser light excites the dye in the flow. The dye is excited because its excitation wavelength corresponds to the laser light wavelength. The illumination brightness of the plume depends on the concentration of the dye at the particular region.

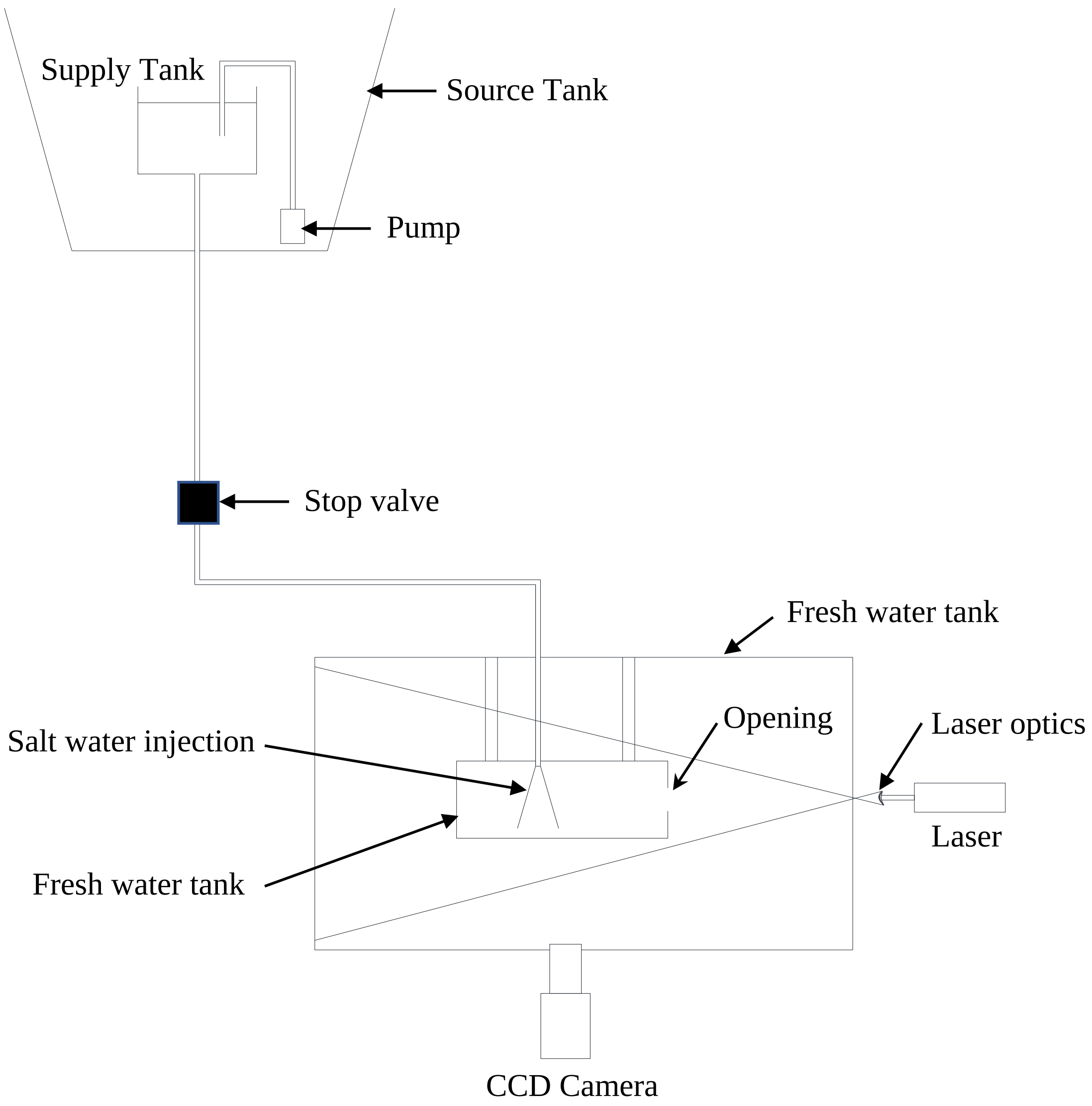

Figure 1.4: Schematic of salt water/fresh water system.

At the initial injecting region the brightness is high as entrainment is minimal. Further away from the injection point, the brightness decreases due to the dilution within the plume. Using the PLIF technique, the density differences across the cross sections of a buoyant plume to its surrounding could be measured. This density manipulation depends on the relative brightness between the buoyant plume to its initial injecting brightness. To convert the brightness data to density data, both the densities of the ambient fluid and the saline solution need to be measured. The density is computed based on ratio between the net brightness in the flow to initial brightness of the plume in the calibration cell. In order to pick up the brightness data from the experiment, a set of image capturing equipment is required. It includes high-speed cameras, computers, light sources etc.

When using a salt water system to model fire induced smoke flows, the denser fluid containing the salt acts in place of the fire source and the leaner fresh water acts as the cold air in the lower layer. For this reason, it is necessary to conduct these experiments upside down, as they appear in real life scenarios. Both the fire and its salt water analogue produce plumes which are a result of the leaner fluid rising (or falling in the salt water system) and entraining ambient fluid, as eddy currents develop due to the density difference (LeQuesne, 2010).

In spite of several advantages of salt water/fresh water system, this analogy has some limitations as follows:

(i) Heat Transfer Deficiency-In any real fire in an enclosure there is a certain amount of heat transfer to the boundaries of the compartment. The result of this is a thermal boundary layer, which is colder than the general ceiling layer immediately adjacent to the compartment boundaries. This phenomenon cannot be directly simulated by salt water modelling, as this would necessitate mass transfer of salt into the surfaces of the model. Salt water modelling is limited to fire induced flows in insulated enclosures.

(ii) Initial Plume Momentum-In a real fire scenario, the buoyant plume created by the fire has no initial momentum as the flow is driven solely by the density difference between the fire gases and the ambient air. In the case of salt water modelling, the rate of heat release of the fire is modelled using the mass flux leaving the source. For the salt water model to best represent the real fire scenario, it is important to reduce this initial momentum as far as possible.

(iii) Salt water Source Geometry-While fire can be considered a volumetric heat source, the extent of its volume is constantly changing and is very difficult to define. In the case of salt water modelling, it is not possible to release fresh water in a precisely scaled volume corresponding to the volumetric extent of a real fire. Therefore, the source geometry is assumed, i.e., the diameter of the planar source.

(iv) Plume Mass Flux-In a real fire scenario the mass flux at the source of the fire is zero as there is no mass introduced into the system. When conducting a salt water modelling experiment, however, mass is introduced in the form of the injected plume. In order to have a negligible effect on the experiment care must be taken to ensure that the mass flux entraining into the plume from the source is large compared to that at the source.

1.3. Objective of thesis

Experiments and appropriate numerical model development for buoyancy or pressure and buoyancy induced flow in multiple compartments connected through horizontal and vertical openings are the main objectives of the present research work to understand the flow pattern at opening locations. In the present work, experiments have been conducted with salt water and fresh water analogy to simulate the stratification behaviour and actual scenario and the data have been used for CFD code validation and model improvement. Other objective of the present research is to explore the potential of using the combined Particle Image Velocimetry (PIV) and PLIF technique in conjunction with saltwater modelling for studying the density driven exchange flow through opening.

The study includes flow pattern characterisation, its flow visualization and determining the suitability of salt water system to simulate accidental fire induced flows, natural convection flows, containment thermal hydraulics, etc. The turbulence quantities were measured using 2D PIV that helped in modelling the effect of buoyancy on turbulence accurately. Non-intrusive laser diagnostics, PLIF and PIV were used to measure the dimensionless density difference and velocity in saltwater plumes. These experiments quantify the effects of different compartment opening geometries on the bulk flow characteristics and internal flow structure arising from hot gas exchange flow through opening in horizontal or vertical partition. Salt water fresh water analogy is a simple and effective approach to model complicated turbulent structures. The behaviour of buoyant turbulent plume, ceiling jet and effects of horizontal and vertical openings were investigated in an integrated manner.

1.4. Accomplishments of the present research

In first part, numerical simulations were performed for buoyant flow through circular ceiling opening and gravity currents related to backdraft through opening in vertical partition. Experimental data from literature was used for validation of CFD code for simulation of flow through horizontal opening due to density difference. For this case model of two compartments one over another, separated by a horizontal partition, with an opening of a specified size was used. Fluid of higher density was filled in the top compartment while the bottom compartment was filled with fluid of lower density. A correlation was developed to predict the frequency of oscillation for a given value of density ratio and opening aspect ratio within a reasonable accuracy. Gravity current related experiments were used for validation of the developed CFD code for simulation of flow through opening in vertical partition due to density difference.

In second part, effect of pressure forces generated by initial fire plume or hydrogen plume and density difference was used to study buoyant plume, ceiling jet, flow through ceiling or vertical opening. Both numerical simulations and experiments were performed in scaled setup. The interior dimension of compartment was decided based on geometric scaling and preliminary numerical simulations. A small tank was placed inside a large tank called as ambient tank. The small tank has the horizontal ceiling or side vertical opening (of different shapes and sizes) and provision for injection of salt water jet from top. Initially both the tanks were filled with fresh water. Salt water was injected from top of the small tank creating buoyant jet/plume then forming buoyant ceiling jet. Stratification/mixing occurred in small tank and salt water from small tank moved in ambient tank through horizontal or vertical openings. The salt water was fed from the bottom of a source tank located above the main tank. Separate experiments were conducted for horizontal opening with closed vertical opening and vice versa. 2D planar PIV and 2D PLIF measurements have been performed in the region of interest. Flow visualization was performed by direct photography and dye visualization.

3D CFD computations of all the cases have been performed using in-house developed CFD code. The computer code has been developed in order to predict the 3D behaviour of the salt water distribution in a large enclosure filled with fresh water. Dynamic LES turbulence model was used for simulations. The buoyant flow is anisotropic hence the assumption of isotropy in conventional two equation turbulence model is not valid for the buoyant flows.

1.5. Organization of thesis

Keeping the research objective in mind, the present thesis is organized into the following chapters.

In **Chapter 2**, the literature review study has been deliberated on the following major parts: experimental work on flow through opening in horizontal and vertical partition and numerical work on flow through opening. An overview of experiments conducted using salt water system to simulate buoyancy, combined buoyancy and pressure driven flow has been given. Numerical studies on oscillations generated during buoyant flow through ceiling opening, stable and unstable stratifications are reviewed. The gravity current experiments and numerical simulations conducted by various authors have been discussed in this chapter.

Chapter 3 describes the mathematical models and numerical methods used to study oscillatory exchange flow due to density difference across opening in horizontal partition. Fluid of higher density located in the upper compartment connected through an opening in a horizontal partition to a lower compartment filled with fluid of lower density creates an unstable system. The fluid flow through the opening is oscillatory, turbulent and irregular. Numerical simulations were performed to characterise this oscillatory exchange flow through a single circular opening in horizontal partition. The effect of density ratio and opening aspect ratio on the oscillation frequency and flow coefficient through the opening is discussed. Numerical model, its validation and application have been discussed in this chapter. Results of parametric study performed with 4 density differences and 5 opening aspect ratios are also explained.

In **Chapter 4**, 3D transient large eddy simulations (LES) of gravity current related to backdraft have been performed for different compartment aspect ratios (1 to 5). Six different opening configurations in vertical partition and five different compartment aspect ratios have been studied for five different density ratios (from 1.005 to 1.1). Salt water-fresh water has been used as working fluid to create the desired density difference. Limited experimental results are available for compartment ratios of 2 and 4 with different opening and density ratios (1.003 to 1.1). Most of the studies on gravity current have been performed for long run up of gravity current. However, the actual compartment may not have very high aspect ratios. Data of small aspect ratios (1 to 5) may be useful for actual compartment.

In **Chapter 5**, CFD simulations have been performed to quantify the amount of pressure difference required to overcome buoyancy force so the flow become unidirectional from bidirectional through a single circular opening in horizontal partition. The configuration of salt water and fresh water system was similar as in chapter 3; however there was provision to impose a pressure field in the bottom compartment. The pressure in lower compartment was raised in steps to find the value of pressure when the flow through opening becomes unidirectional from bidirectional. Two dimensional axisymmetric simulations were performed using Finite Volume Method in transient manner with in-house CFD code.

Chapter 6 presents the results of 3D transient LES based CFD simulations performed for combined buoyancy and pressure driven flow across a square opening in a horizontal or vertical partition using salt water analogy. The salt water was injected in a small compartment connected to a larger compartment through opening; both were pre-filled with fresh water. CFD results have been validated quantitatively against PIV/PLIF data obtained from experiments and qualitatively with dye visualization experiments. The numerical model reasonably predicts the movement of salt-water plume, mixing and formation of stratified layer in injection compartment and flow through opening

Chapter 7 provides the summary of the work and conclusions of the current work. Recommendations for future work are also described in this chapter. All major findings of the present research work have been summarised.

CHAPTER 2: REVIEW OF LITERATURE

2.1. Experimental work on flow through opening in horizontal partition

One of the first experiments on heat and mass transfer through opening in horizontal and vertical partition were performed by Brown and Salvason (1962a, 1962b). The exchange flow rate through opening was determined and found proportional to the opening aspect ratio. Air was used as working fluid and experiments were performed for opening aspect ratio from 0.0825 to 0.66.

Epstein (1988) studied buoyancy driven exchange flow through horizontal opening using salt water and fresh water using a simple setup shown in figure 2.1. The upper compartment was filled with heavier density fluid while the lower compartment was filled with lighter density fluid. Both of the compartments were connected by an opening in horizontal partition. Flow was initiated by removing the stopper and closed by placing the stopper. Mass balance was used to determine the exchange flow based on following Eq. (2.1).

$$Q = \frac{-V_H (d\rho_H / dt)}{(\rho_H - \rho_{L,0}) - {V_H}/{V_L} (\rho_{H,0} - \rho_H)} \qquad \textbf{(2.1)}$$

For measuring density variation with respect to time for upper compartment, the mixing was stopped by closing the opening at regular interval of time. A hydrometer reading was taken after stirring the brine solution. Round opening of diameter (D) 0.0254 m, 0.0339 m, 0.0437 m, 0.0445 m and 0.0525 m and a square opening of side length (S) 0.0292 m were studied.

Volume exchange flow rate in the form of dimensionless Froude number as a function of L/D was examined. 4 different regimes for exchange flow were determined:

Regime 1 for 0.01<L/D<0.16	Oscillatory exchange flow
Regime 2 for 0.16<L/D<0.4	Bernoulli Flow
Regime 3 for 0.4<L/D<1.32	Combined turbulent diffusion and Bernoulli flow
Regime 4 for 1.32<L/D<20	Turbulent diffusion

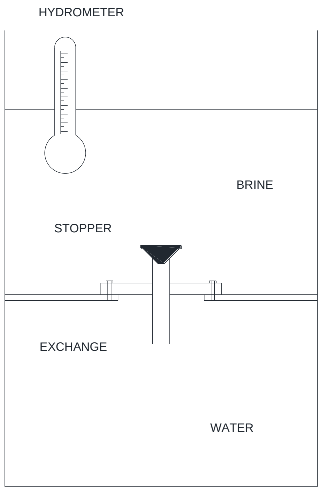

Figure 2.1: Experimental set up used by Epstein (1988)

From this detailed study, a purely empirical correlation (Eq. (2.2)) for the exchange flow rate was computed over the entire range of L/D investigated

$$\frac{Q}{(D^5 g\Delta\rho/\bar{\rho})^{1/2}} = \frac{0.055[1+400(L/D)^3]^{1/6}}{[1+0.00527(1+427(L/D)^3)^{1/2}((L/D)^6+117(L/D)^2)^{3/4}]^{1/3}} \quad \textbf{(2.2)}$$

The above equation is valid in the range 0.01< L/D <20, and 0.025< $\Delta\rho/\rho$ <0.17. This work was extended for multiple openings in the horizontal partition.

Epstein (1989) extended his work on the same setup to study combined natural convection and forced flow through small horizontal opening. The flow across a vertical opening was analysed using Bernoulli equation and an equation for flooding flow rate was deduced. By supplying water into the lower compartment to initiate unidirectional flow in upward direction or by draining water from the lower compartment to initiate unidirectional flow in downward direction, he calculated the flooding flow rate (q) through the opening. The relation for dimensionless flooding flow rate $q/(D^5 g\Delta\rho/\rho)^{1/2}$ against L/D was obtained (Eq. (2.3))

$$\frac{q}{(D^5 g\Delta\rho/\rho)^{1/2}} = \frac{0.19[1+4*10^3(L/D)^3]^{1/9}}{(1+5.091*10^{-2}(L/D)^{16/7}[1+4*10^3(L/D)^3]^{4/9})^{1/4}} \qquad \textbf{(2.3)}$$

The eq. (2.3) is valid for the same range of L/D and $\Delta\rho/\rho$ as described earlier. Jaluria et al. (1998) also performed experimental study to characterise the combined buoyancy and pressure driven flow through a single opening in horizontal partition. The density difference was maintained by using salt water and fresh water in liquid system, while in air system, the temperature of compartment was kept higher to study natural convection across opening. For liquid system, setup was same as used by Epstein (1989), except that there was provision to pressurize the water in bottom compartment by injecting additional fresh water. The density variation of the upper compartment was measured and flow rate was determined as described by Epstein. The pressure difference was increased and conversion from bidirectional to unidirectional flow was found. The entire process was visualised using shadowgraph and photographs were taken at regular interval. In the heated air system, compartment was heated and smoke was introduced into the chamber for flow visualization. A vertical laser sheet was passed through the centre of exit duct and resulting scattering of the smoke particle was recorded.

Similar type of experiments were also conducted by Tan and Jaluria (2001), the pressure in the lower compartment was increased gradually and a pressure value known as purging or flooding pressure was found when the flow through the opening is unidirectional. During the experiments flow visualisation was done using shadowgraph and unidirectional flow was determined by these images. They showed that this critical pressure difference is of the order of ($g\Delta\rho D$). The parameters studied were 0.25< L/D <6.08, 0.043< $\Delta\rho/\rho$ <0.13 and 30< Δp <100 N/m^2. They developed a correlation for net flow rate Q_0 in terms of Δp as given below (Eq. (2.4))

$$Q_0 = 2.313*10^{-7}(\Delta p + 30.12)^{0.914}(\Delta\rho)^{-0.157}(L/D)^{0.037} \qquad \textbf{(2.4)}$$

The above correlation can be used for estimation of growth of fire in a compartment.

Christensen and Peterson (2001) developed BMIX code to simulate the mixing in large stable stratified enclosures. They developed 1-D model based on Langrangian approach. The BMIX code was validated against an earlier developed code and also by experimental data. The density stratification was produced in the same way as in salt water and fresh water experiment. Two openings were used to form convective current loop. The density variation along height was measured and plotted with data obtained by developed code.

Kuhn et al. (2001) conducted similar type of study to simulate density stratification in the compartment due to combined density and pressure driven flow in presence of opening in horizontal partition. They assumed that there is density variation only in vertical direction. Since there is stratification in both the tanks, they showed that Epstein equation for flow rate based on mass balance has limitations. It is only valid for well-mixed conditions in the upper and lower compartment. A convective loop was established through two openings in horizontal partition which was unidirectional. The fluid velocity was measured with hot film probes to compute the exchange flow rate. In order to determine vertical density variation a laser was injected through the corner of tank and the reflected laser image provided the density at a point. A digital camera recorded the density curves on the target screen.

Oscillatory exchange flow through opening of small aspect ratio in horizontal partition was also studied by Conover et al. (1995). The axial velocity at a point was measured using LDV in the oscillatory region and frequency of oscillation was obtained. The flow visualisation was performed using shadowgraph and snapshots were taken by a standard camera. From the axial velocity measured and shadowgraph images the pulsating exchange flow was characterised. The frequency of pulsation was measured by carefully measuring the time required for repeating the flow of a blob from one compartment to another.

Salt water-freshwater analogy was also used by Linden et al. (1990) to simulate natural ventilation flow through an opening in horizontal partition. Use of salt water-fresh water analogy was also explored by Tovar et al. (2009) for experiments to study flow and stratification in two coupled rooms connected to the exterior by a single vent related to natural ventilation. The two rooms were connected by two openings one at high-level and the other at low-level in the dividing wall. One “forced” room had a buoyancy source, while the outlet vent was in the “unforced” room, placed in such a way that the buoyancy in the room could potentially drive an exchange flow through it. The effect of the size of the outlet vent on the resulting stratification in the two rooms was studied. For a small vent, only unidirectional flow occurred, and since no ambient fluid entered the rooms, the buoyancy in both rooms became uniform and approached asymptotically to the buoyancy of the source. Above a critical vent size, a bidirectional flow was observed through the vent.

Salt water fresh water analogy was also used by Yao (2006) and Yao and Marshall (2005) to study ceiling jet dynamics. Salt water was injected in a tank filled with fresh water to generate circular jet followed by ceiling jet when the round jet interacted with ceiling wall. Suitable scaling was developed to compare the result of salt water experiments with fire plume and ceiling jet. PLIF technique was used to measure salt concentration during the experiments.

Clement and Fleischmann (2003) have performed salt-water experiments that resemble the smoke flow in the early stages of a residential scale building fire. In the experiments, a salt-water plume was injected into a two-room model where a simple rectangular opening connected the two compartments. As a whole, the model was a rectangular compartment 400 mm high, 400 mm wide and 1200 mm long. The density of the fluid within vertical plane was measured from the fluorescence emitted by the tracer dye in the salt water.

Hunt and Linden (2001) examined the steady flow and stratification generated in a ventilated enclosure by a single point source of buoyancy on the floor and a flow of wind which assists the buoyancy-driven flow. Laboratory experiments were conducted in water tanks to study these flows and the results compared with the predictions of a theoretical model. Stack-driven flows were simulated in the laboratory using brine and fresh water to create density differences and, therefore, the buoyancy forces acted downwards.

Cholemari and Arakeri (2005) conducted experimental measurements of buoyancy driven turbulent exchange flow in a vertical pipe (L/D ratios of 9–12). The flow was driven by an unstable density difference across the ends of the pipe, created using brine and distilled water. The large pipe was connected by two tanks, with the top tank fluid having higher density than the bottom tank fluid.

Yao and Marshall (2006, 2007) studied plumes behaviour created by gently introducing salt-water into quiescent fresh water. Turbulent mixing patterns were visualized via PLIF. The

PLIF salt-water modelling technique was used to characterize canonical, unconfined and impinging plumes.

Blomqvist and Sandberg (2000) performed salt water fresh water experiments for natural ventilation study through a square horizontal opening, the size of setup was 0.495mX0.495mX0.595m; the compartment was divided into two parts by a horizontal 10 mm thick plate. In the centre of plate, there was a square opening of side length size 80 mm. The upper compartment was filled with salt water of density 1006.3 kg/m^3. The time-averaged results with well-mixed compartment were reported for the average value of density of upper compartment with respect to time.

LeQuesne (2010) has also performed saltwater modelling of fire gas flow through a horizontal ceiling opening. A $1/10^{th}$ scale model was made for square and slot opening in horizontal partitions for two different density ratios of fresh water and salt water.

Zhigang (2007) performed two cases of full-scale measurements of buoyancy driven natural ventilation through a horizontal opening and a combined horizontal and vertical opening. For case one, opening in horizontal partition the experiments was performed for opening aspect ratio 0.027 to 4.455. The characteristics of flow i.e. airflow rate, velocity, difference in temperature were measured. Flow visualisation was done using inclusion of smoke, which showed the nature of flow as highly transient, unstable and complex and oscillating with time. For case two, combined opening in horizontal as well as in vertical partition; the experiments was performed for opening aspect ratio from 0.11 to 25. Three modes of flow were identified depending on different parameters.

2.2. Numerical work on flow through opening

Apart from the experiments, various analytical and numerical computations have been performed by researchers to find the oscillatory nature of flow through an opening in a horizontal partition separating heavier fluid salt water at the top with lighter fluid fresh water in the lower enclosure. Singhal and Kumar (1995) studied the transient density driven flow through a circular opening in horizontal partition numerically. Spall and Anderson (1999) also studied the counter current exchange flow through a circular opening in horizontal partition for very thin opening. The oscillatory nature of flow was characterised by two dominant pulsation frequencies.

Effect of partition thickness on oscillatory exchange flow using water as the working fluid was numerically studied by Harrison and Spall (2003). Five different opening aspect ratio were considered in the analysis. It was found that the exchange coefficient first increases with opening aspect ratio up to 0.3 and after that it decreases with increases in opening aspect ratio.

Sleiti (2008) performed 2D numerical simulations for such type of oscillatory exchange flow at low Rayleigh number. Three different opening aspect ratio and air as working fluid were considered during the analysis. It was found that if opening aspect ratio is decreased to 0.5 from 1, exchange flow from upper to lower compartment was increased while if opening aspect ratio is increased to 2 from 1, exchange flow from upper to lower compartment was decreased.

Many similar analytical studies have also been performed with air as the working media slightly overheated in the lower enclosure when compared to the upper enclosure. Chow and Gao (2009) have developed a mathematical model and applied linear perturbation theory. A wave function was introduced as a perturbation to a control volume concerned. Oscillation growth, amplification, response and frequency have been studied by solving equations under practical conditions. Useful semi-empirical formula on these parameters is derived for fire safety engineering design.

Cooper (1996) developed a model for calculating combined density and pressure driven flow through an opening in horizontal partition in a gravitationally unstable configuration and used to solve the problem of steady burning in a ceiling-vented enclosure. The study led to a general finding that relates the rate of energy release of the fire to the area of the vent and the temperature and oxygen concentration of the upper portion of the enclosure environment.

Mishra et al. (2008) investigated the dynamics of the transient, two-dimensional buoyancy driven thermal mixing of two fluid masses at different temperatures, initially at rest and confined to separate portions of a horizontally partitioned adiabatic enclosure numerically within the framework of the Boussinesq approximation. Spanning the range $500 \leq Ra \leq 10^4$ at $Pr=0.71$ and unity aspect ratios of the vent and the enclosures, the dominant spatial and temporal flow structures, in the asymptotic approach of the system towards a state of thermo mechanical equilibrium, had been identified.

Kerrison et al. (1998) performed a comparison of CFD model predictions with experiment for the case of a fire within a compartment, which is vented (buoyancy-driven) to the outside by a single horizontal ceiling, vent. The flow through the vent produced oscillatory behaviour in vent temperatures with puffs of smoke emerging from the fire compartment.

Siang (2010) used the salt-water analogy modelling as an effective diagnostic, predictive and scaling tool for understanding fire dispersion in a beam ceiling complex compartment using the PIV and PLIF techniques. Dimensionless dispersion signatures and front arrival times were compared between the fire and salt-water experiments, which showed excellent agreement.

2.3. Experimental work on flow through opening in vertical partition

Fleischmann et al. (1994) modelled the fire compartment gravity current using salt water fresh water system. Four different openings in vertical partition were studied viz. full, slot, window and door; 2D flow for first 2 openings and 3D for last two openings was assumed. It was determined that length and velocity should be scaled down using geometric similarity and Froude number similarity $v^* = v / \sqrt{\beta g h}$, where $\beta = \Delta\rho / \rho$. Density ratio 2.2 was studied using salt water and fresh water where the ratio is 1.003-1.101. Gravity currents using a camera were recorded and Froude numbers for various values of β were examined. It was found that the value is constant differing only with geometry over the range of β investigated, i.e., 0.003-0.101. Maintaining Froude number similarity, the salt water results could be directly applied to typical fire compartment irrespective of same Reynolds number.

Mixing that happens in gravity current followed by backdraft was studied using salt water fresh water analogy by Fleischmann and McGrattan (1999). They also performed numerical simulations and lab scale back draft experiments to study flow behaviour across a large opening in vertical partition. In experiments, an active indicator phenolphthalein was used for flow visualization. The colour of mixture becomes red as the mixing causes a change in pH. To study gravity current an acrylic chamber of 0.3X0.15X0.15 m containing fresh water placed into the tank of 0.6X0.3X0.45 m filled with salt solution was constructed. Both tanks were separated by a vertical partition, when the opening was clear, mixing occurred and current was recorded using a 8 mm video camcorder at 30 frames/sec. Backdraft experiments on large scale setup were also performed. The compartment was filled with hot gases from a methane fuel gas burner. Bi-directional probes were used to measure velocity distribution across the opening.

Weng et al. (2002) and Weng et al. (2005) investigated the speed and clarity of the extent of the mixed region of gravity currents prior to backdrafts in building fires, by conducting a series of scaled salt water experiments using flow visualization and digital particle image velocimetry. The scaled compartment (0.4 m X 0.1 m X 0.1 m) was fitted with a variety of end and ceiling opening geometries, respectively: full, middle slot, upside-slot, downside-slot, door and window. The experimental results show that the gravity currents in salt water experiments are similar to other naturally occurring gravity currents and the experiments can model the gravity currents prior to backdrafts in building fires and predict the time of ignition for backdrafts in compartments with the same opening geometries.

Clement (2000) conducted a series of buoyant salt water experiments, with the purpose of generating experimental data for comparison with computational fluid dynamics (CFD) models. Two types of buoyant flows were generated in the experiments; a natural transitional flow, and flows that resemble fire induced smoke flow within a residential building. Laser Induced dye Fluorescence (LIF) was used to measure the fluid density in a single vertical plane of the flow.

Jankiewicz (2004) used salt-water modelling as a predictive tool for determining the response time of ionization type smoke detectors. A quantitative technique was developed using salt-water modelling and PLIF diagnostics. The non-intrusive diagnostic technique was used to temporally and spatially characterize the dispersion of a buoyant plume within a $1/7^{th}$ scale room-corridor-room enclosure. This configuration was geometrically similar to a full-scale fire test facility, where local conditions were characterized near five ionization type smoke detectors placed throughout the enclosure. The full-scale fire and salt-water model results were scaled using the fundamental equations that govern dispersion.

McBryde (2008) performed scale salt water modelling to generate Boussinesq, fully turbulent gravity currents for different opening geometries, typical of fire compartments. Experimental concentration and velocity fields were generated using the non-intrusive flow visualization technique.

Yii (1998) investigated the potential of applying salt water modeling using the PLIF flow visualization technique to study balcony spill plume phenomena. A 1/20 scale perspex model was used to conduct a series of salt water experiments. The testing parameters include two balcony settings (125 mm and 250 mm in model scale) and two spilling densities (0.5% and 1.0% of salt by weight). The smoke layer within the compartment was simulated by the injection of a saline layer. By doing this, a quantitatively correct counter flow at the doorway was achieved, as in the real fire situation. This method also provided greater control over the injected flow and the flow was found to be repeatable.

2.4. Gap areas

From the literature, it is clear that most of the work for opening in horizontal partition has been done for small opening size compared to the compartment size. Limited results are available for large opening. Most of the experimental results are time averaged with well-mixed compartment assumption. Only qualitative and average measurements have been performed. Detailed 2D PIV and PLIF measurement for flow through opening in horizontal partition has not been performed. PLIF measurement for density driven flow through opening in vertical partition has been performed but flow through opening in vertical partition has not been examined in detail using PIV and PLIF.

2.5. Scope of the work

A. Experimental Work

The scope of the present work is to investigate the potential of applying salt water modelling using the PLIF flow visualization and salt concentration measurement technique to study the influence of vertical and ceiling opening on movement of fire induced smoke flow. Experiments have been conducted for combined pressure and buoyancy driven fire induced flow through horizontal and vertical opening. A 1/16th scale Perspex model was constructed. The testing parameters were as follows:

(i) 2 different configuration of vertical opening (window/door)

(ii) 2 different sizes of horizontal opening (square shape)

(iii) 4 different salt water densities.

B. Numerical Work

(i) 3D CFD computation were carried out for transient turbulent movement of salt water buoyant plume, its interaction with ceiling, oscillatory exchange flow through ceiling opening and bi-directional flow through vertical opening. Developed 3D transient CFD code will be used for simulation of all above experiments.

(ii) 2D transient simulation of oscillatory exchange flow through opening in horizontal partition (two compartments one over another separated by a horizontal partition) were carried out.

(iii) 3D transient simulations of flow through opening in vertical partition due to density difference (the left hand side compartment will be filled with salt water and the other with the fresh water) were carried out.

2.6. Closure

Detailed literature review related to experimental and numerical work related to flow through openings has been performed. Use of salt water analogy for this type of study has also been reviewed. The gap areas in this field have been identified. Based on these findings, the scope of the present research work has been defined.

CHAPTER 3: NUMERICAL INVESTIGATION OF BUOYANT FLOW THROUGH OPENING IN HORIZONTAL PARTITION

3.1. Introduction

The flow of hot gases/smoke through opening in horizontal partition is important for stratification inside the enclosure and spread of hot gases outside the enclosure. The application of these flows is important during natural ventilation, spread of smoke during fire, release of steam in helium-steam stratified atmosphere inside nuclear reactor containment and during passive cooling of heated structures. It is essential to characterize such flow through large openings to determine the exchange from one compartment to another compartment accurately in presence of buoyancy and combined buoyancy and pressure driven force. Current zone based model calculates the flow using standard vent models based on pressure difference using flow coefficients that do not accurately take in to account the buoyancy component of the flow and predict no flow in case of only density difference across the opening. The applications of such studies are in the areas of containment thermal hydraulics, fire modelling in nuclear power plants and hydrogen transport in nuclear reactor containment. In nuclear reactor containment resulting flow after an accidental condition will be a function of the initial pressure difference, but in the long-term, the flow field will be principally driven by density differences between the two compartments as soon as the pressures have equalized. In accidental fires, the compartment below the partition contains lighter fluid (hot gases) compared to heavier fluid located in the upper compartment (ambient air). A gravitational unstable system is created when fluid of higher density is placed in a compartment connected to a compartment filled with lighter density fluid having an opening in connecting horizontal partition. The nature of flow in this condition is turbulent, unstable and bi-directional. A large number of analytical, numerical and experimental studies have been performed to quantify flow through single large opening (Chow and Gao, 2009, Kerrison et al., 1998).

Significant researches have been done to characterise such type of flow across the openings using salt water/fresh water analogy. Salt water modelling technique is a useful tool to simulate such flows, which takes into accounts most of the flow characteristics and allows for good flow visualization (Yao and Marshall, 2006). The main advantages of the salt water modelling experiments are that they are clean and relatively inexpensive compared to the conventional fire test and CFD modelling.

3.2. Problem Description

Influence of density difference as well as opening aspect ratio has been studied with salt water analogy. Flow coefficient is weakly varying with time and one can say that flow coefficient is weakly dependent on density ratio across the opening at low value of density difference. The effect of larger density difference on oscillation frequency has been studied in present work as it is not considered previously by other investigators and as identified in the literature review presented in Chapter 2. A correlation has been developed to compute the frequency of oscillation for known values of L/D and $\Delta\rho_0 / \rho_{L,0}$. In-house buoyancy modified turbulent 2D axisymmetric CFD code was used which can simulate buoyancy driven oscillatory exchange flow through a circular opening in a horizontal partition. The effect of opening aspect ratio and initial non-dimensional density difference has been studied numerically for partitions of finite thickness over the range 0.008 ≤ L/D ≤ 0.9 and 0.012 ≤ $\Delta\rho_0 / \rho_{L,0}$ ≤ 0.2. The characteristic of flow was defined by flow coefficient and computed numerically as recommended by Epstein (1988) and compared with the experimental results for validation of the present axisymmetric CFD code. The frequency of oscillation has been determined from instantaneous velocity at the opening location. Epstein (1988) initiated a study on the buoyancy driven exchange flow through opening in horizontal partition between two compartments using salt water/fresh water. Based on the mass balance of the upper and lower compartments, Eq. (3.1) for flow rate from the top enclosure to bottom enclosure was developed. For a particular opening diameter, the theoretical volumetric exchange flow rate at any instant was calculated using Eq. (3.2). The flow is considered as exchanged if some of the quantity of salt is transported from top enclosure to bottom enclosure. The exchange flow in upward and downward direction was equal. Based on these two equations flow coefficient was defined as Eq. (3.3)

$$Q(t) = \frac{-V_H (d\rho_H / dt)}{(\rho_H - \rho_{L,0}) - {}^{V_H}\!/_{V_L} (\rho_{H,0} - \rho_H)} \tag{3.1}$$

$$Q_s(t) \equiv \sqrt{\frac{D^5 g \Delta\rho(t)}{\rho(t)}} \tag{3.2}$$

$$Q^* = \frac{Q(t)}{Q_s(t)} \tag{3.3}$$

For numerical simulations, the computational domain was chosen from the test set up of Conover et al. (1995). The experimental setup was made of transparent material and comprised of two separate compartments connected by an opening in horizontal partition. The lower enclosure has dimension of 0.381X0.381X0.316 m. The upper enclosure has dimension of 0.381X0.381X0.265 m. Both the enclosure was separated by a partition plate. A plate having 0.127 m diameter hole at centre was attached to the partition plate and sealed by an O-ring. Holes of 0.0508 m (2 inches) in diameter were served in the plates of varying thickness to be used as vents.

The top enclosure was occupied with fluid of higher density while the bottom enclosure was occupied with fluid of lower density, thus creating a density differential between the two chambers. The code was validated against reported experiments of this nature. The flow coefficients and pulsation frequency were determined. Various cases were studied by varying the density ratio from 1.012 to 1.2 while the opening aspect ratio was varied from 0.008 to 0.9. The effect of these parameters was investigated on oscillation frequency and flow coefficient.

3.3. Mathematical model and numerical method

The computations were carried out assuming a cylindrical geometry for ease in computation. The volume of simplified geometry was kept similar to actual set up. To further simplify the computation the computational domain was considered as 2D axisymmetric.

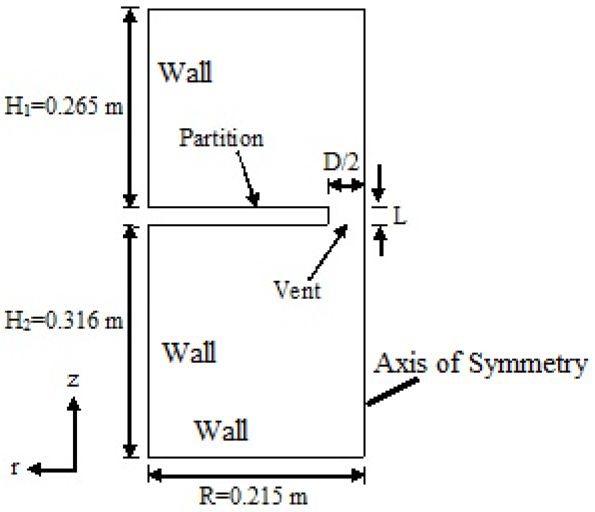

Figure 3.1: Simplified geometric configuration for CFD computation

The domain dimensions were taken as radius (R) 0.215 m and height of lower enclosure 0.316 m (H_2) and height of upper enclosure 0.265 m (H_1) connected by a thin partition of specified thickness, containing a hole of diameter (D) 0.0508 m (2 inches). The simplified geometry of computational domain is depicted in Fig. 3.1.

The governing equations are as follows

Continuity equation

$$\frac{\partial \rho}{\partial t}+\frac{\partial(\rho u)}{\partial z}+\frac{1}{r}\frac{\partial(r\rho v)}{\partial r}=0 \tag{3.4}$$

Z-momentum equation

$$\frac{\partial(\rho u)}{\partial t}+\frac{\partial(\rho uu)}{\partial z}+\frac{1}{r}\frac{\partial(r\rho vu)}{\partial r}=-\frac{\partial p}{\partial z}+\frac{\partial}{\partial z}\left(2\mu_{eff}\left(\frac{\partial u}{\partial z}\right)\right)+\frac{1}{r}\frac{\partial}{\partial r}\left(r\mu_{eff}\left(\frac{\partial u}{\partial r}+\frac{\partial v}{\partial z}\right)\right)-(\rho-\rho_{\infty})g \tag{3.5}$$

R-momentum equation

$$\frac{\partial(\rho v)}{\partial t}+\frac{\partial(\rho uv)}{\partial z}+\frac{1}{r}\frac{\partial(r\rho vv)}{\partial r}=-\frac{\partial p}{\partial r}+\frac{\partial}{\partial z}\left(\mu_{eff}\left(\frac{\partial u}{\partial r}+\frac{\partial v}{\partial z}\right)\right)+\frac{1}{r}\frac{\partial}{\partial r}\left(2r\mu_{eff}\left(\frac{\partial v}{\partial r}\right)\right)-\frac{2}{r^2}\left(\mu_{eff}\,v\right) \tag{3.6}$$

Species transport equation

$$\frac{\partial(\rho Y_S)}{\partial t}+\frac{\partial(\rho uY_S)}{\partial z}+\frac{1}{r}\frac{\partial(r\rho vY_S)}{\partial r}=\frac{\partial}{\partial z}\left((\rho D_{ab}+\mu_t/Sc_t)\frac{\partial Y_S}{\partial z}\right)+\frac{1}{r}\frac{\partial}{\partial r}\left(r(\rho D_{ab}+\mu_t/Sc_t)\frac{\partial Y_S}{\partial r}\right) \tag{3.7}$$

Salt water density has been determined in terms of the salt mass fraction using an empirical expression as suggested by Yao and Marshall (2006) as given by Eq. (3.8)

$$\rho=\rho_{L,0}(1.0+\beta_{SW}Y_s) \tag{3.8}$$

Turbulence Modelling:

For modelling turbulence RNG k-ε model (Yakhot el al., 1992) was used with buoyancy modification. The y+ was in the range of 30-80 near the walls that is required to use the standard wall function. The renormalization group (RNG) theory represents the effects of the small-scale turbulence by means of a random forcing function in the Navier–Stokes equation. The RNG procedure systematically removes the small scales of motion from the governing equations by expressing their effects in terms of larger scale motions and a modified viscosity. The RNG k–ε model equations for high Reynolds number flows derived by Yakhot et al. (1992) are as follows:

For the RNG k-ε model, the turbulent viscosity is modelled as (Eq. (3.9))

$$\mu_t = \rho C_\mu \frac{k^2}{\varepsilon} \tag{3.9}$$

For turbulent kinetic energy, the equation is given by (Eq. (3.10))

$$\frac{\partial(\rho k)}{\partial t} + \frac{\partial(\rho u k)}{\partial z} + \frac{1}{r}\frac{\partial(r\rho v k)}{\partial r} = \frac{\partial}{\partial z}\left(\alpha_k \mu_{eff}\frac{\partial k}{\partial z}\right) + \frac{1}{r}\frac{\partial}{\partial r}\left(r\alpha_k \mu_{eff}\frac{\partial k}{\partial r}\right) + \tau_{ij}.S_{ij} + G_B - \rho\varepsilon \tag{3.10}$$

The turbulent dissipation rate is computed by Eq. (3.11)

$$\frac{\partial(\rho \varepsilon)}{\partial t} + \frac{\partial(\rho u \varepsilon)}{\partial z} + \frac{1}{r}\frac{\partial(r\rho v \varepsilon)}{\partial r} = \frac{\partial}{\partial z}\left(\alpha_\varepsilon \mu_{eff}\frac{\partial \varepsilon}{\partial z}\right) + \frac{1}{r}\frac{\partial}{\partial r}\left(r\alpha_\varepsilon \mu_{eff}\frac{\partial \varepsilon}{\partial r}\right) + \frac{\varepsilon}{k}\left(C_{1\varepsilon}^{*}\tau_{ij}.S_{ij} - C_{2\varepsilon}\rho\varepsilon + C_3 G_B\right) \tag{3.11}$$

Where $\mu_{eff} = \mu + \mu_t$, $\alpha_k = \alpha_\varepsilon = 1.39$, $C_{1\varepsilon} = 1.42$, $C_{2\varepsilon} = 1.68$ and $C_{1\varepsilon}^{*}$ is given by Eq. (3.12)

$$C_{1\varepsilon}^{*} = C_{1\varepsilon} - \frac{\eta(1-\eta/\eta_0)}{1+\beta_{RNG}\eta^3} \tag{3.12}$$

$$\eta = \frac{k}{\varepsilon}\sqrt{2S_{ij}.S_{ij}}\ ,\ \eta_0 = 4.377\ ,\ \beta_{RNG} = 0.012$$

The term G_B can be modelled by Eq. (3.13), which is based on Simple Gradient Diffusion Hypothesis (SGDH) (Markatos et al., 1982) or by Eq. (3.14) which is based on Generalised Gradient Diffusion Hypothesis (GGDH) (Daly &Harlow, 1970). In the present work GGDH approach has been used as GGDH is better approach since it considers density gradient in all the 3 directions.

$$G_B = -\frac{\mu_t}{\Pr_t}\frac{1}{\rho^2}\frac{\partial\rho}{\partial x_j}\left(\frac{\partial p}{\partial x_j} + \rho_\infty g_j\right) \tag{3.13}$$

$$G_B = -\frac{3}{2}\frac{\mu_t}{\Pr_t}\frac{1}{\rho^2 k}\left(\overline{u'_j u'_k}\frac{\partial\rho}{\partial x_k}\right)\left(\frac{\partial p}{\partial x_j} + \rho_\infty g_j\right) \tag{3.14}$$

In Eq. (3.14), pressure gradient was assumed as negligible. The assumption is reasonable as the fluid velocity is relatively low thus causing low pressure gradients. There are various approaches to determine the value of C_3 for Eq. (3.11); in the present work the approach suggested by Viollet (1987) was adopted. Depending on the sign of G_B (the term denoting the buoyancy production of turbulence in k), the value of C_3 is determined. If $G_B > 0$; $C_3 = 1.44$ and $C_3 = 0$, if $G_B < 0$. The stability of flow determines the sign of G_B. If $G_B > 0$; the flow is unstable since density gradient is positive and, if $G_B < 0$; the flow is stable density gradient is negative. Table 3.1 shows the parameters used in the computation.

Table 3.1: Values of parameters used in computation (McBryde, 2008)

Parameter	Value
Mass diffusivity of salt (D_{ab})	1.5e-9 m^2/ s
Dynamic viscosity of water (μ)	1.003e-3 m^2/s

Turbulent Schmidt number (Sc_t)	0.7

Solver Details:

The 2D axisymmetric, incompressible, unsteady momentum, continuity, species and turbulent quantities were solved. In-house CFD code was developed based on pressure based SIMPLE algorithm. The code written in C language is for this specific purpose and solver is very fast for this problem as compared to any commercial or open source code. Third order QUICK scheme (Hayase et al., 1992) was employed for convective terms to capture the oscillation pattern and second order central differencing was employed for diffusive term. The time discretization was done using second-order-accurate Crank-Nicolson scheme.

Initially the lower compartment was filled with fresh water; hence mass fraction of salt was assigned as zero and in the upper compartment salt water, mass fraction was assigned as per the required density of salt water solution evaluated using Eq. (3.8). The characteristic velocity is $\sqrt{(\Delta\rho / \rho) gD}$, which is of the range of 0.077 m/s to 0.316 m/s for the parameters considered, which gives densimetric Reynolds number (Re) in the range of ~ 4000-16000. The flow is turbulent in all the cases. For initialisation, the velocity components were set to zero values. All the walls and partition have been modelled as a no-slip impermeable wall. Staggered grid system was used in which scalar i.e. pressure, species mass fraction and turbulent quantities ware calculated at cell centre while fluid velocities were calculated at the cell faces. The set of algebraic equations were solved iteratively using Gauss-Seidal method. For momentum equation under-relaxation value of 0.05 was used to have easy convergence since the solutions were oscillating in nature. For species transport equation under-relaxation value of 1 was chosen. The solution was assumed as converged in each time step if mass residual was below 10^{-5}. For a single simulation on a Xeon machine, the computational time was approximately 24 hours for the 3000 seconds of a transient duration. 4 simulations were run simultaneously on a 4-core 2.67 GHz processor with L2 cache size of 8 MB.

3.4. Grid resolution and Time step selection

Two different time step, i.e. 0.05 s and 0.1 s were used to perform time step independence study. It was observed that the smaller time step gives nearly similar results. Hence time step of 0.1 s was used for final runs. To achieve the convergence in each time step maximum one hundred internal iteration per time step were performed. Non-uniform mesh was adopted for accurately predicting the flow gradients. The y+ was kept in the range of 30-80 near the walls which is essential to use the standard wall function. In the axial direction, the grids were made fine near the partition and it was made coarser away from the partition. In the radial direction a uniform grid was employed up to the opening region after which the grid was made non-uniformly coarser towards the outer radius. Four different grid sizes were tested to obtain the results which are independent of grid size. Flow coefficient was computed for each grid size. The different grids used were 86 X 50, 128 X 75, 170 X 100 and 212 X 130 in axial and radial directions respectively and opening region was meshed by 10, 15, 20, 30 grids in radial direction respectively for these four grids. A coarse and finer mesh used in present work is depicted in Fig. 3.2. The results of the grid independence study performed for the window opening for opening aspect ratio of 0.3 used in the present work is depicted in Fig. 3.3.

Figure 3.3 shows that the exchange flow coefficients increases with grid size and approached towards a fix value as the grid size is refined. From the Fig. 3.34 it was concluded that that a grid size 170 X 100 is sufficiently fine to obtain grid independent results. Since the flow is unstable, flow established by itself even when the initial velocity components were set as zero value. During simulation, flow is initiated automatically without any perturbation due to initial round off error.

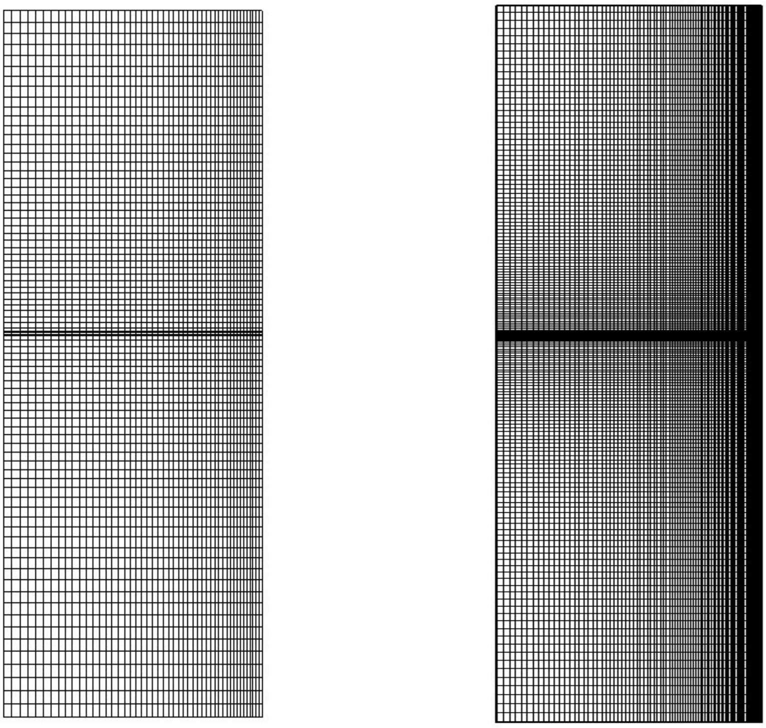

Figure 3.2: Meshes used coarse mesh 86 X 50 (left) and fine mesh 170 X 100 (right)

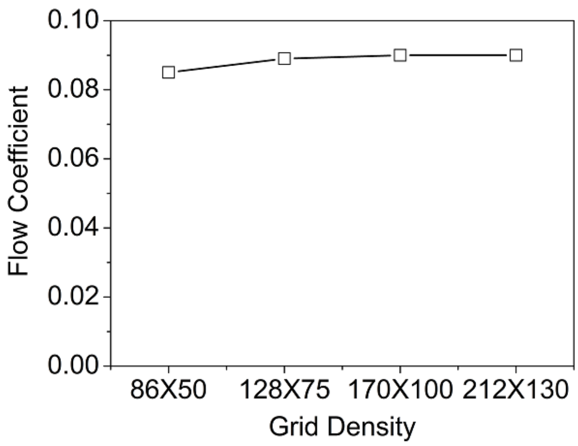

Figure 3.3: Grid independence results for opening L/D=0.3 for flow coefficient

3.5. Model Validation

The code was validated against the experimental data for two different opening aspect ratios of 0.008 and 0.106 as used by Conover et al. (1995). The density of upper compartment was computed and compared with experimental values as shown in Fig. 3.4. The initial density of salt water was 1011.5 kg/m^3 and 1012 kg/m^3 respectively in the experiment as well as in simulations. The code predictions are in very good agreement with experiments for low aspect ratio. For higher aspect ratios, the code was validated against available experimental data from Epstein (1988) and numerical data from Harrison and Spall (2003). Figure 3.5 shows the time averaged flow coefficient and comparison with available data.

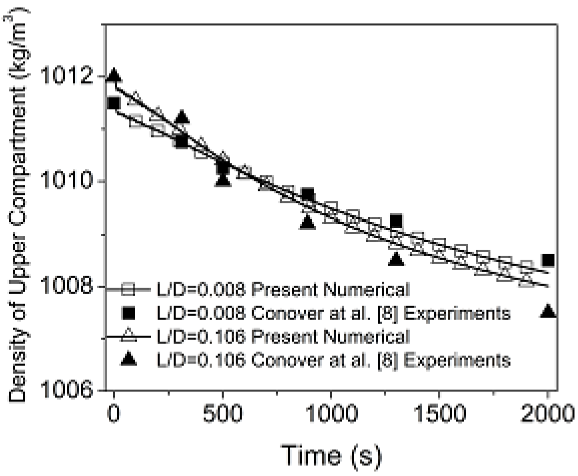

Figure 3.4: Variation of upper compartment density with time for validation

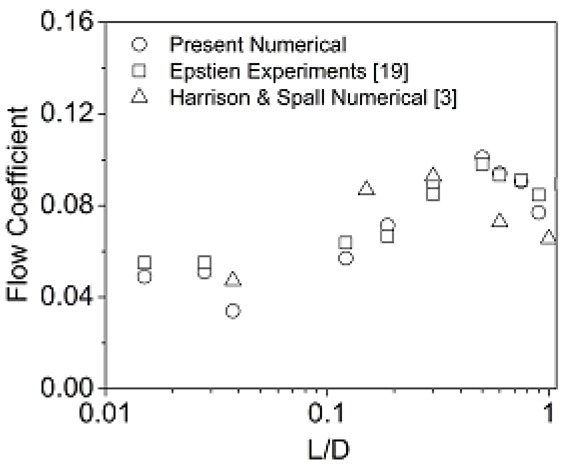

Figure 3.5: Comparison of numerically determined flow coefficients with available data

3.6. Application of model

Flow Coefficient:

When the flow is oscillating, the flow coefficient is also oscillating as shown in Figs. 3.6-3.7 for two opening aspect ratio at different densities. The effect of $\Delta\rho_0 / \rho_{L,0}$ and L/D on time averaged flow coefficient is shown in Fig. 3.8. It is clear that effect of $\Delta\rho_0 / \rho_{L,0}$ on average flow coefficient is not significant but effect of L/D is significant. As the density ratio is varied, the actual exchange flow rate as well as theoretical exchange flow rate gets altered and net effect on flow coefficient is small. A larger L/D configuration creates a flow resistance and flow coefficient increases with L/D as flow gets streamlined, however at low L/D, oscillations are significant but net exchange flow is reduced. The peak value of flow coefficient at L/D = 0.6 is consistent with Epstein (1988). Harrison and Spall (2003) have also obtained flow oscillation at higher value of L/D = 0.9. To explain the effect of density on flow coefficient, the normalised density is plotted against non-dimensional time in Fig. 3.9-3.10. The normalised density $\left(\rho^*\right)$ and non-dimensional time $\left(t^*\right)$ are defined as follows

$$\rho^* = \left(\rho_H\left(t\right) - \rho_{L,0}\right) / \Delta\rho_0 \tag{3.15}$$

$$t^* = t / \left(D / \sqrt{\left(\Delta\rho / \rho_{L,0}\right) gD}\right) \tag{3.16}$$

This phenomenon that non-dimensional flow or velocity is independent of density difference ratio also exists for buoyancy driven flows through opening in vertical partition (Fleischmann et al., 1994). Results from modelling of gravity currents prior to backdraft have shown the value of non-dimensional velocity as 0.5 (Weng et al., 2002) for all density ratios.

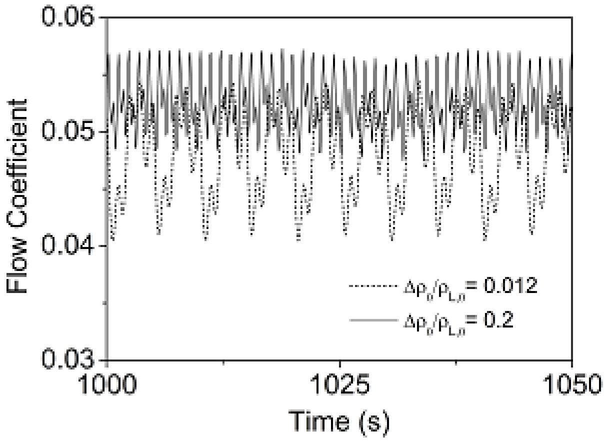

Figure 3.6: Variation of flow coefficient with time for L/D=0.008

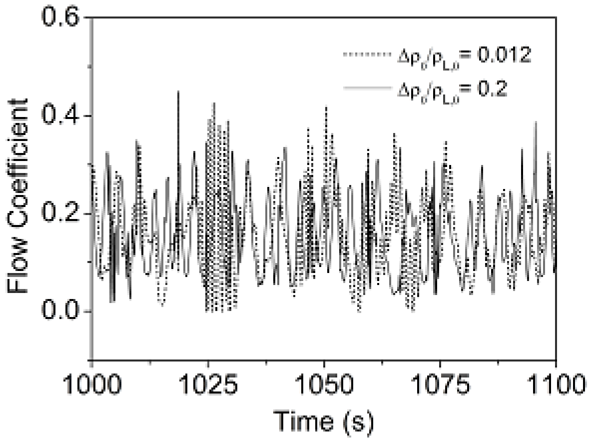

Figure 3.7: Variation of flow coefficient with time for L/D=0.9

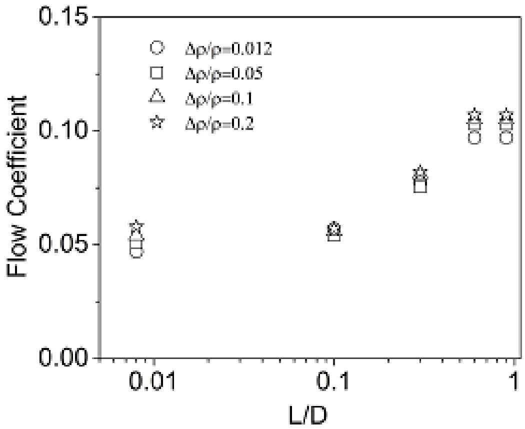

Figure 3.8: Time averaged flow coefficient for different L/D and $\Delta\rho_0 / \rho_{L,0}$

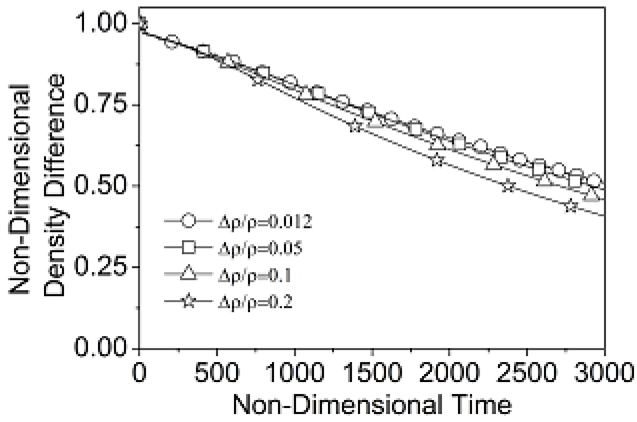

Figure 3.9: Variation of Normalised density difference with non-dimensional time for L/D = 0.008

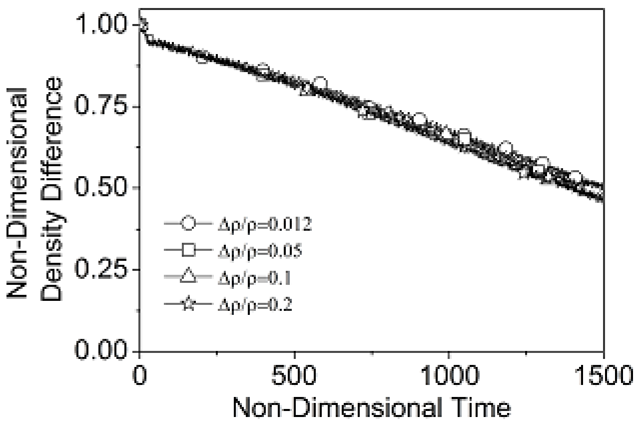

Figure 3.10: Variation of Normalised density difference with non-dimensional time for L/D = 0.9

Axial Velocity:

The axial velocity near opening was monitored with time to compute the pulsation frequency, and is shown in Figs. 3.11-3.12 for different $\Delta\rho_0 / \rho_{L,0}$ and for 2 different L/D. The velocity at the opening is oscillatory in nature in a well-defined pattern so that a single dominant frequency was obtained during FFT analysis. As expected, velocity as well as oscillation frequency increases with increase in $\Delta\rho_0 / \rho_{L,0}$. Transient flow field was captured by numerical simulation. The magnitude of velocity increases with L/D. To compute the dominant frequency in all the cases, FFT analysis was performed on point velocity data.

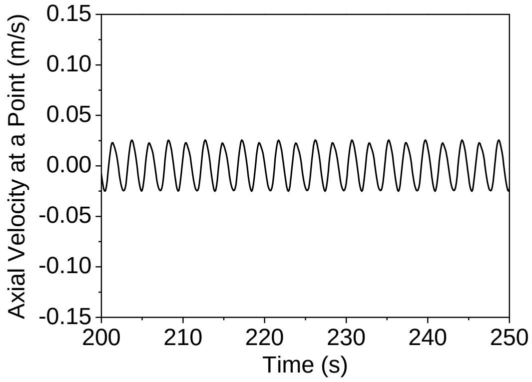

(a) $\Delta\rho_0 / \rho_{L,0}$ =0.012

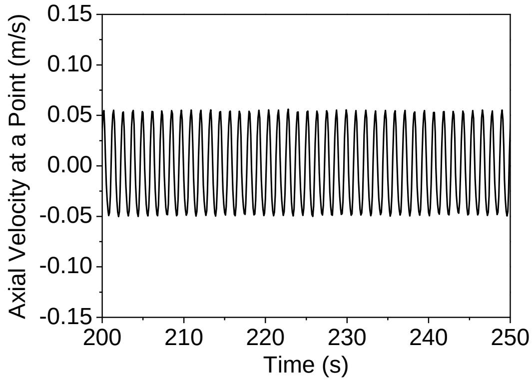

(b) $\Delta\rho_0 / \rho_{L,0}$ =0.05

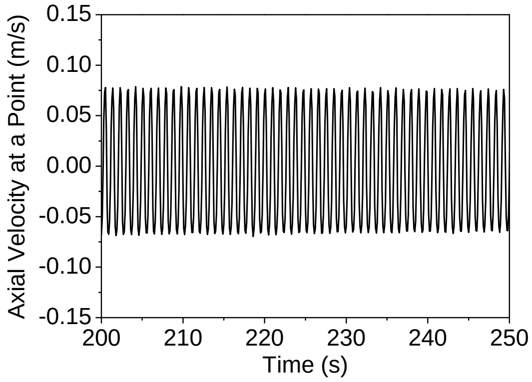

(c) $\Delta\rho_0 / \rho_{L,0}$ =0.1

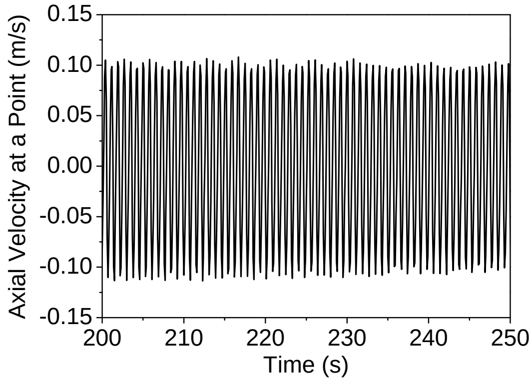

(d) $\Delta\rho_0 / \rho_{L,0}$ =0.2

Figure 3.11: Axial velocity at the centre of opening for different $\Delta\rho_0 / \rho_{L,0}$ at L/D = 0.008

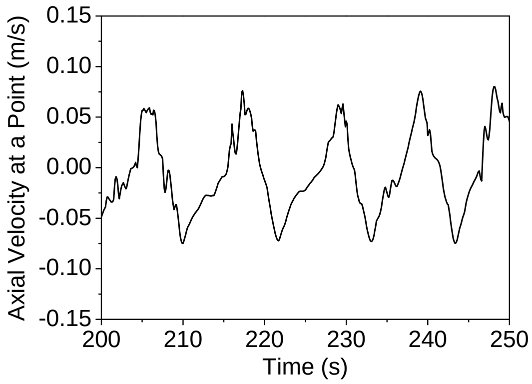

(a) $\Delta\rho_0 / \rho_{L,0}$ =0.012

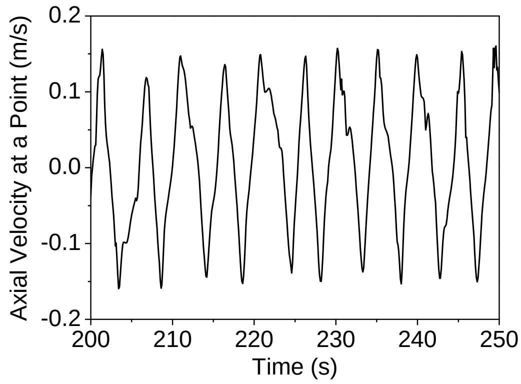

(b) $\Delta\rho_0 / \rho_{L,0}$ =0.05

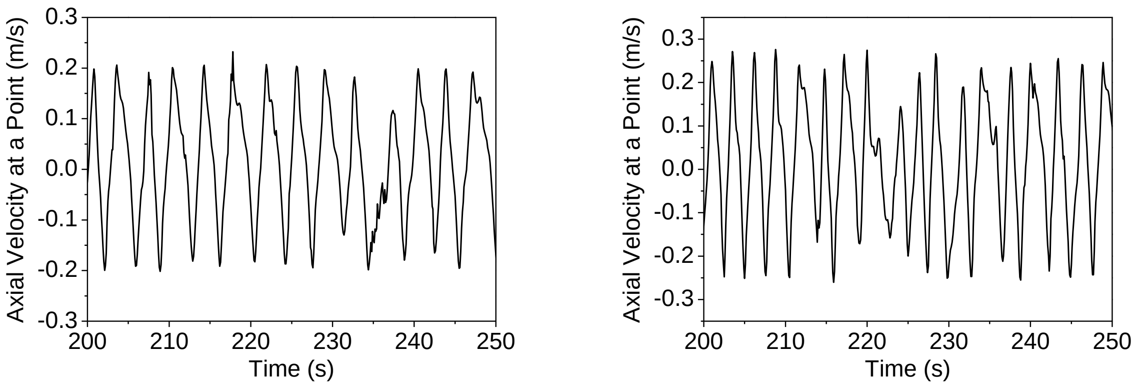

(c) $\Delta\rho_0 / \rho_{L,0}$ =0.1 (d) $\Delta\rho_0 / \rho_{L,0}$ =0.2

Figure 3.12: Axial velocity at the centre of opening for different $\Delta\rho_0 / \rho_{L,0}$ at L/D = 0.9

Pulsation Frequency:

The frequencies of oscillation during initial 200 seconds for all cases are shown in Figs. 3.13-3.17. The dominant frequency for all the cases is plotted in Fig. 3.18. Oscillation frequency is dependent on driving potential and frictional resistance. The driving potential for the flow is $\Delta\rho_0 / \rho_{L,0}$ and opening length creates a flow resistance. At very low L/D, the flow is highly oscillatory and due to increase in opening length, flow becomes streamlined up to L/D≤0.6. For L/D greater than 0.6, viscous resistance is prominent and flow coefficient reduces. The peak value of flow coefficient is obtained at L/D=0.6. As reported in literature, at the interface of both the fluid the pressure is same in both the enclosures. However, the interface remains always unstable as the fluid of higher density is staying over the fluid of lower density. A small disturbance initiates an oscillatory exchange flow through the opening. This is a classic example of “Taylor instability”, due to which exchange flow takes place from one enclosure to another. The exchange flow is oscillatory and these oscillation are quantified by the oscillatory nature of the vertical velocity component at the opening location.

The density difference causes the flow from the upper compartment to lower compartment through the opening, since the lower compartment has a fixed volume, the fresh water from the lower compartment moves towards the upper chamber through the same opening. As time proceeds, the density difference is reduced due to mixing, hence driving potential is decreased and a small decrease in velocity magnitude and pulsation frequency is observed. For L/D=0.6 and 0.9, the velocity magnitude is doubled as compared to other L/D.

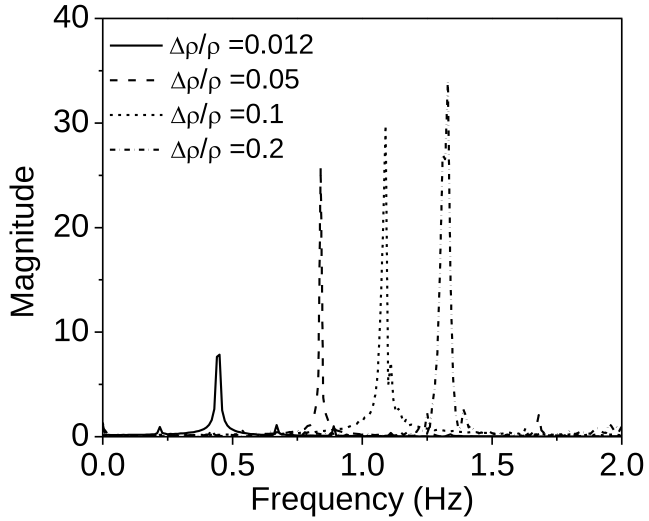

Figure 3.13: FFT analysis results for L/D = 0.008

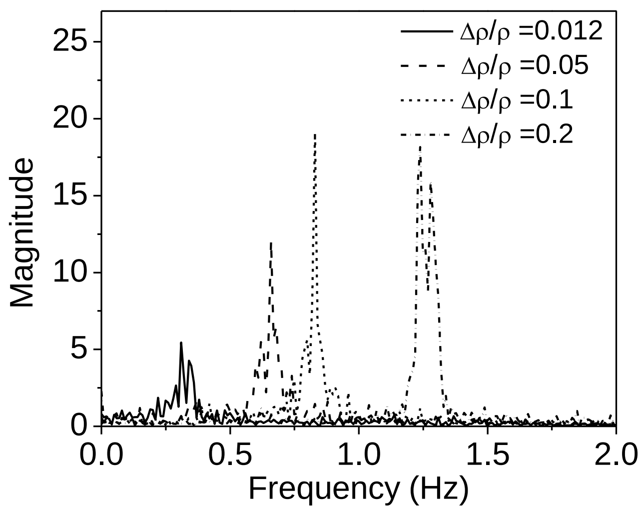

Figure 3.14: FFT analysis results for L/D = 0.1

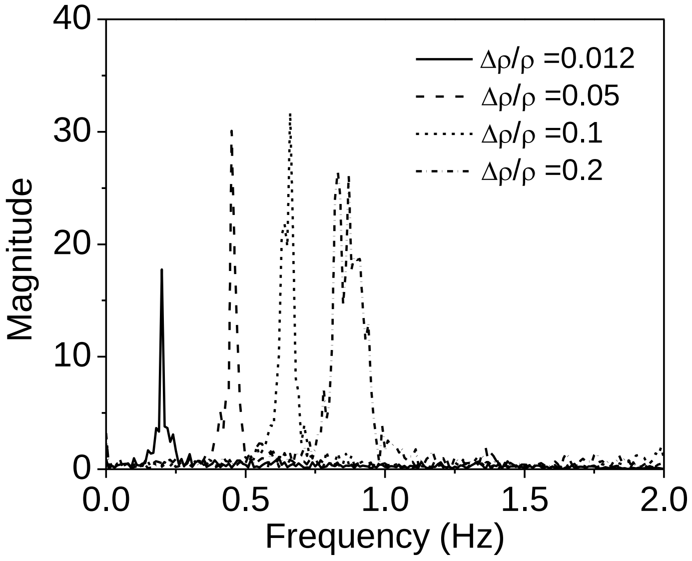

Figure 3.15: FFT analysis results for L/D = 0.3

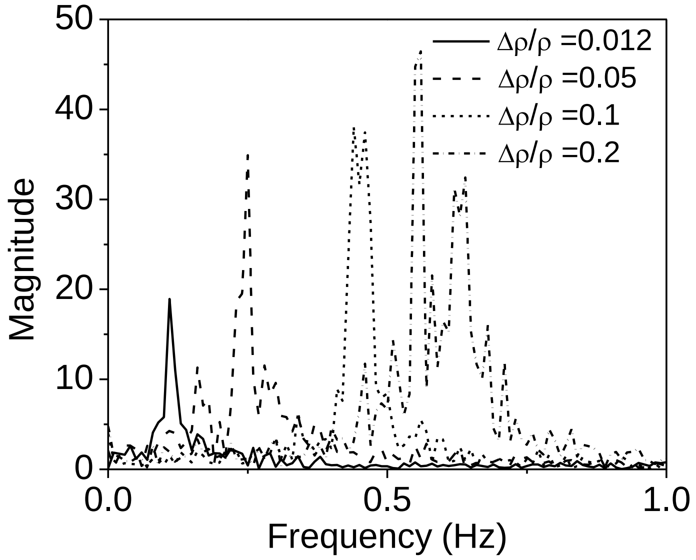

Figure 3.16: FFT analysis results for L/D = 0.6

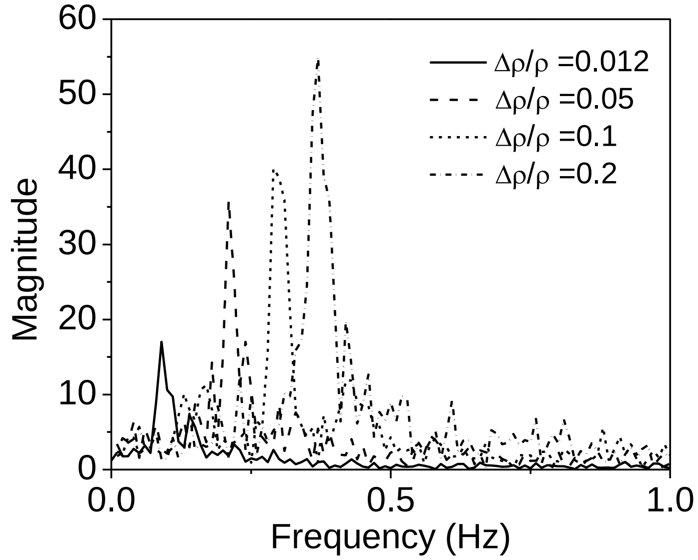

Figure 3.17: FFT analysis results for L/D = 0.9

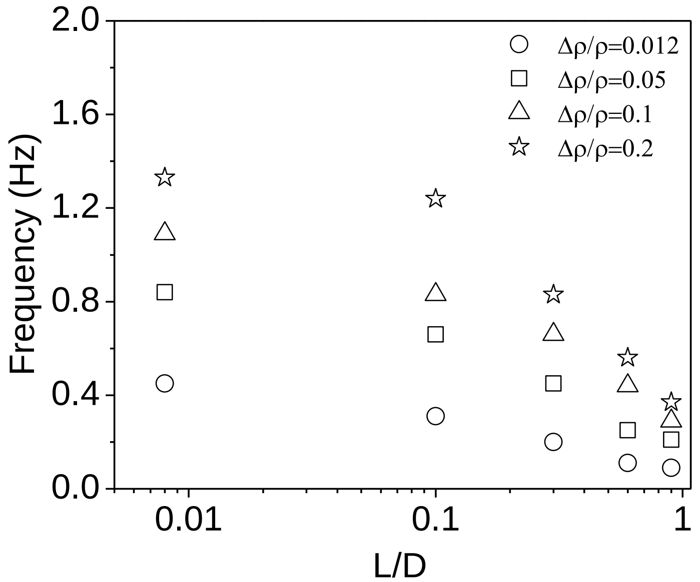

Figure 3.18: Pulsation frequency for all the cases

Flow Pattern:

The non-dimensional density contours in both the compartments at different times for L/D = 0.008 and $\Delta\rho_0 / \rho_{L,0}$ = 0.012 are shown in Fig. 3.19. The evolution of flow with time is explained by this figure. Blob of salt water formed move in both the compartment, vortices are formed near the opening edge and generate turbulence, which results in free jet in both the compartments. The velocity vectors shown in Fig. 3.20 depict the free jet in both the compartments. The zoomed vectors are also shown in that figure; these velocity vectors near the opening keep on changing with time as the flow is oscillatory. The lighter jet moves up to free surface of upper compartment and spreads. Similarly, the downward jet impinges on bottom wall on lower compartment. Stable stratification is formed in both the compartments. The stratification is clearly visible in density contours. A complete cycle of oscillation is shown in Fig. 3.21, which shows that the vortex formed near opening edge moves in upper and lower compartment alternatively. The normalised mass fraction contours for a fixed L/D=0.008 and different density ratio are shown in Fig. 3.22 at a time of 200 s from initiation of the flow. The normalised mass fraction contours for a fixed density ratio 0.1 and different L/D are shown in Fig. 3.23 at a time of 200 s from initiation of the flow.

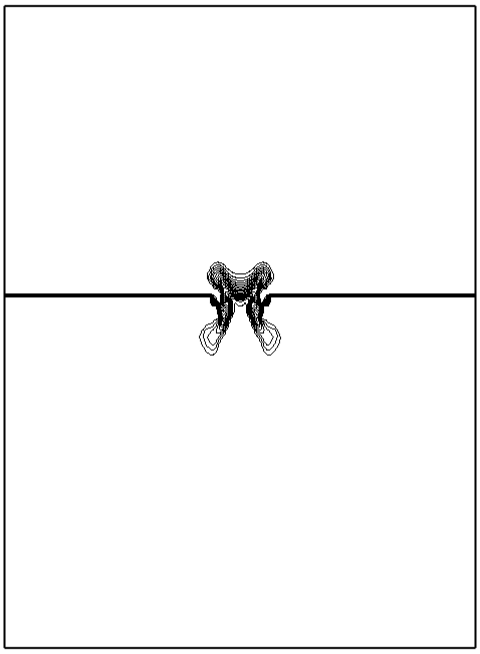

(a) 2 second

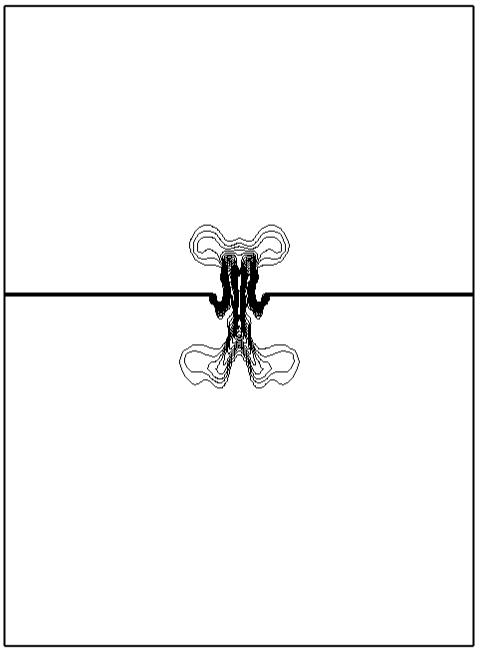

(b) 3 second

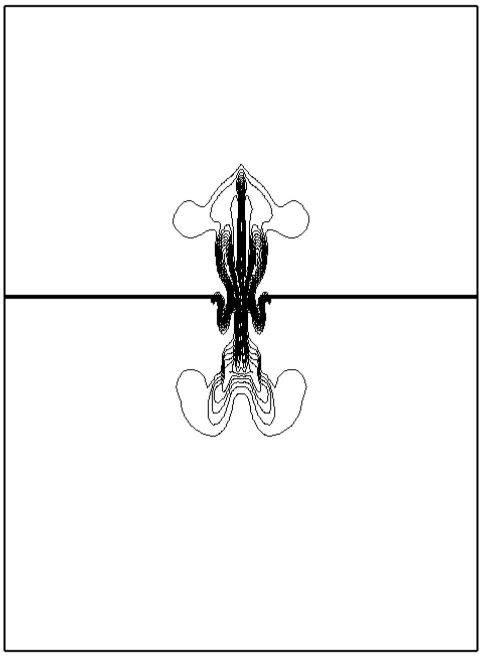

(c) 4 second

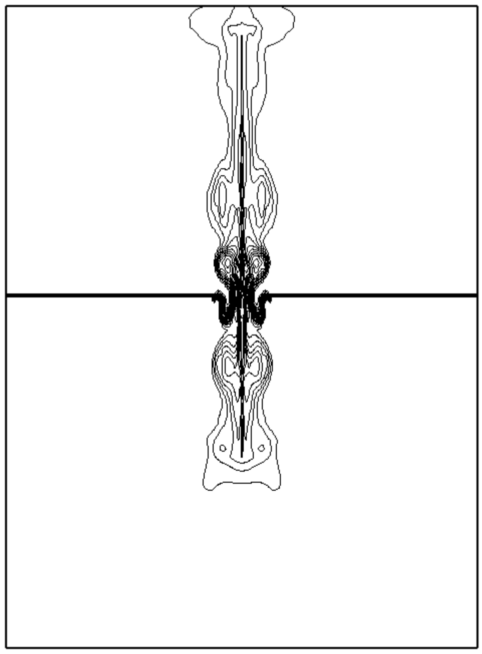

(d) 9 second

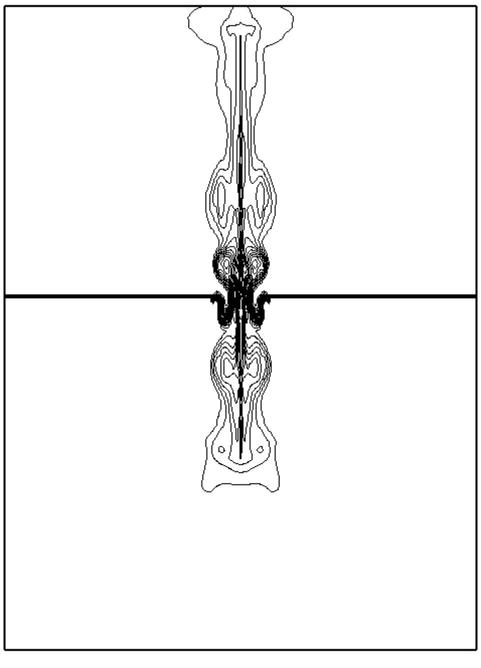

(e) 20 second

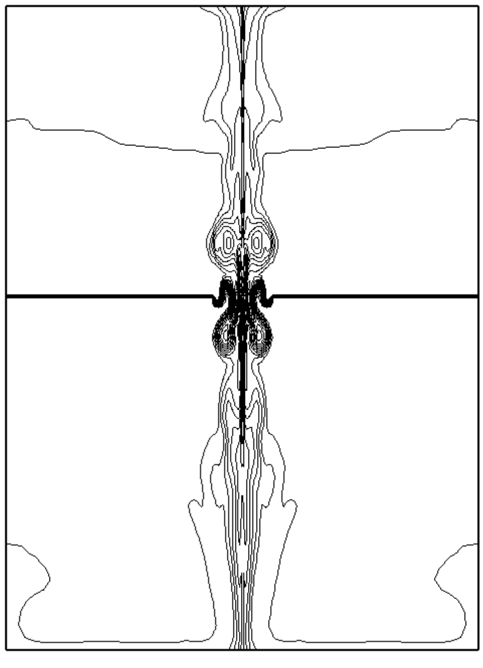

(f) 50 second

Figure 3.19: Non-dimensional density contour at different time for L/D=0.008

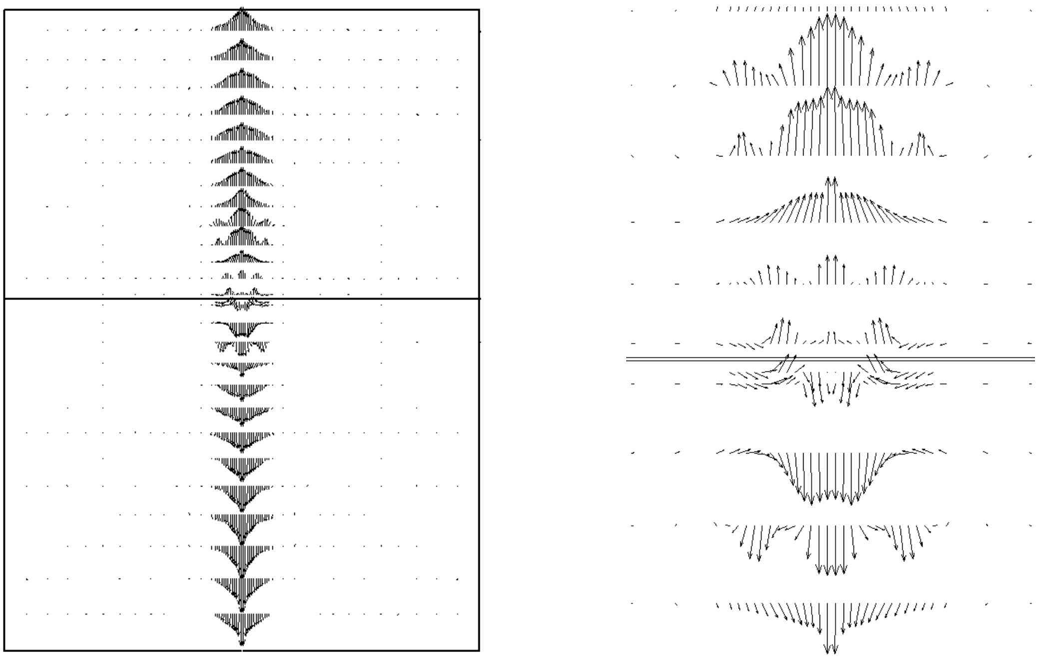

(a) Instantaneous vectors (b) Zoomed view

Figure 3.20: Instantaneous vectors and zoomed view near opening for L/D=0.008

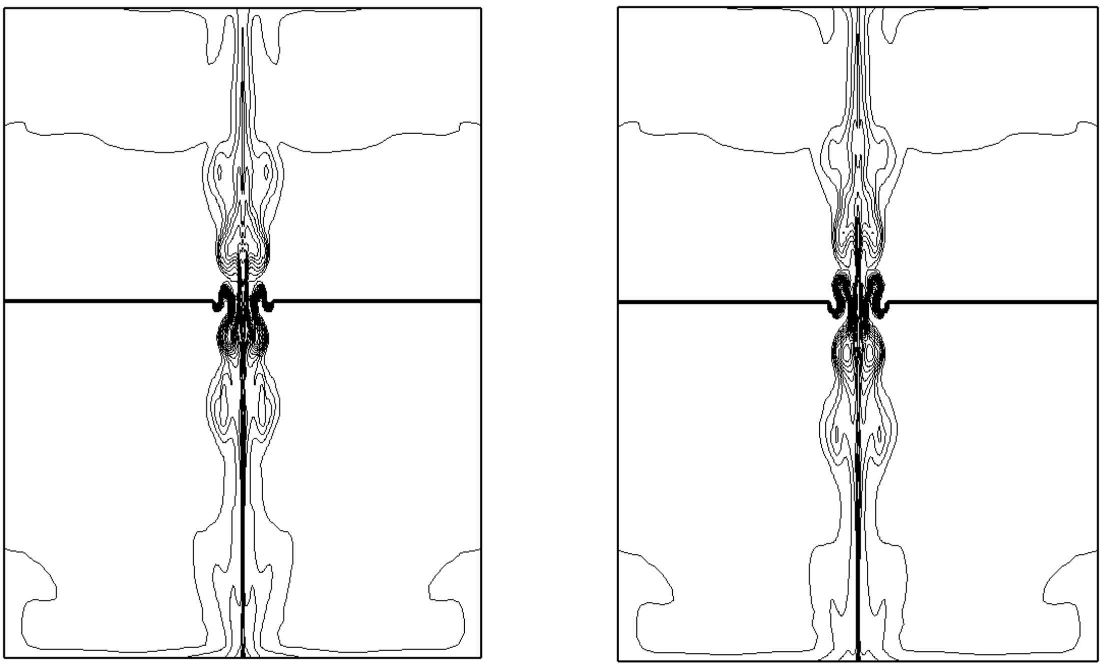

(a) 50.8 second (b) 51.0 second

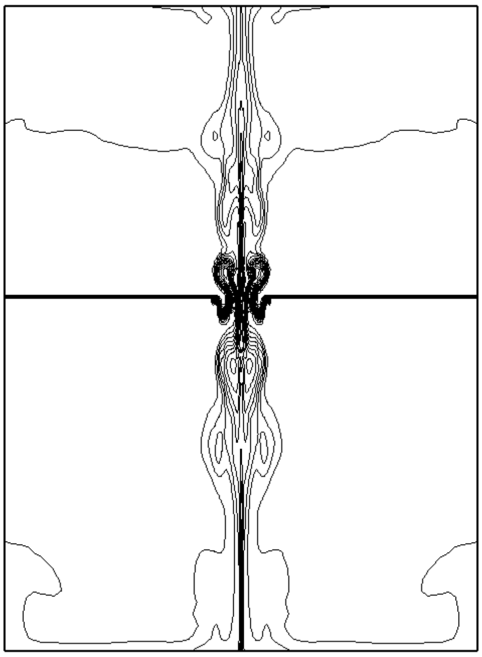

(c) 51.2 second

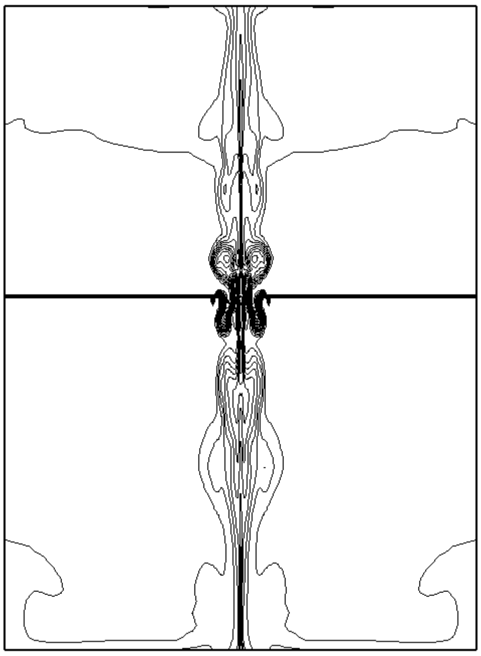

(d) 51.4 second

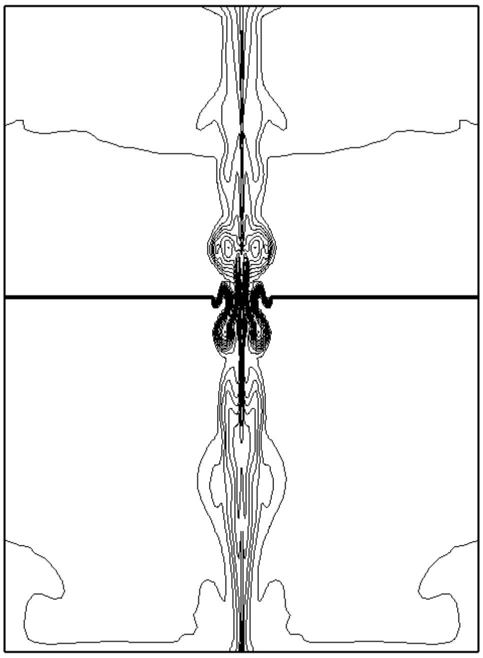

(e) 51.6 second

Figure 3.21: Non-dimensional density contour for complete oscillation cycle for L/D=0.008

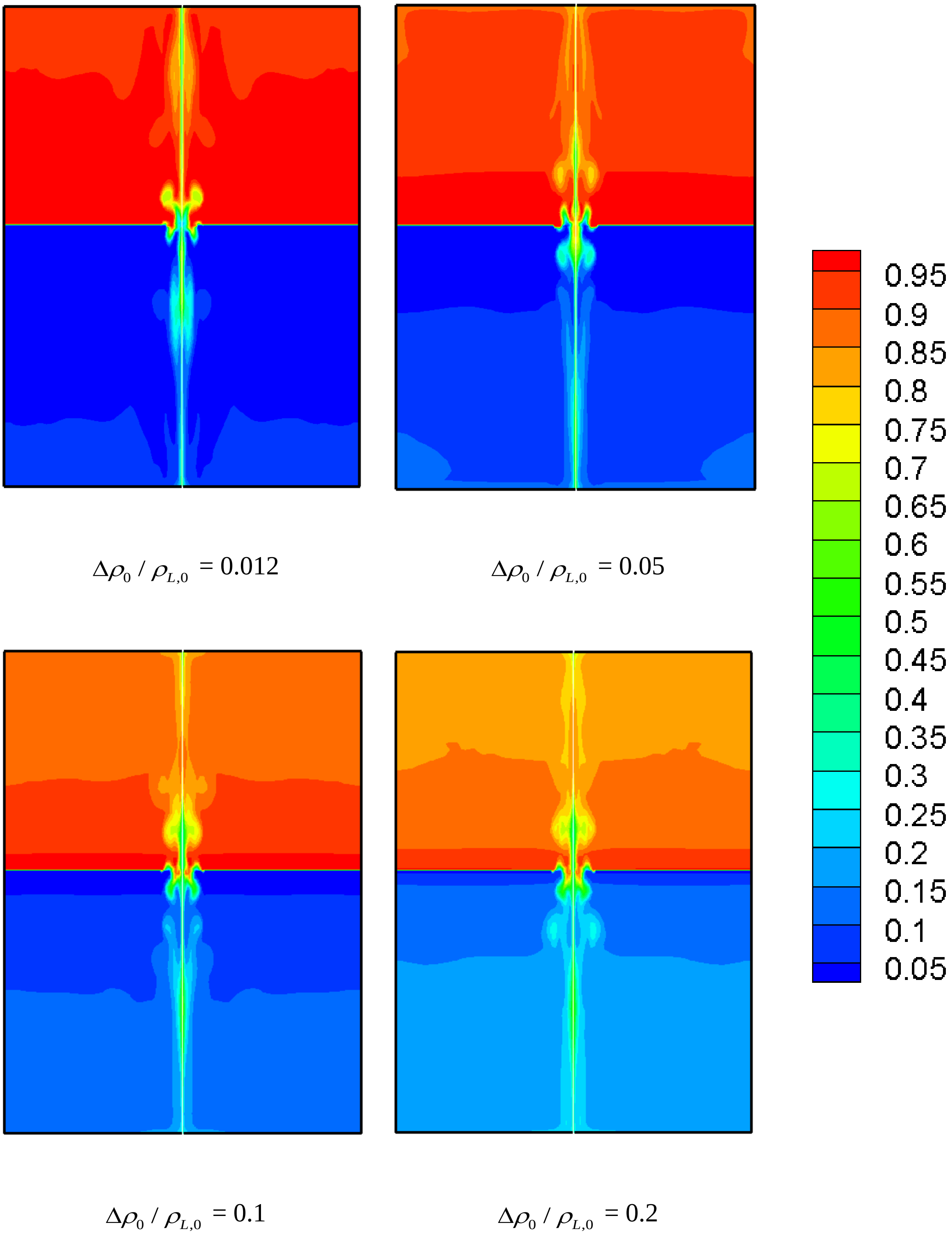

Figure 3.22: Normalised mass fraction for L/D=0.008 at 200 s

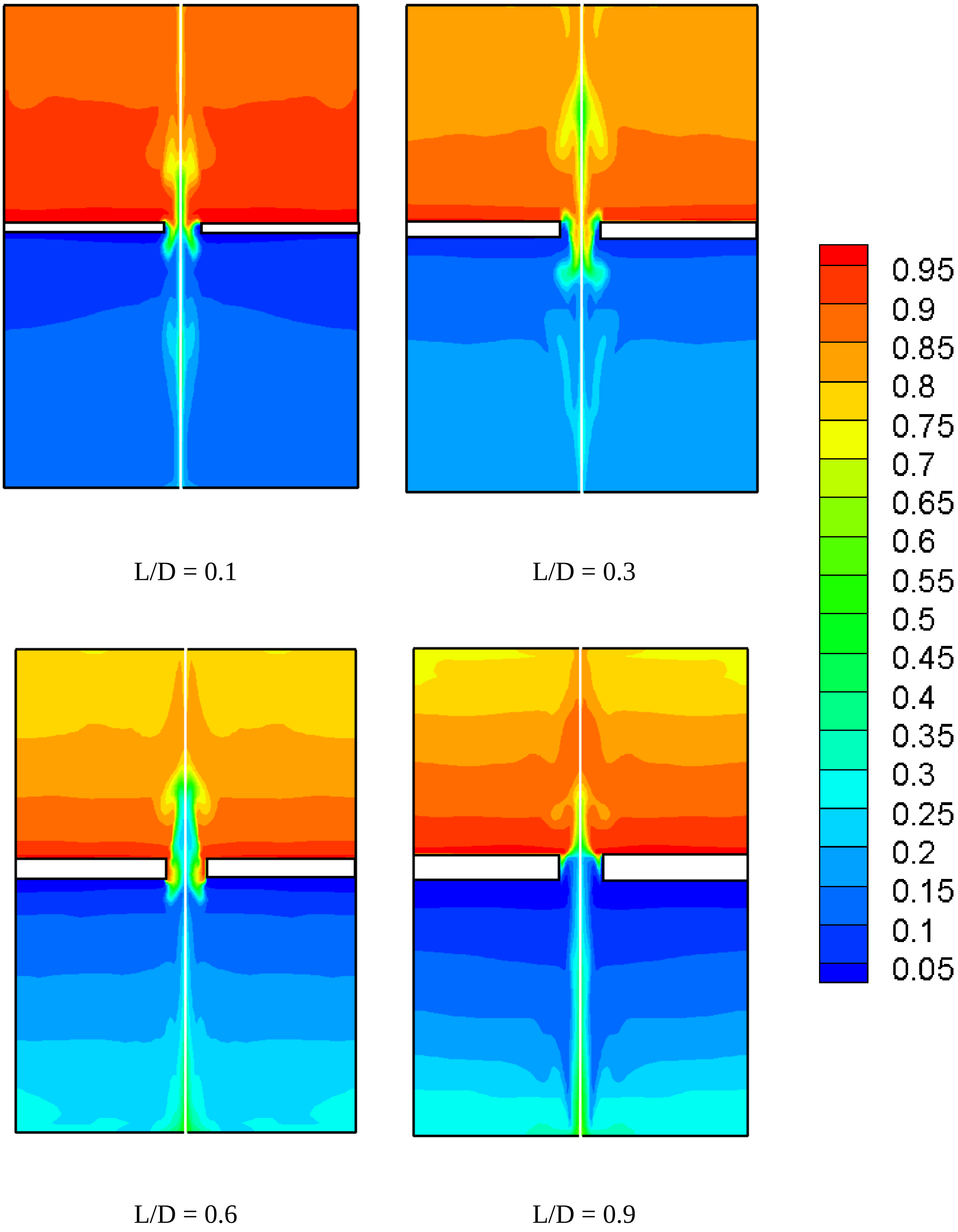

Figure 3.23: Normalised mass fraction for $\Delta\rho_0 / \rho_{L,0}$=0.1 at 200 s

Correlations based on CFD Simulation Data:

The following correlation was developed to predict the frequency (f) or Strouhal number (St) for a given value of density ratio ($\Delta\rho_0 / \rho_{L,0}$) and opening aspect ratio (L/D) within a reasonable accuracy, i.e.,

$$f = 1.103\left(\Delta\rho_0/\rho_{L,0}\right)^{0.5}\left(L/D\right)^{-0.279} \quad \textbf{(3.17)}$$

$$St = 0.079\left(L/D\right)^{-0.279} \quad \textbf{(3.18)}$$

Chao and Gao (2009) have also shown that frequency of oscillation is proportional to square root of fire strength (heat release rate) similar to that shown in above equation 3.28. This is also consistent with Kerrison et al. (1998) for fire strength lying between 3.6 and 5.6 kW. Thus the density ratio in salt water fresh water system represents the temperature difference generated by fire source.

3.7. Closure

2D axisymmetric CFD simulations for oscillatory exchange flow through opening in horizontal partition were carried out. Turbulent flows along with oscillations in the flow were observed in all the cases. Effect of density ratio on flow coefficient is less significant as normalised density and non-dimensional time for a given aspect ratio was approximately the same. The flow coefficient was maximum at L/D 0.6. Pulsation frequency increases with increase in $\Delta\rho_0 / \rho_{L,0}$. The effect of $\Delta\rho_0 / \rho_{L,0}$ is significant on axial velocity and pulsation frequency. Oscillatory frequency is proportional to square root of density ratio. The velocity magnitude also increases with increase in L/D but pulsation frequency decreases with increase in L/D.

CHAPTER 4: SIMULATION OF GRAVITY CURRENTS RELATED TO BACKDRAFT FOR VARIOUS COMPARTMENT ASPECT RATIOS

4.1. Introduction

Backdrafts are developed from an enclosure due to combustion of heated unburnt fuel (remaining due to oxygen starvation) with fresh air if any large opening is suddenly pushed opened. This situation will happen in an under ventilated enclosure having large inventory of unburnt combustibles. If any opening is suddenly pushed opened, fresh air enters and rapid deflagration may occur. The deflagration moving through the building and out of the opening is a backdraft. Backdraft is a hazard and can become dangerous to people specially fire-fighters (Fleischmann, 1994). Due to density difference across opening, shear flow occurs where heavier fluid from outside the compartment travels underneath the lighter fluid. This fluid flow is known as gravity current and is mainly responsible for mixing between high temperature unburnt fuel and fresh air. Gravity currents are generated due to density difference in horizontal direction arising from difference in temperature or/and concentration in fluid systems. A sound knowledge of gravity currents can help in explaining the backdraft phenomena. The consideration of air/smoke movement during fire through doors and windows requires an understanding of buoyancy driven fluid motion through vertical vents connecting different rooms in a building. Most of the studies have used salt water lab scale set up to explain the physics of gravity currents. The concept of using scaled salt water models to investigate gas and smoke flows was first formally documented by Steckler et al. (1986). Since then, the use of salt water modelling in the fire research community has continuously been significant.

In large number of gravity current studies the length of the floor over which gravity current travel is large (Baum et al., 1994, Mcgrattan et al., 1994, Rehm et al., 1994). In this scenario, the non-dimensional velocity of gravity current follows closely the perfect fluid theory $\left(v^{*}=0.5\right)$. However, gravity current related to backdraft may not travel a long distance. Backdrafts commonly occur in residential and industrial locations, where enclosure length to height ratio is not large. Main studies on gravity current in compartments have been performed for compartment ratio of two (Fleischmann et al., 1994) and four (Weng el al., 2002) respectively.

In this chapter transient simulation of gravity currents related to backdrafts has been simulated using 3D CFD in-house code using salt water analogy. Influence of compartment aspect ratio (L/H) as well as opening geometry on the time required for gravity current to touch the rear wall from initiation has been computed over the range 1 ≤ L/H ≤ 5 and 0.005 ≤ $\Delta\rho_0 / \rho_{L,0}$ ≤ 0.1. Six different openings, i.e., full, middle slot, top slot, bottom slot, window and door have been considered. Froude number for all the cases is calculated. Salt water analogy modelling is an effective diagnostic, predictive and scaling tool for understanding such complex flows through ceiling opening using the PIV and PLIF techniques. Hence salt water/fresh water has been considered as working fluids in present numerical work. Salt water modelling has limitations in terms of exact representation of Schmidt and Prandtl number of water and gases; non-modelling of heat transfer to wall during gas flow and creations of large density differences. In salt water modelling, Boussinesq assumption is made, which assumes that variations in fluid properties (viscosity, thermal diffusivity and mass diffusivity), except density, are completely ignored and that density variations are only included in terms involving gravity. This assumption is justified when the density difference between fluids is small (density differences less than approximately 10% (Shin et al., 2004)), which is relevant for some, but not all, backdraft gravity currents (McBryde, 2008). The scaling of gravity currents for salt water modelling is described by Fleischmann et al. (1994) where characteristic length, velocity and time scale are as follows:

$$X_C = H \tag{4.1}$$

$$V_C = \sqrt{\beta g H} \tag{4.2}$$

$$t_C = \sqrt{H/\beta g} \tag{4.3}$$

The dimensional variables have been non-dimensionalised using their corresponding characteristic variable. To maintain the Boussinesq approximation, all simulations were restricted to $\beta \leq 0.1$.

4.2. Problem Description

The computational domain was selected based on experimental facility of Fleischmann et al. (1994). The height (H) and width of small compartment was kept same as 0.15 m and length of compartment (L_C) was varied depending on the aspect ratio. The small compartment was placed in large compartment of size $2L_C$ X 0.3 m X 0.45 m. A typical computational domain is shown in Fig. 4.1 for aspect ratio 2. Both the compartments are connected by a vertical opening, different types of opening considered in present analysis are shown in Fig. 4.2.

Initial density difference was created between two chambers. The large compartment was initially filled with fresh water while the small compartment was initially filled with fresh water. The code was validated against reported experiments of Fleischmann et al. (1994) and Weng et al. (2002) for compartment ratio of two and four respectively. The dimensionless velocity (Froude number) has been determined for all cases. Various cases were studied by varying the normalised density difference from 0.005 to 0.1 with different opening and compartment aspect ratio was varied from 1 to 5.

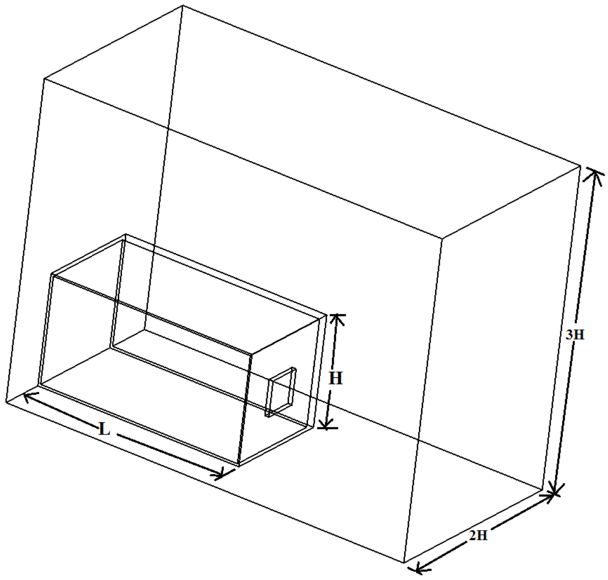

Figure 4.1: Geometric configuration for CFD computation

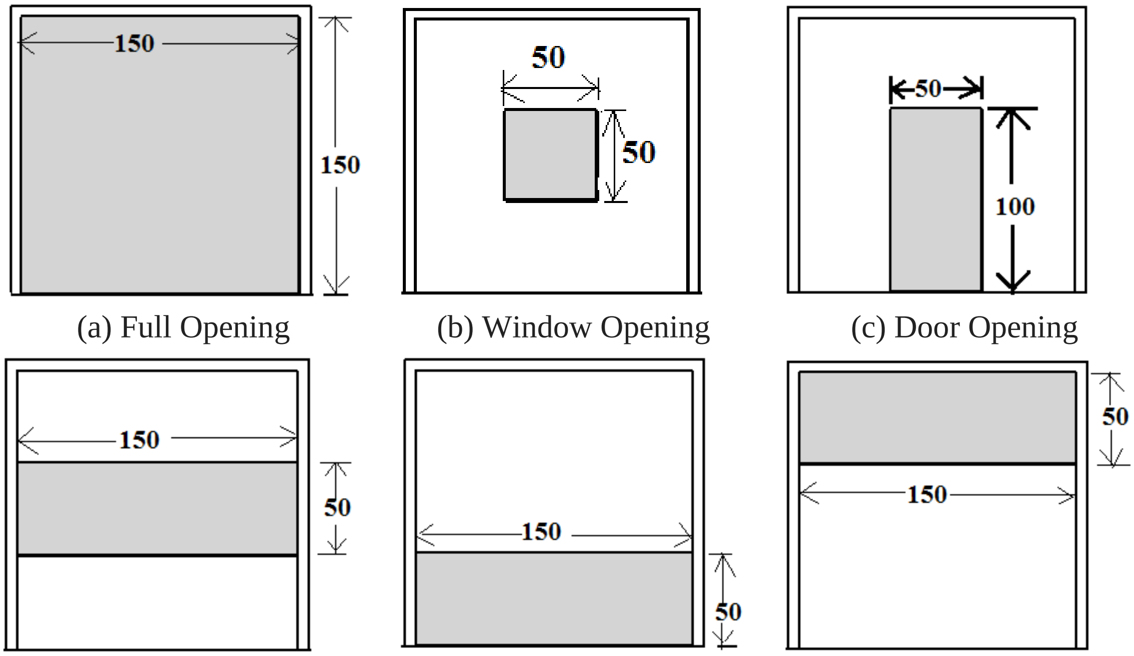

(a) Full Opening
(b) Window Opening
(c) Door Opening
(d) Middle Slot Opening (M-Slot)
(e) Downside/Bottom Slot Opening (B-Slot)
(f) Upside/Top Slot Opening (T-Slot)

Figure 4.2: Different opening configuration

4.3. Numerical Modelling

Dynamic LES based 3D transient simulations were performed to characterise the flow behaviour of gravity current in enclosures. The 3D, incompressible, filtered unsteady momentum, continuity, species, and SGS kinetic energy were solved. In-house CFD code was developed based on pressure based SIMPLE algorithm. Third order QUICK scheme was employed for convective terms to capture the gravity current and second order central differencing was employed for diffusive term. The time discretization was done using second order Crank-Nicolson method. In LES, the Navier–Stokes equations of incompressible flow are filtered using a spatial filter and governing equations are as follows:

$$\frac{\partial \bar{u}_i}{\partial x_i} = 0 \tag{4.4}$$

$$\frac{\partial \bar{u}_i}{\partial t} + \frac{\partial \bar{u}_i \bar{u}_j}{\partial x_j} = -\frac{\partial \bar{p}}{\partial x_i} + \nu \frac{\partial^2 \bar{u}_i}{\partial x_j \partial x_j} - \frac{\partial \tau_{ij}}{\partial x_j} \tag{4.5}$$

The SGS stress tensor is defined as

$$\tau_{ij} = \overline{u_i u_j} - \bar{u}_i \bar{u}_j \tag{4.6}$$

The SGS stress tensor can be decomposed into three parts, the Leonard term L_{ij} , the cross term C_{ij} and the SGS Reynolds stress term R_{ij} .

In one equation model or sub-grid kinetic energy model, the SGS stress is modelled as:

$$\tau_{ij} \approx \frac{2}{3} k_{sgs} \delta_{ij} - 2\nu_t \bar{S}_{ij}$$

(4.7)

Where $S_{ij} = \frac{1}{2}\left(\frac{\partial \bar{u}_i}{\partial x_j} + \frac{\partial \bar{u}_j}{\partial x_i}\right)$ and $k_{sgs} = \frac{1}{2}\left(\overline{u_k u_k} - \bar{u}_k \bar{u}_k\right)$ is the SGS kinetic energy. The SGS eddy viscosity is modelled as: $\nu_t = C_d \sqrt{k_{sgs}} \Delta$. k_{sgs} is obtained by solving the following transport equation:

$$\frac{\partial k_{sgs}}{\partial t} + \bar{u}_j \frac{\partial k_{sgs}}{\partial x_j} = -\tau_{ij} \frac{\partial \bar{u}_i}{\partial x_j} - C_\varepsilon \frac{k_{sgs}^{1.5}}{\Delta} + \frac{\partial}{\partial x_j}\left[\left(\frac{\nu_t}{\sigma_k} + \nu\right)\frac{\partial k_{sgs}}{\partial x_j}\right]$$

(4.8)

Right-hand side of Eq. (4.8) represents the production, dissipation, and diffusion of the SGS kinetic energy respectively. Through this one-equation approach, the KEM improves the accuracy of SGS stress modelling when compared to other eddy-viscosity models (Menon, and Rizk, 1996). In the dynamic approach, the constant C_d and C_ε are evaluated dynamically as mentioned below:

$$C_d = \frac{1}{2} \frac{L_{ij} \sigma_{ij}}{\sigma_{kl} \sigma_{kl}}$$

(4.9)

$$\sigma_{ij} = -\tilde{\Delta} k_{test}^{1/2} \tilde{S}_{ij}$$

(4.10)

$$L_{ij} = \widetilde{\bar{u}_i \bar{u}_j} - \tilde{\bar{u}}_i \tilde{\bar{u}}_j$$

(4.11)

$$k_{test} = \frac{1}{2} L_{ii}$$

(4.12)

$$C_\varepsilon = \frac{\tilde{\Delta}}{k_{test}^{3/2}}\left(\nu+\nu_t\right)\left(\frac{\partial \overline{u}_i}{\partial x_j}\frac{\partial \overline{u}_i}{\partial x_j}-\frac{\partial \tilde{\overline{u}}_i}{\partial x_j}\frac{\partial \tilde{\overline{u}}_i}{\partial x_j}\right) \tag{4.13}$$

$$L_{ij} = -\frac{\tilde{\Delta}^2}{12}\frac{\partial \overline{u}_i}{\partial x_k}\frac{\partial \overline{u}_j}{\partial x_k} \tag{4.14}$$

$$C_d = \frac{1}{2}\frac{L_{ij}\sigma_{ij}}{\sigma_{kl}\sigma_{kl}} = 0.5*\left(\begin{array}{l}
\frac{L_{11}\sigma_{11}}{\sigma_{11}\sigma_{11}}+\frac{L_{11}\sigma_{11}}{\sigma_{12}\sigma_{12}}+\frac{L_{11}\sigma_{11}}{\sigma_{13}\sigma_{13}}+\frac{L_{11}\sigma_{11}}{\sigma_{21}\sigma_{21}}+\frac{L_{11}\sigma_{11}}{\sigma_{22}\sigma_{22}}+\frac{L_{11}\sigma_{11}}{\sigma_{23}\sigma_{23}}+\frac{L_{11}\sigma_{11}}{\sigma_{31}\sigma_{31}}+\frac{L_{11}\sigma_{11}}{\sigma_{32}\sigma_{32}}+\frac{L_{11}\sigma_{11}}{\sigma_{33}\sigma_{33}} \\
+\frac{L_{12}\sigma_{12}}{\sigma_{11}\sigma_{11}}+\frac{L_{12}\sigma_{12}}{\sigma_{12}\sigma_{12}}+\frac{L_{12}\sigma_{12}}{\sigma_{13}\sigma_{13}}+\frac{L_{12}\sigma_{12}}{\sigma_{21}\sigma_{21}}+\frac{L_{12}\sigma_{12}}{\sigma_{22}\sigma_{22}}+\frac{L_{12}\sigma_{12}}{\sigma_{23}\sigma_{23}}+\frac{L_{12}\sigma_{12}}{\sigma_{31}\sigma_{31}}+\frac{L_{12}\sigma_{12}}{\sigma_{32}\sigma_{32}}+\frac{L_{12}\sigma_{12}}{\sigma_{33}\sigma_{33}} \\
+\frac{L_{13}\sigma_{13}}{\sigma_{11}\sigma_{11}}+\frac{L_{13}\sigma_{13}}{\sigma_{12}\sigma_{12}}+\frac{L_{13}\sigma_{13}}{\sigma_{13}\sigma_{13}}+\frac{L_{13}\sigma_{13}}{\sigma_{21}\sigma_{21}}+\frac{L_{13}\sigma_{13}}{\sigma_{22}\sigma_{22}}+\frac{L_{13}\sigma_{13}}{\sigma_{23}\sigma_{23}}+\frac{L_{13}\sigma_{13}}{\sigma_{31}\sigma_{31}}+\frac{L_{13}\sigma_{13}}{\sigma_{32}\sigma_{32}}+\frac{L_{13}\sigma_{13}}{\sigma_{33}\sigma_{33}} \\
+\frac{L_{21}\sigma_{21}}{\sigma_{11}\sigma_{11}}+\frac{L_{21}\sigma_{21}}{\sigma_{12}\sigma_{12}}+\frac{L_{21}\sigma_{21}}{\sigma_{13}\sigma_{13}}+\frac{L_{21}\sigma_{21}}{\sigma_{21}\sigma_{21}}+\frac{L_{21}\sigma_{21}}{\sigma_{22}\sigma_{22}}+\frac{L_{21}\sigma_{21}}{\sigma_{23}\sigma_{23}}+\frac{L_{21}\sigma_{21}}{\sigma_{31}\sigma_{31}}+\frac{L_{21}\sigma_{21}}{\sigma_{32}\sigma_{32}}+\frac{L_{21}\sigma_{21}}{\sigma_{33}\sigma_{33}} \\
+\frac{L_{22}\sigma_{22}}{\sigma_{11}\sigma_{11}}+\frac{L_{22}\sigma_{22}}{\sigma_{12}\sigma_{12}}+\frac{L_{22}\sigma_{22}}{\sigma_{13}\sigma_{13}}+\frac{L_{22}\sigma_{22}}{\sigma_{21}\sigma_{21}}+\frac{L_{22}\sigma_{22}}{\sigma_{22}\sigma_{22}}+\frac{L_{22}\sigma_{22}}{\sigma_{23}\sigma_{23}}+\frac{L_{22}\sigma_{22}}{\sigma_{31}\sigma_{31}}+\frac{L_{22}\sigma_{22}}{\sigma_{32}\sigma_{32}}+\frac{L_{22}\sigma_{22}}{\sigma_{33}\sigma_{33}} \\
+\frac{L_{23}\sigma_{23}}{\sigma_{11}\sigma_{11}}+\frac{L_{23}\sigma_{23}}{\sigma_{12}\sigma_{12}}+\frac{L_{23}\sigma_{23}}{\sigma_{13}\sigma_{13}}+\frac{L_{23}\sigma_{23}}{\sigma_{21}\sigma_{21}}+\frac{L_{23}\sigma_{23}}{\sigma_{22}\sigma_{22}}+\frac{L_{23}\sigma_{23}}{\sigma_{23}\sigma_{23}}+\frac{L_{23}\sigma_{23}}{\sigma_{31}\sigma_{31}}+\frac{L_{23}\sigma_{23}}{\sigma_{32}\sigma_{32}}+\frac{L_{23}\sigma_{23}}{\sigma_{33}\sigma_{33}} \\
+\frac{L_{31}\sigma_{31}}{\sigma_{11}\sigma_{11}}+\frac{L_{31}\sigma_{31}}{\sigma_{12}\sigma_{12}}+\frac{L_{31}\sigma_{31}}{\sigma_{13}\sigma_{13}}+\frac{L_{31}\sigma_{31}}{\sigma_{21}\sigma_{21}}+\frac{L_{31}\sigma_{31}}{\sigma_{22}\sigma_{22}}+\frac{L_{31}\sigma_{31}}{\sigma_{23}\sigma_{23}}+\frac{L_{31}\sigma_{31}}{\sigma_{31}\sigma_{31}}+\frac{L_{31}\sigma_{31}}{\sigma_{32}\sigma_{32}}+\frac{L_{31}\sigma_{31}}{\sigma_{33}\sigma_{33}} \\
+\frac{L_{32}\sigma_{32}}{\sigma_{11}\sigma_{11}}+\frac{L_{32}\sigma_{32}}{\sigma_{12}\sigma_{12}}+\frac{L_{32}\sigma_{32}}{\sigma_{13}\sigma_{13}}+\frac{L_{32}\sigma_{32}}{\sigma_{21}\sigma_{21}}+\frac{L_{32}\sigma_{32}}{\sigma_{22}\sigma_{22}}+\frac{L_{32}\sigma_{32}}{\sigma_{23}\sigma_{23}}+\frac{L_{32}\sigma_{32}}{\sigma_{31}\sigma_{31}}+\frac{L_{32}\sigma_{32}}{\sigma_{32}\sigma_{32}}+\frac{L_{32}\sigma_{32}}{\sigma_{33}\sigma_{33}} \\
+\frac{L_{33}\sigma_{33}}{\sigma_{11}\sigma_{11}}+\frac{L_{33}\sigma_{33}}{\sigma_{12}\sigma_{12}}+\frac{L_{33}\sigma_{33}}{\sigma_{13}\sigma_{13}}+\frac{L_{33}\sigma_{33}}{\sigma_{21}\sigma_{21}}+\frac{L_{33}\sigma_{33}}{\sigma_{22}\sigma_{22}}+\frac{L_{33}\sigma_{33}}{\sigma_{23}\sigma_{23}}+\frac{L_{33}\sigma_{33}}{\sigma_{31}\sigma_{31}}+\frac{L_{33}\sigma_{33}}{\sigma_{32}\sigma_{32}}+\frac{L_{33}\sigma_{33}}{\sigma_{33}\sigma_{33}}
\end{array}\right) \tag{4.15}$$

Initially, the smaller inner compartment was filled with fresh water; hence mass fraction of salt was assigned as zero and in the outer compartment salt water mass fraction was assigned as per the required density of salt water solution using Eq. (3.8). The characteristic velocity is $V_C = \sqrt{\beta g H}$ which is in the range of 0.121-0.54 m/s for the parameters considered. The flow is turbulent since it is free shear flow in all the cases. The initial velocity components were assigned zero values. All the walls and partition have been modelled as a no-slip impermeable wall. Staggered grid system was used in which scalar i.e. pressure, species mass fraction and turbulent quantities ware calculated at cell centre while fluid velocities were calculated at the cell faces. The set of algebraic equations were solved iteratively using

Gauss-Seidal method. For momentum equation under-relaxation value of 0.3 was used to have easy convergence. For species transport equation under-relaxation value of 1 was chosen. The solution was assumed as converged in each time step if mass residual was below 10^{-5}. To achieve the convergence maximum 50 internal iteration per time step were performed. For a single simulation on a Xeon machine, the computational time was approximately 72 hours for the full transient duration. Three different times step 0.01 s, 0.001 s and 0.0005 s were used to perform time step independence study. It was observed that the smaller time step gives nearly similar results. Hence time step of 0.001 s was used for final runs. Since the vertical interface between two fluids is unstable, flow initiates by itself even when the initial velocity components are zero.

4.4. Application of model

The results were evaluated in terms of non-dimensional velocity i.e. the Froude number for all the cases. The mixture density near the centre of left wall in small compartment was monitored at a point during simulation. This gives the value of time taken by gravity current (t_{in}) to reach the left wall. Average velocity of entering gravity current was computed by dividing the compartment length to the time taken by entering current $v = L / t_{in}$. This velocity was non-dimensionalised by characteristic velocity as defined by Equation (4.2). As the gravity current reached to leftmost centre point, a sharp increase in mixture density was observed. A typical density profile with time at the monitored point for compartment aspect ratio 3, β =0.1 and full opening is depicted in Fig. 4.3.

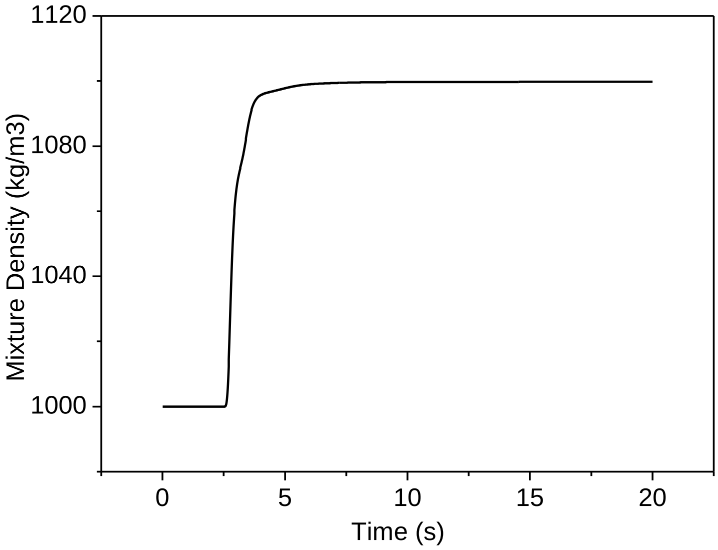

Figure 4.3: Mixture density at monitored point for AR=3, β =0.1 and full opening

Grid Independence Study:

First a grid independence study was done for all the compartments aspect ratio for window configuration as it has the highest flow gradient. A non-uniform grid in each direction was employed for mesh generation. The grids were finer in the inner compartment zone and coarser away from it. The inner compartment height (H) was resolved by 102 uniform grids as suggested by McBryde (2008) and total 200 grids were used in z-direction, grid size was fine near walls and coarser away from the walls. Four different grid sizes were tested to obtain the results which are independent of grid size. Non-dimensional velocity was computed for each grid size. The different grids used were 100 X 30 X 150, 100 X 30 X 200, 100 X 50 X 200 and 150 X 50 X 200 in x, y and z direction respectively for compartment aspect ratio of 2. The results of the grid independence study performed for the window opening for compartment aspect ratio of 2 used in the present work is depicted in Fig. 4.4. It clearly shows that the Froude number has more or less a constant value and attains a fix value if the grid size is refined further. From the Fig. 4.4 it was concluded that that a grid size 100 X 50 X 200 is sufficiently fine to obtain grid independent results for aspect ratio 2.

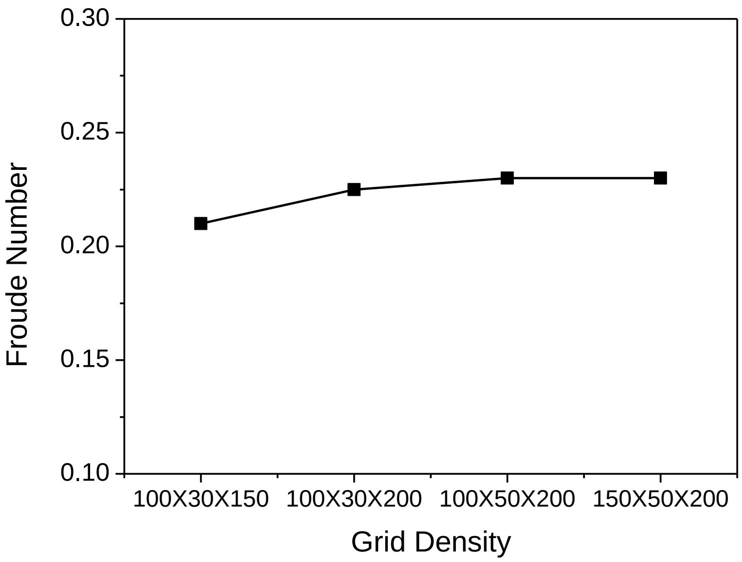

Figure 4.4: Grid independence results for AR=2, β =0.1 and window opening

Validation of Model:

The CFD code was validated with the available experimental results for compartment aspect ratio 2 (Fleischmann et al., 1994) and 4 (Weng et al., 2002). Figures 4.5 and 4.6 show the comparison of present numerical results with that of experiments from Fleischmann et al. (1994) and Weng et al. (2002) respectively. The numerical results are in good agreement (within 5%) with experimental data.

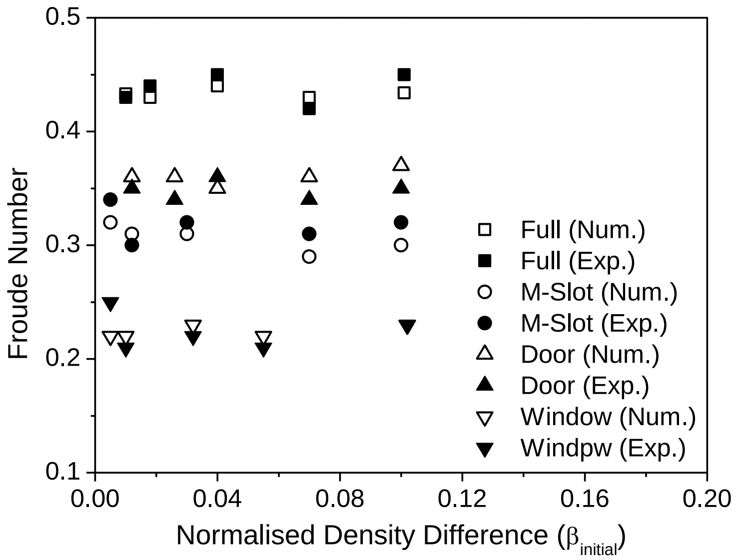

Figure 4.5: Comparison of numerically determined Fr with available data for AR=2

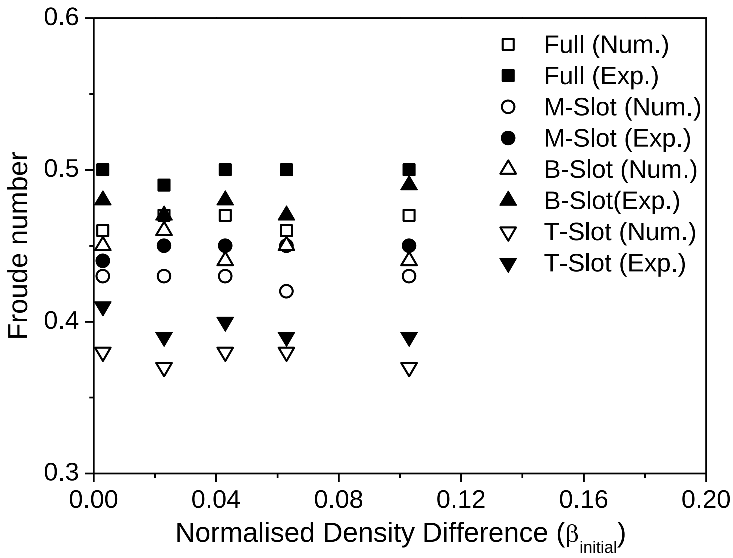

Figure 4.6: Comparison of numerically determined Fr with available data for AR=4

Evaluation of Froude Number:

The code was further utilised to predict the Froude Number for aspect ratio 1, 3 and 5 for all six opening geometries at five different levels of density differences. The Froude number for AR 1, 3 and 5 are shown in Figs. 4.7-4.9 respectively. It is observed that Froude number increases with aspect ratio for all the opening configurations. Froude number is the highest for full opening and lowest for window opening, since window opening possess highest resistance for salt water to flow inside the small compartment. It is observed that Froude number increases with increase in compartment aspect ratio for the entire opening configuration.

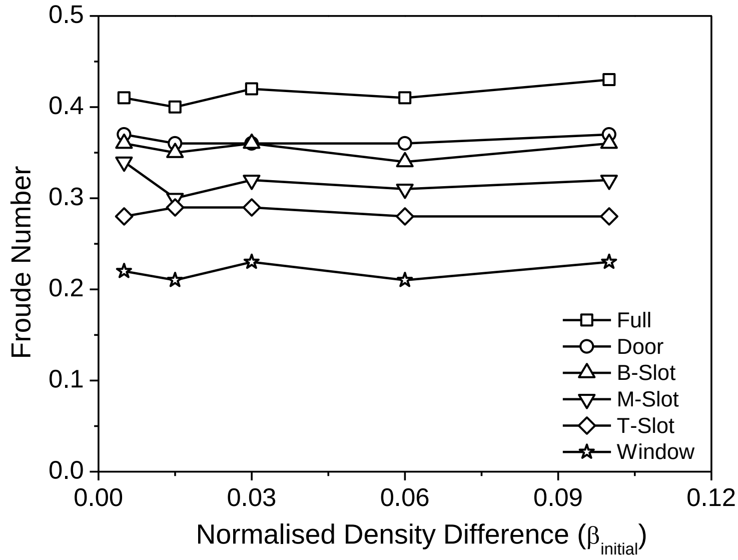

Figure 4.7: Computed Froude number for AR=1 for all opening configurations

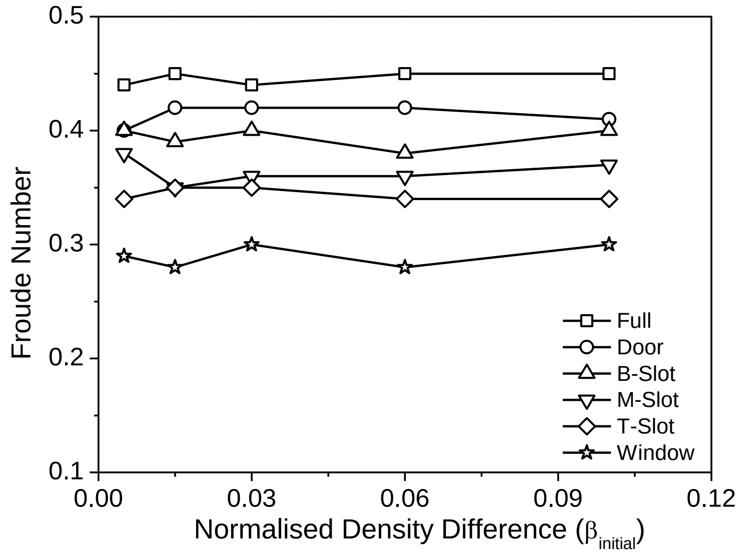

Figure 4.8: Computed Froude number for AR=3 for all opening configurations

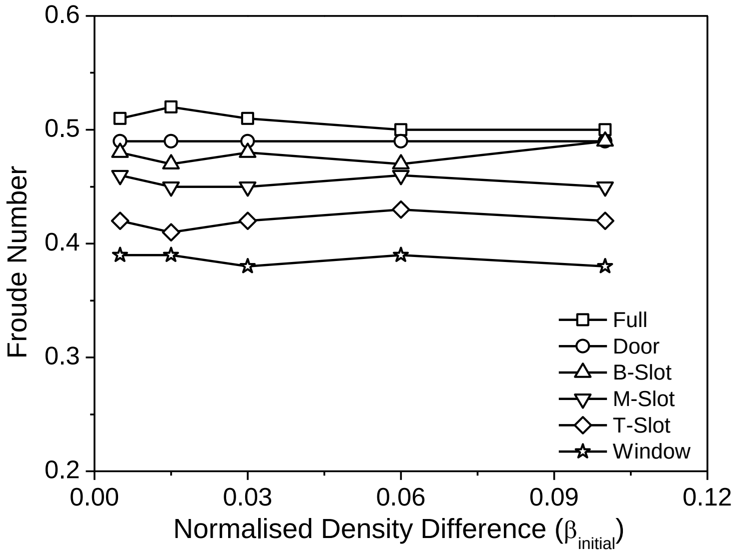

Figure 4.9: Computed Froude number for AR=5 for all opening configurations

Transient Behaviour of Gravity Current:

The transient behaviour of gravity current for AR=5, β=0.1 and full opening is shown in Fig. 4.10. As the gravity current enters, initial length of gravity current called as head, has higher height. Higher density fluid replaces the lower density fluid in the lower part of the inner compartment and lighter density fluid moves out of the inner compartment from the upper region of opening. The front of gravity current moves over lighter fluid and does not touch the bottom boundary. The front of gravity current (called as nose) is slightly above the bottom no slip wall, and a small quantity of lighter fluid is there below the nose. As gravity current touches the rear wall, it is reflected up, and then it travels towards the opening.

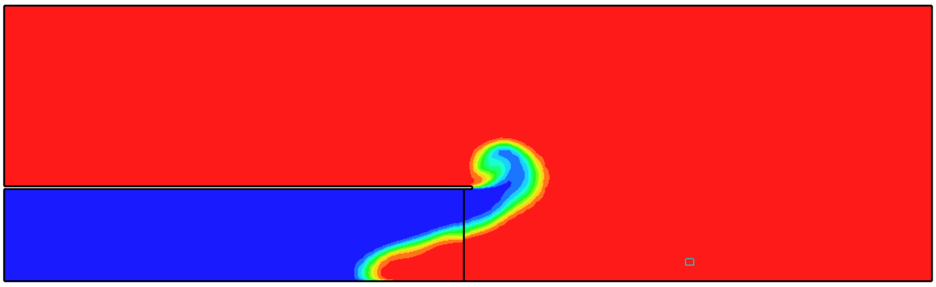

(a) 1 second

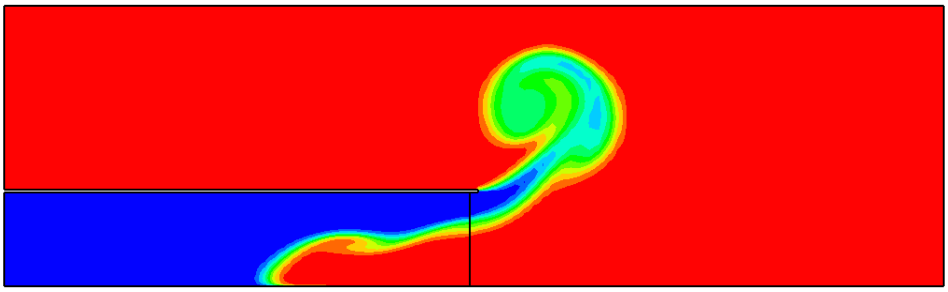

(b) 2 second

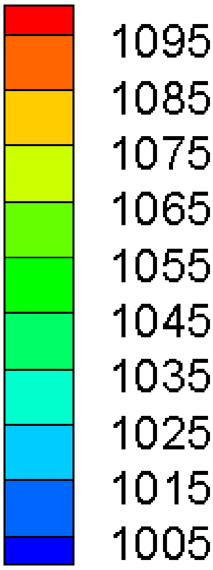

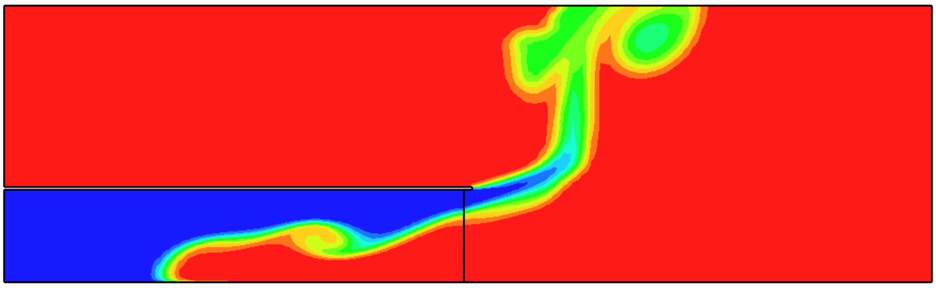

(c) 3 second

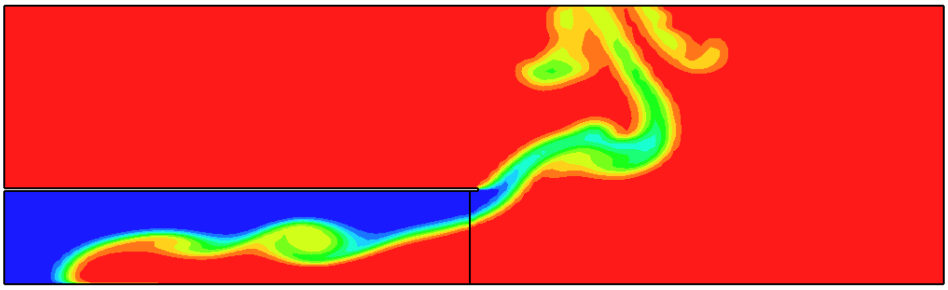

(d) 4 second

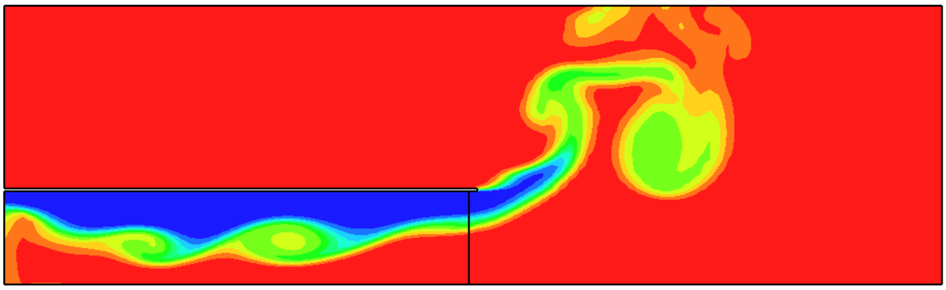

(e) 5 second

Figure 4.10: Transient behaviour of Gravity Current (Density contours) for AR=5, β =0.1 and full opening

The transient velocity of gravity current front is shown in Fig. 4.11; the gravity current decelerates as it moves into the inner compartment. During its movement of gravity current, shear flow occurs and vortices are formed at the interface of fresh water and salt water. Fig 4.12 shows the flow pattern of gravity current for AR=1, β =0.1 and full opening at 1 s.

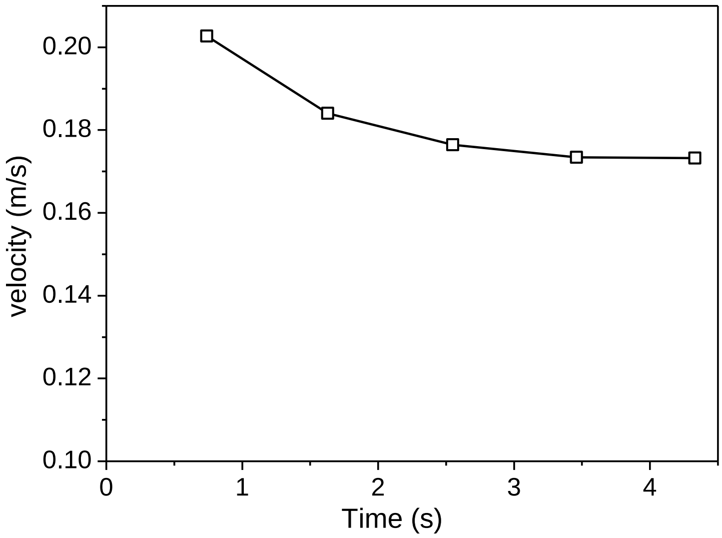

Figure 4.11: Transient velocity of gravity current front

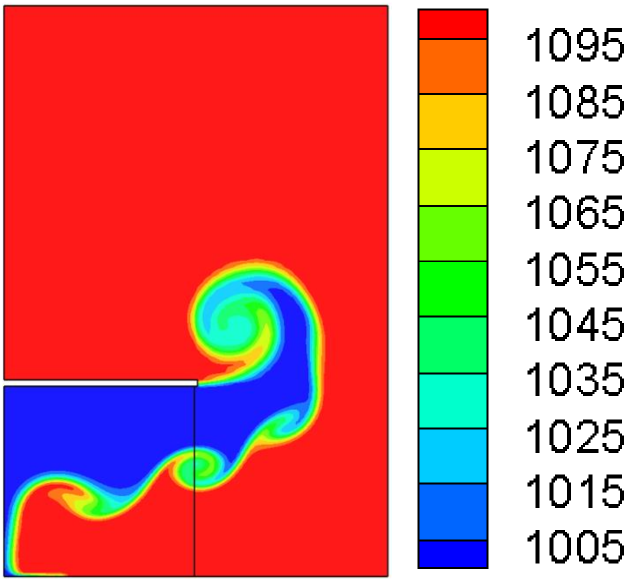

Figure 4.12: Density contour at 1 s for AR=1, β =0.1 and full opening

Effect of Compartment Aspect Ratio:

Fig. 4.13 shows the effect of compartment aspect ratio on gravity current (density contours at 2 s) for β =0.1 and M-slot opening. The initial structure of gravity current is similar for all the aspect ratios except for AR=1 at 2 seconds. As the aspect ratio is increased, time required to reach the rear wall is increased, however the basic structure of gravity current remains the same. The opening configuration has a strong influence on the gravity current structure. Figs. 4.14 and 4.15 show the effect of opening configuration on gravity current at 2 second for β =0.1 and AR=2 and 4 respectively. The figures are arranged in the sequence of increasing opening resistance.

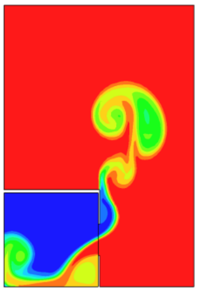

(a) AR=1

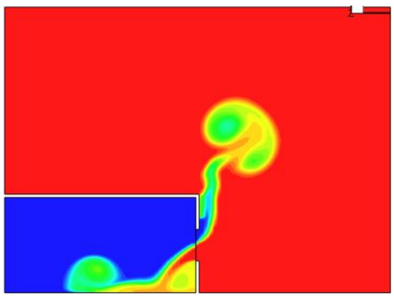

(b) AR=2

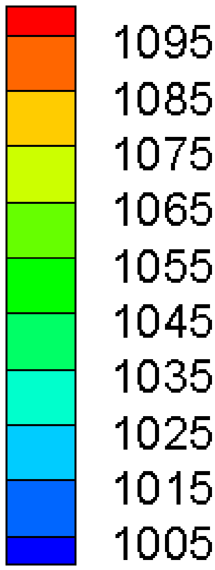

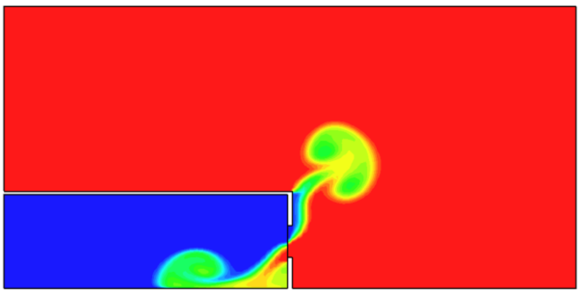

(c) AR=3

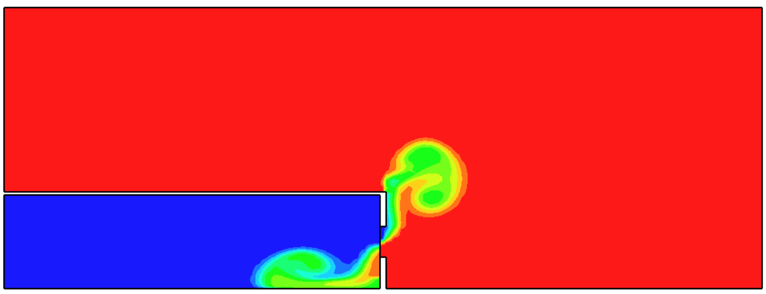

(d) AR=4

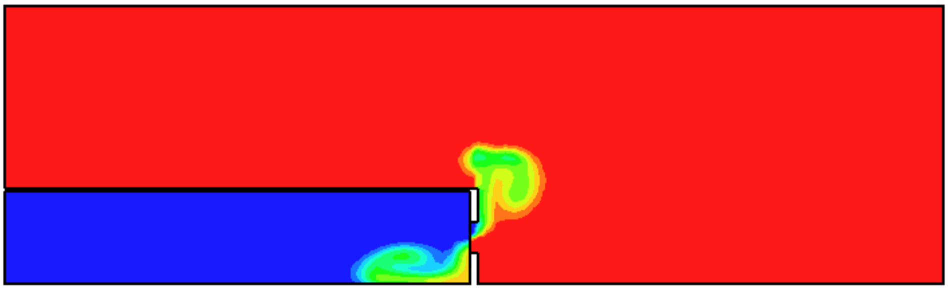

(e) AR=5

Figure 4.13: Effect of aspect ratio on gravity current (density contours at 2 s) for β =0.1 and M-slot opening

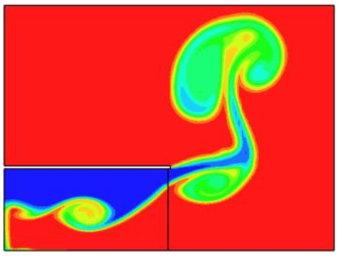

(a) Full Opening

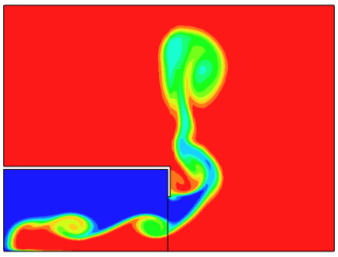

(b) Door Opening

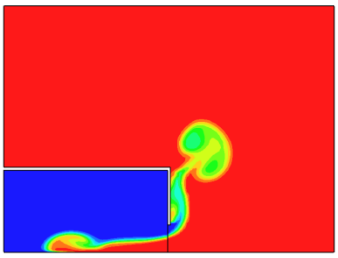

(c) B-slot opening

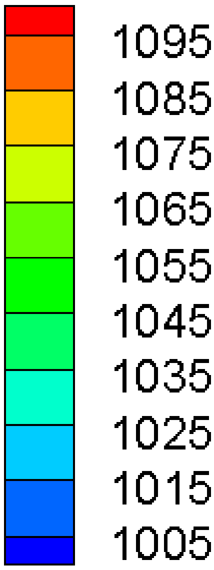

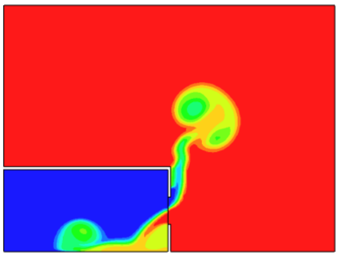

(d) M-slot opening

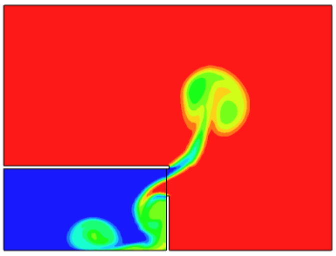

(e) T-slot opening

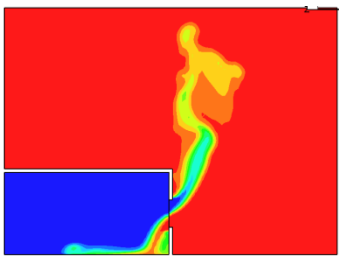

(f) Window opening

Figure 4.14: Effect of opening configuration on gravity current (density contours at 2 s) for AR=2, β =0.1

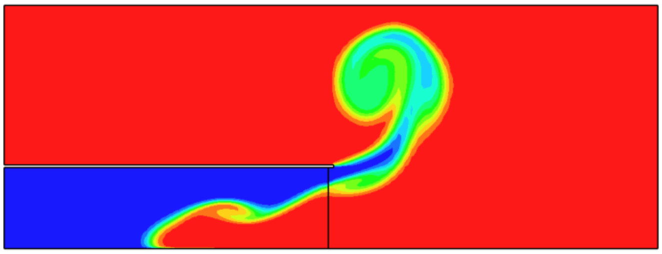

(a) Full Opening

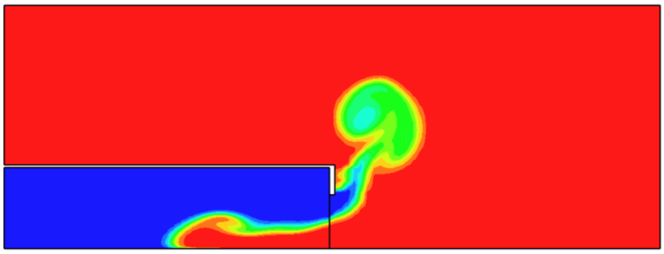

(b) Door Opening

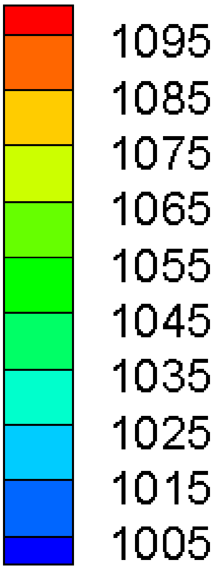

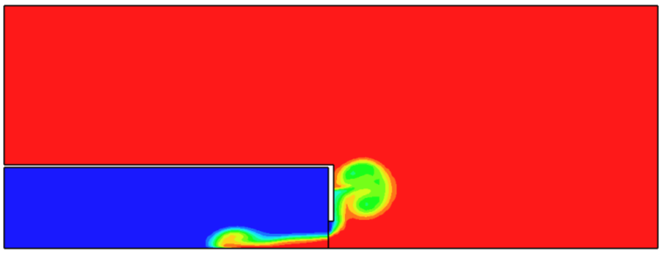

(c) B-slot opening

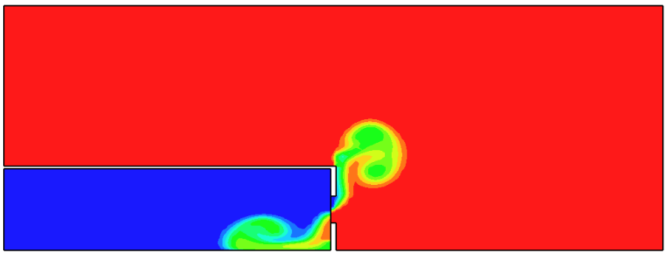

(d) M-slot opening

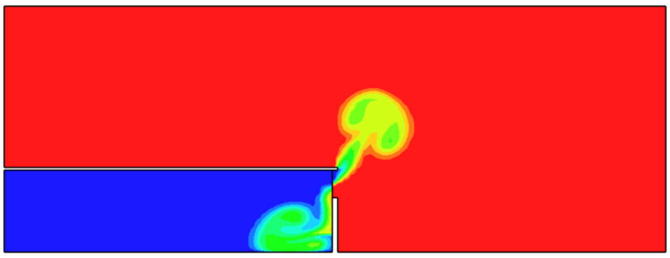

(e) T-slot opening

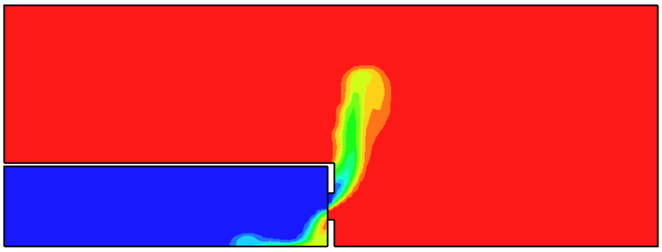

(f) Window opening

Figure 4.15: Effect of opening configuration on gravity current (density contours at 2 s) for AR=4, β =0.1

For description of 3D features of gravity currents, 3D iso-surfaces of mid-level density have been plotted in Figs. 4.16-4.18. Fig 4.16 shows the transient behaviour of gravity current for a full opening of compartment AR= 2 and β =0.1. The head of the current is clearly visible at 1 s. Between 1 and 2 seconds, the gravity current touches the rear wall. Fig 4.17 shows the transient behaviour of gravity current for a slot opening of compartment AR= 2 and β =0.1. Fig 4.18 shows the transient behaviour of gravity current for a full opening of compartment AR= 3 and β =0.1. Fig. 4.18 (a-d) clearly shows that the gravity current head is slightly over the fresh water. The head is slightly revolved and not a sharp edge. These results show the capability of salt water modelling to simulate gravity currents similar to other naturally occurring gravity currents. The fresh water is fast moving fluid compared to salt water. The velocity vectors at mid-plane confirm the same in Fig 4.19. The head is highly convoluted in case of slot opening as compared to full opening. Slot opening possess more resistance as compared to full opening. The height of current is very low in case of slot opening owing to small path available to the heavy fluid. The gravity current has wavy structure from the top. More turbulence is generated when the currents are forced back from the rear wall.

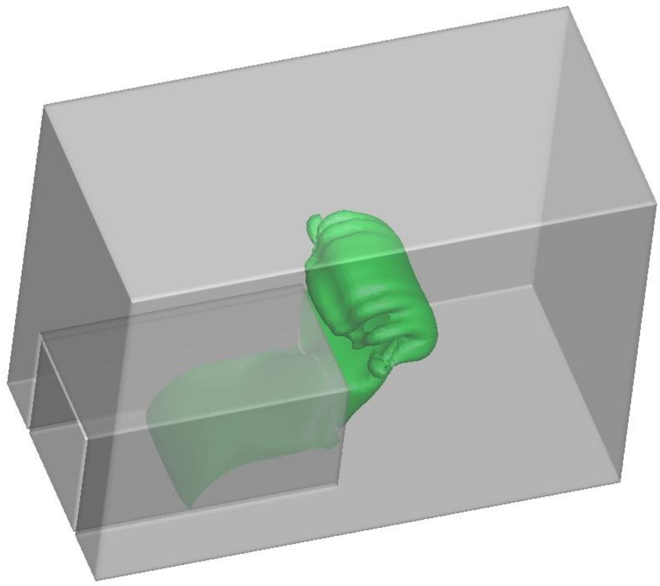

(a) 1 s

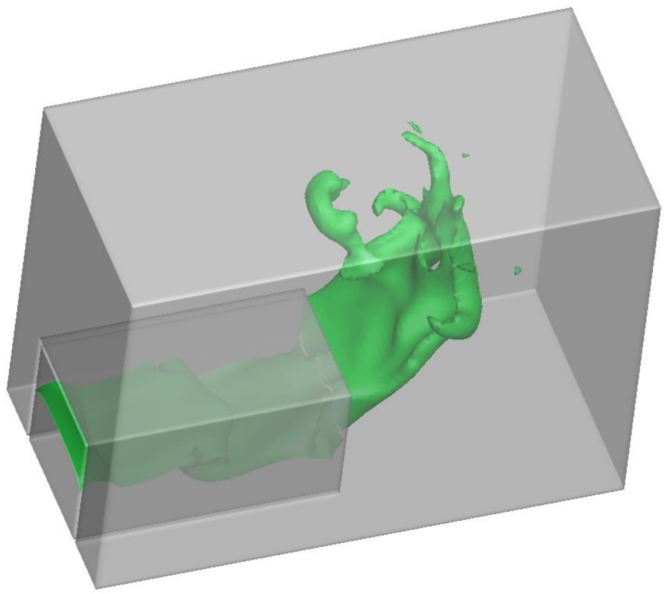

(b) 2 s

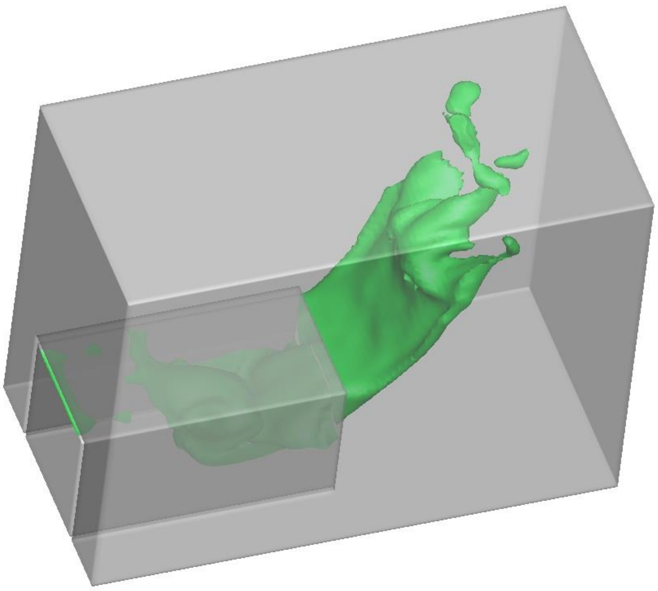

(c) 3s

Figure 4.16: Iso-surface of mid level density (1050 kg/m^3) for AR=2, β =0.1, Full opening

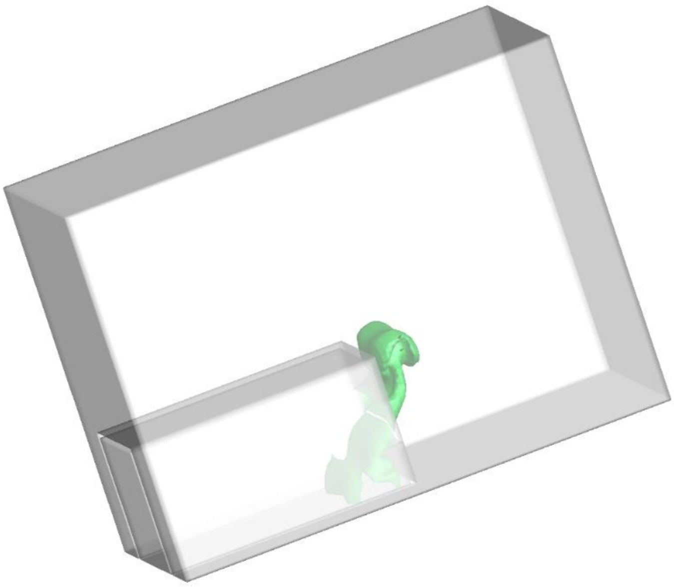

(a) 1 s

(b) 2 s

(c) 3 s

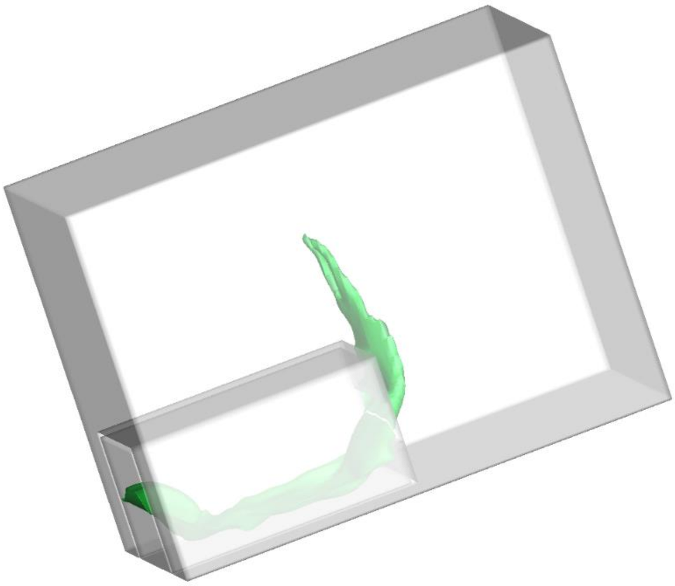

(d) 5 s

(e) 6 s

Figure 4.17: Iso-surface of mid level density (1050 kg/m^3) for AR=2, β =0.1, M-slot pening

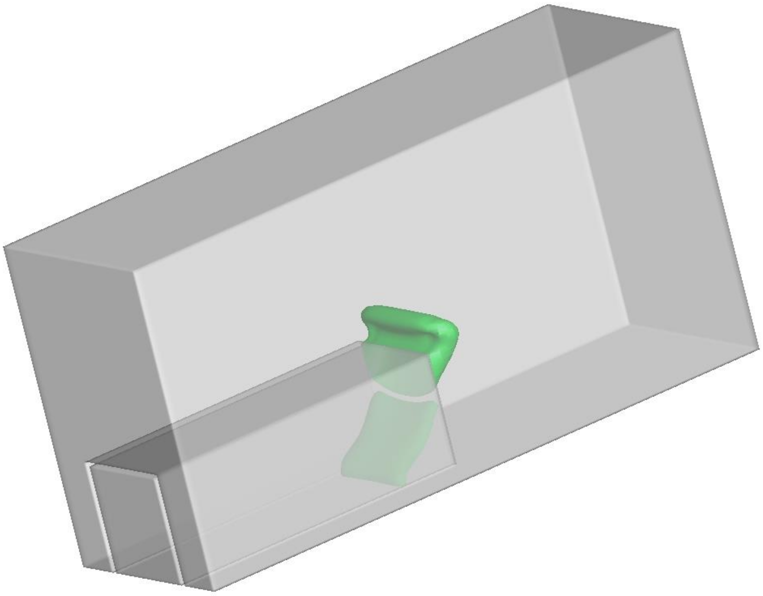

(a) 1 s

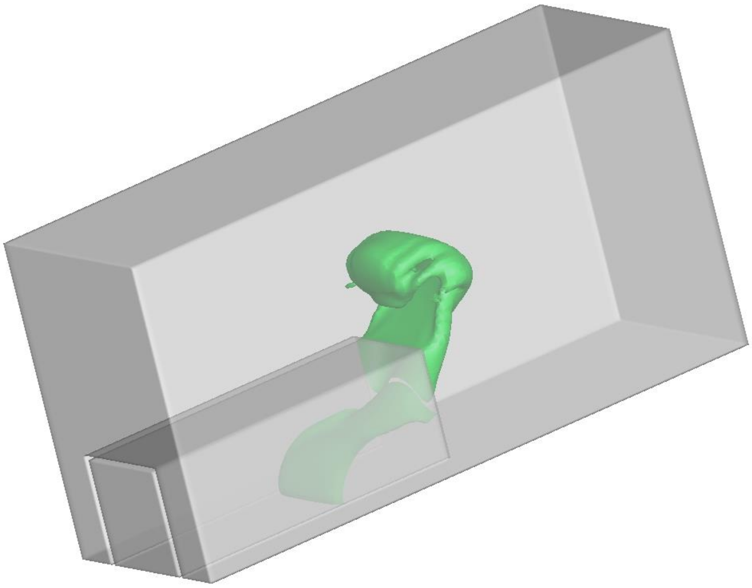

(b) 2 s

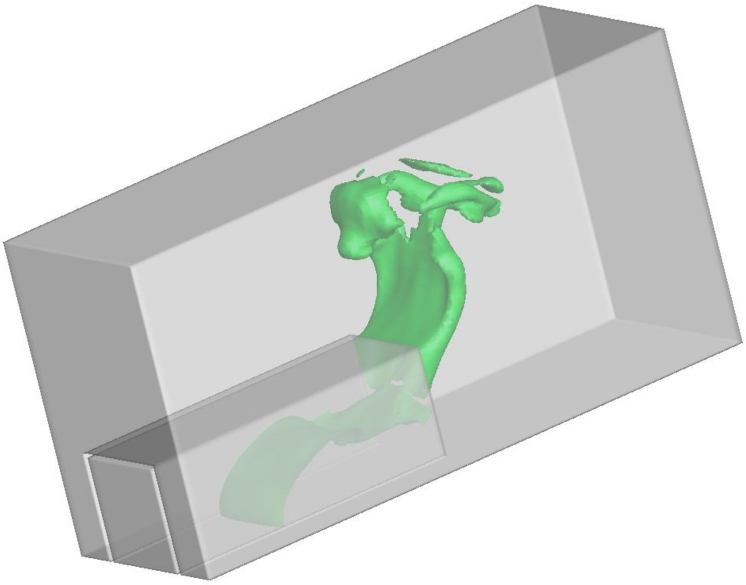

(c) 3 s

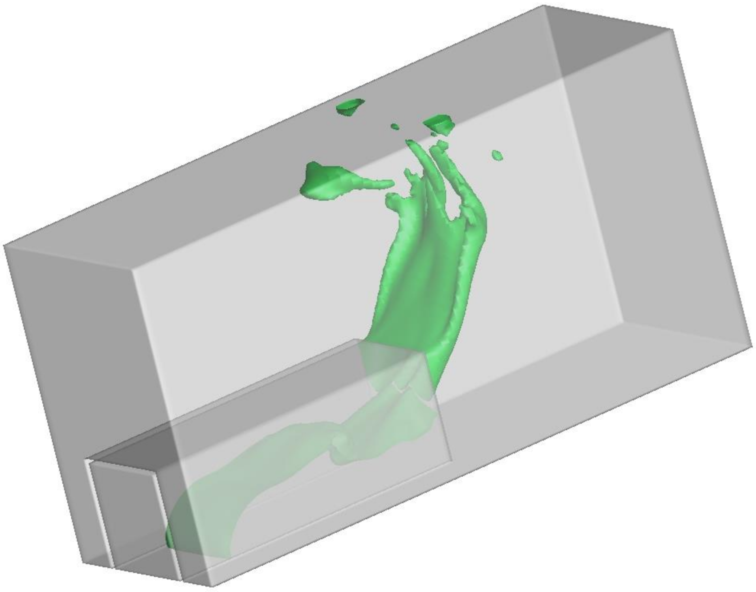

(d) 4 s

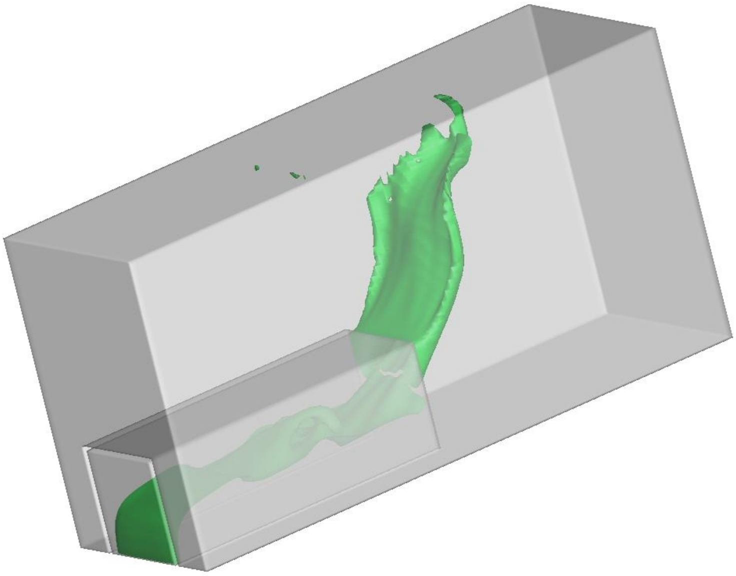

(e) 5 s

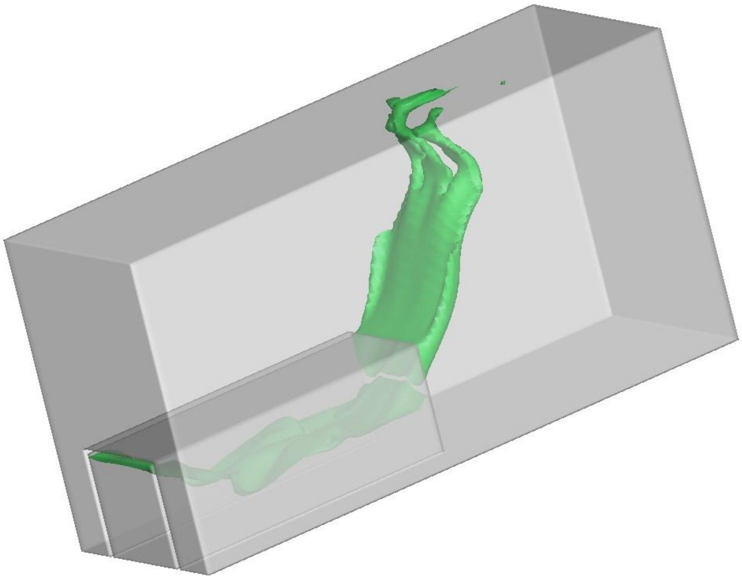

(f) 6 s

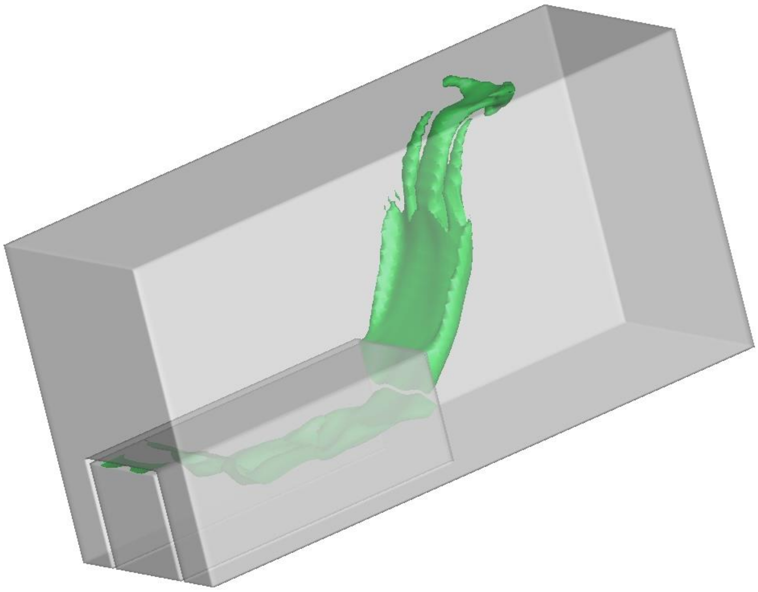

(g) 7 s

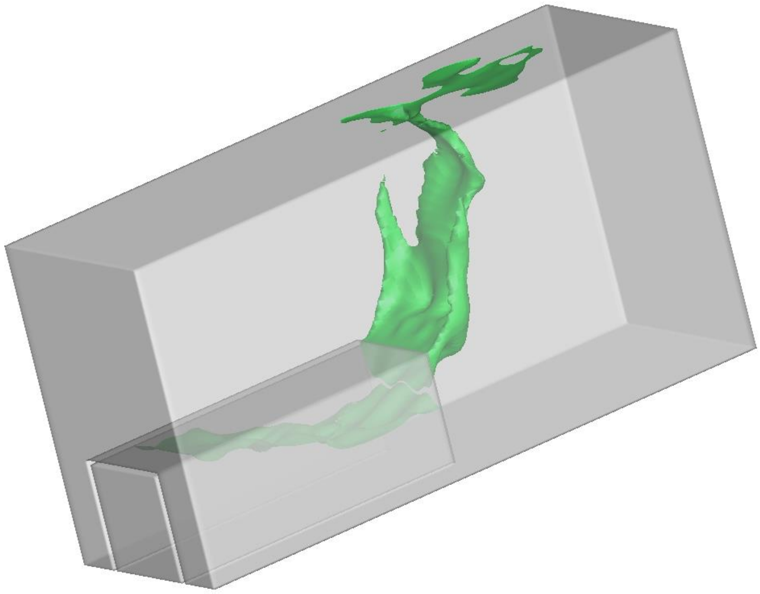

(h) 8 s

Figure 4.18: Iso-surface of mid level density (1015 kg/m^3) for AR=3, β =0.03, Full opening

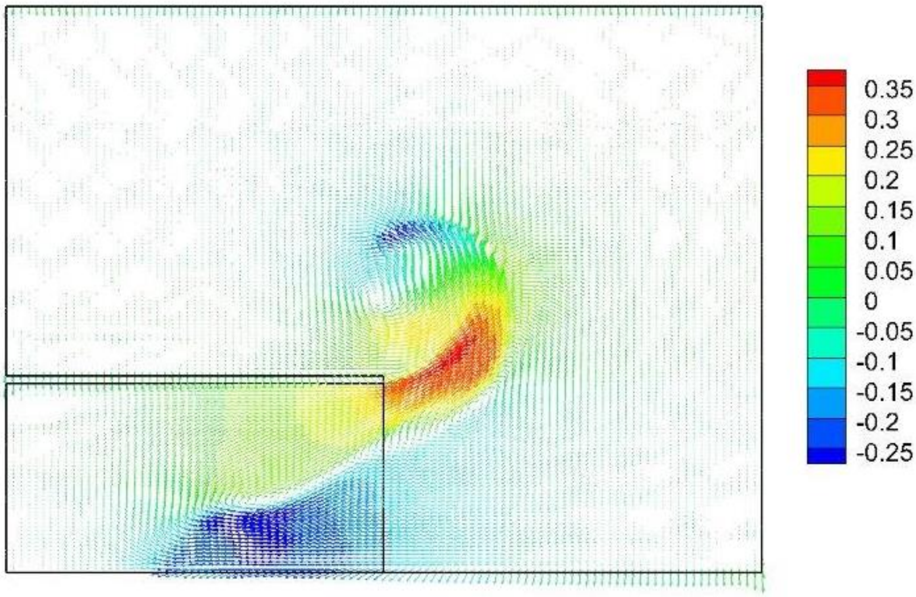

(a) AR 2

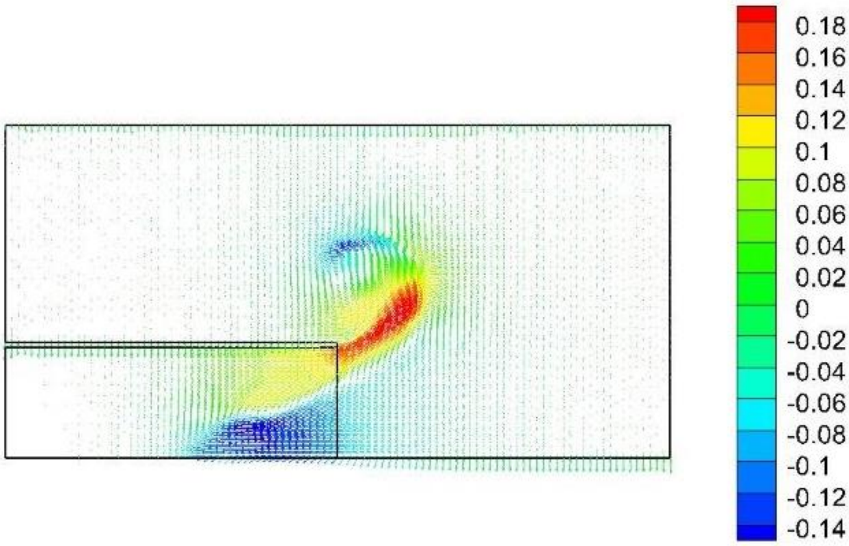

(b) AR3

Figure 4.19: Velocity vectors at mid plane for β =0.1, Full opening at 1 s

4.5. Closure

3D transient LES of gravity currents related to backdraft for various compartment aspect ratios using salt water analogy have been carried out for opening in vertical partition. Six different opening configurations, five compartment aspect ratios and five density ratios were varied to characterise the gravity current under these scenarios. The time required for gravity current to reach the rear wall has been computed for all the cases and dimensionless Froude number is determined. The opening shape has strong influence on gravity current. As the compartment aspect ratio increases, the time required for gravity current to reach the rear wall increases. It is shown that gravity current decelerates during its flow in inner compartment.

CHAPTER 5: CFD ANALYSIS OF FLOW THROUGH HORIZONTAL CEILING OPENING DUE TO BUOYANCY AND PRESSURE DIFFERENCE

5.1. Introduction

Evaluation of density and pressures driven hot gas flows through opening in horizontal partition has been a great interest for fire propagation, natural ventilation and containment of nuclear reactors. It is significant to evaluate the inflow and outflow flow rates through these openings accurately as the flow near the opening in 3D, unstable and bi-directional. It is essential to characterize such flow through large opening in horizontal partition to determine the strength of stratification inside enclosure and escaped flow from enclosure to outside accurately in presence of combined buoyancy and pressure driven force. In this case flow through opening is three-dimensional and complete details of velocity and density field is necessary to achieve the best accuracy for computed parameters such as mass flow rate. CFD based study has been performed to quantify the required pressure for transition to unidirectional flow from bidirectional flow due to buoyancy and forced effects. Use of salt water/fresh water analogy to model such type of flow is an excellent alternative approach as this system requires less cost and flow visualization is easy. The pressure in the lower compartment was increased until transition from bidirectional flow to unidirectional flow is obtained. The 2D axisymmetric, incompressible, unsteady momentum, continuity, species and turbulent quantities were solved. In-house CFD code was developed based on pressure based SIMPLE algorithm. The model is explained in chapter 3 with validation examples performed with this code. Numerical simulations were performed for various cases for different opening aspect ratio. In the present work, the effect of pressurizing the lower compartment has been studied for partitions of finite thickness over the range $0.008 \leq L/D \leq 0.9$. The flooding pressure corresponding to transition to unidirectional flow from bi-directional flow was computed for opening diameter of 0.0254 m and 0.0508 m.

5.2. General Description of the Problem

For numerical simulations, the computational domain was chosen from the test set up of Conover et al. (1995) as shown in Fig. 5.1. The experimental setup was made of transparent material and comprised of two separate compartments connected by an opening in horizontal partition.

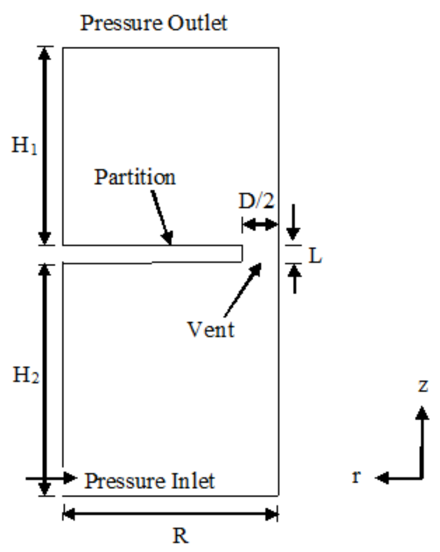

Figure 5.1: Simplified geometric configuration for CFD computation

The lower enclosure has dimension of 0.381X0.381X0.316 m. The upper enclosure has dimension of 0.381X0.381X0.265 m. Both the enclosure was separated by a partition plate. A plate having 0.127 m diameter hole at centre was attached to the partition plate and sealed by an O-ring. Holes of 0.0508 m (2 inches) in diameter were served in the plates of varying thickness to be used as vents.

The top enclosure was occupied with fluid of higher density while the bottom enclosure was occupied with fluid of lower density, thus creating a density differential between the two chambers. The code was validated against reported experiments of this nature. The flow coefficients and pulsation frequency were determined. Various cases were studied by varying the density ratio from 1.012 to 1.2 while the opening aspect ratio was varied from 0.008 to 0.9. The effect of these parameters was investigated on oscillation frequency and flow coefficient.

The computations were carried out assuming a cylindrical geometry for ease in computation. The volume of simplified geometry was kept similar to actual set up. To further simplify the computation the computational domain was considered as 2D axisymmetric. The domain dimensions were taken as radius (R) 0.215 m and height of lower enclosure 0.316 m (H_2) and height of upper enclosure 0.265 m (H_1) connected by a thin partition of specified thickness, containing a hole of diameter (D) 0.0508 m (2 inches) or 0.0254 m (1 inch). The bottom inlet boundary was modelled as specified pressure and top outlet boundary was also defined as specified pressure.

The governing equations are as follows

Continuity equation

$$\frac{\partial \rho}{\partial t} + \frac{\partial (\rho u)}{\partial z} + \frac{1}{r}\frac{\partial (r\rho v)}{\partial r} = 0$$

(5.1)

Z-momentum equation

$$\frac{\partial (\rho u)}{\partial t} + \frac{\partial (\rho u u)}{\partial z} + \frac{1}{r}\frac{\partial (r\rho v u)}{\partial r} = -\frac{\partial p}{\partial z} + \frac{\partial}{\partial z}\left(2\mu_{eff}\left(\frac{\partial u}{\partial z}\right)\right) + \frac{1}{r}\frac{\partial}{\partial r}\left(r\mu_{eff}\left(\frac{\partial u}{\partial r}+\frac{\partial v}{\partial z}\right)\right) - (\rho-\rho_{\infty})g$$

(5.2)

R-momentum equation

$$\frac{\partial(\rho v)}{\partial t}+\frac{\partial(\rho uv)}{\partial z}+\frac{1}{r}\frac{\partial(r\rho vv)}{\partial r}=-\frac{\partial p}{\partial r}+\frac{\partial}{\partial z}\left(\mu_{eff}\left(\frac{\partial u}{\partial r}+\frac{\partial v}{\partial z}\right)\right)+\frac{1}{r}\frac{\partial}{\partial r}\left(2r\mu_{eff}\left(\frac{\partial v}{\partial r}\right)\right)-\frac{2}{r^{2}}\left(\mu_{eff}v\right) \quad \textbf{(5.3)}$$

Species transport equation

$$\frac{\partial(\rho Y_s)}{\partial t}+\frac{\partial(\rho uY_s)}{\partial z}+\frac{1}{r}\frac{\partial(r\rho vY_s)}{\partial r}=\frac{\partial}{\partial z}\left((\rho D_{ab}+\mu_t/Sc_t)\frac{\partial Y_s}{\partial z}\right)+\frac{1}{r}\frac{\partial}{\partial r}\left(r(\rho D_{ab}+\mu_t/Sc_t)\frac{\partial Y_s}{\partial r}\right) \quad \textbf{(5.4)}$$

Salt water density has been determined in terms of the salt mass fraction using an empirical expression as suggested by Yao and Marshall (2006) as given by Eq. (5.5)

$$\rho=\rho_{L,0}(1.0+\beta_{SW}Y_s) \quad \textbf{(5.5)}$$

Turbulence Modelling:

For modelling turbulence RNG k-ε model (Yakhot el al., 1992) was used with buoyancy modification. The y+ was in the range of 30-80 near the walls that is required to use the standard wall function. The renormalization group (RNG) theory represents the effects of the small-scale turbulence by means of a random forcing function in the Navier–Stokes equation. The RNG procedure systematically removes the small scales of motion from the governing equations by expressing their effects in terms of larger scale motions and a modified viscosity. The RNG k–ε model equations for high Reynolds number flows derived by Yakhot et al. (1992) are as follows:

For the RNG k-ε model, the turbulent viscosity is modelled as (Eq. (5.6))

$$\mu_t = \rho C_\mu \frac{k^2}{\varepsilon} \tag{5.6}$$

For turbulent kinetic energy, the equation is given by (Eq. (5.7))

$$\frac{\partial(\rho k)}{\partial t} + \frac{\partial(\rho u k)}{\partial z} + \frac{1}{r}\frac{\partial(r\rho v k)}{\partial r} = \frac{\partial}{\partial z}\left(\alpha_k \mu_{eff} \frac{\partial k}{\partial z}\right) + \frac{1}{r}\frac{\partial}{\partial r}\left(r\alpha_k \mu_{eff} \frac{\partial k}{\partial r}\right) + \tau_{ij}.S_{ij} + G_B - \rho\varepsilon \tag{5.7}$$

The turbulent dissipation rate is computed by Eq. (5.8)

$$\frac{\partial(\rho \varepsilon)}{\partial t} + \frac{\partial(\rho u \varepsilon)}{\partial z} + \frac{1}{r}\frac{\partial(r\rho v \varepsilon)}{\partial r} = \frac{\partial}{\partial z}\left(\alpha_\varepsilon \mu_{eff} \frac{\partial \varepsilon}{\partial z}\right) + \frac{1}{r}\frac{\partial}{\partial r}\left(r\alpha_\varepsilon \mu_{eff} \frac{\partial \varepsilon}{\partial r}\right) + \frac{\varepsilon}{k}\left(C_{1\varepsilon}^{*}\tau_{ij}.S_{ij} - C_{2\varepsilon}\rho\varepsilon + C_3 G_B\right) \tag{5.8}$$

Where $\mu_{eff} = \mu + \mu_t$, $\alpha_k = \alpha_\varepsilon = 1.39$, $C_{1\varepsilon} = 1.42$, $C_{2\varepsilon} = 1.68$ and $C_{1\varepsilon}^{*}$ is given by Eq. (5.9)

$$C_{1\varepsilon}^{*} = C_{1\varepsilon} - \frac{\eta(1-\eta/\eta_0)}{1+\beta_{RNG}\eta^3} \tag{5.9}$$

$$\eta = \frac{k}{\varepsilon}\sqrt{2S_{ij}.S_{ij}}\,,\ \eta_0 = 4.377\,,\ \beta_{RNG} = 0.012$$

The term G_B can be modelled by Eq. (5.10), which is based on Simple Gradient Diffusion Hypothesis (SGDH) (Markatos et al., 1982) or by Eq. (5.11) which is based on Generalised Gradient Diffusion Hypothesis (GGDH) (Daly &Harlow, 1970). In the present work GGDH approach has been used as GGDH is better approach since it considers density gradient in all the 3 directions.

$$G_B = -\frac{\mu_t}{\Pr_t}\frac{1}{\rho^2}\frac{\partial \rho}{\partial x_j}\left(\frac{\partial p}{\partial x_j} + \rho_\infty g_j\right) \tag{5.10}$$

$$G_B = -\frac{3}{2}\frac{\mu_t}{\mathrm{Pr}_t}\frac{1}{\rho^2 k}\left(\overline{u'_j u'_k}\frac{\partial \rho}{\partial x_k}\right)\left(\frac{\partial p}{\partial x_j} + \rho_\infty g_j\right) \tag{5.11}$$

In Eq. (5.11), pressure gradient was assumed as negligible. The assumption is reasonable as the fluid velocity is relatively low thus causing low pressure gradients. There are various approaches to determine the value of C_3 for Eq. (5.8); in the present work the approach suggested by Viollet (1987) was adopted. Depending on the sign of G_B (the term denoting the buoyancy production of turbulence in k), the value of C_3 is determined. If $G_B > 0$; $C_3 = 1.44$ and $C_3 = 0$, if $G_B < 0$. The stability of flow determines the sign of G_B. If $G_B > 0$; the flow is unstable since density gradient is positive and, if $G_B < 0$; the flow is stable density gradient is negative. Table 5.1 shows the parameters used in the computation.

Table 5.1. Values of parameters used in computation (McBryde, 2008)

Parameter	Value
Mass diffusivity of salt (D_{ab})	1.5e-9 m^2/ s
Dynamic viscosity of water (μ)	1.003e-3 m^2/s
Turbulent Schmidt number (Sc_t)	0.7

Solver Details

The 2D axisymmetric, incompressible, unsteady momentum, continuity, species and turbulent quantities were solved. In-house CFD code was developed based on pressure based SIMPLE algorithm. The code written in C language is for this specific purpose and solver is very fast for this problem as compared to any commercial or open source code. Third order QUICK scheme (Hayase et al., 1992) was employed for convective terms to capture the oscillation pattern and second order central differencing was employed for diffusive term. The time discretization was done using second-order-accurate Crank-Nicolson scheme.

Initially the lower compartment was filled with fresh water; hence mass fraction of salt was assigned as zero and in the upper compartment salt water, mass fraction was assigned as per the required density of salt water solution evaluated using Eq. (5.8). The characteristic velocity is $\sqrt{(\Delta\rho/\rho)gD}$, which is of the range of 0.077 m/s to 0.316 m/s for the parameters considered, which gives densimetric Reynolds number (Re) in the range of ~ 4000-16000. The flow is turbulent in all the cases. For initialisation, the velocity components were set to zero values. All the walls and partition have been modelled as a no-slip impermeable wall. The inlet location at the bottom of lower compartment was modelled as pressure inlet and top boundary of upper compartment was modelled as pressure outlet. At the inlet specified gauge pressure was applied while at pressure outlet zero gauge pressure was specified. Staggered grid system was used in which scalar i.e. pressure, species mass fraction and turbulent quantities ware calculated at cell centre while fluid velocities were calculated at the cell faces. The set of algebraic equations were solved iteratively using Gauss-Seidal method. For momentum equation under-relaxation value of 0.05 was used to have easy convergence since the solutions were oscillating in nature. For species transport equation under-relaxation value of 1 was chosen. The solution was assumed as converged in each time step if mass residual was below 10^{-5}.

5.3. Simulation Results

The results were evaluated in terms of flooding pressure for two opening diameter 0.0254 m and 0.0508 m. The flooding pressure corresponding to transition from bi-directional flow to unidirectional flow has been evaluated for two opening diameter 0.0254 m and 0.0508 m and shown in Figs. 5.2-5.3 as a function of $g\Delta\rho D$. Below the lower values of pressure, flow is bi-directional and at high pressure, flow is unidirectional. The velocity vectors for flooding pressure 60 Pa is shown in Fig 5.4-5.5 for density difference of 100 kg/m^3 for both the openings at 10 seconds after initiation of the flow. The density contours for both the openings are shown in Fig. 5.6-5.7. As the density difference increases across the opening, high value of purging pressure is required to overcome the downward flow. The required value of purging pressure increases with increase in opening diameter. The required value of purging pressure also increases with increase in L/D to overcome the frictional resistance offered by opening length.

5.4. Closure

In this chapter, CFD analyses have been carried to compute the flooding pressure corresponding to transition to unidirectional flow from bi-directional flow. As the density difference increases across the opening, high value of purging pressure is required to overcome the downward flow. The required value of purging pressure increases with increase in opening diameter. The required value of purging pressure also increases with increase in L/D to overcome the frictional resistance offered by opening length for the flow to remain unidirectional.

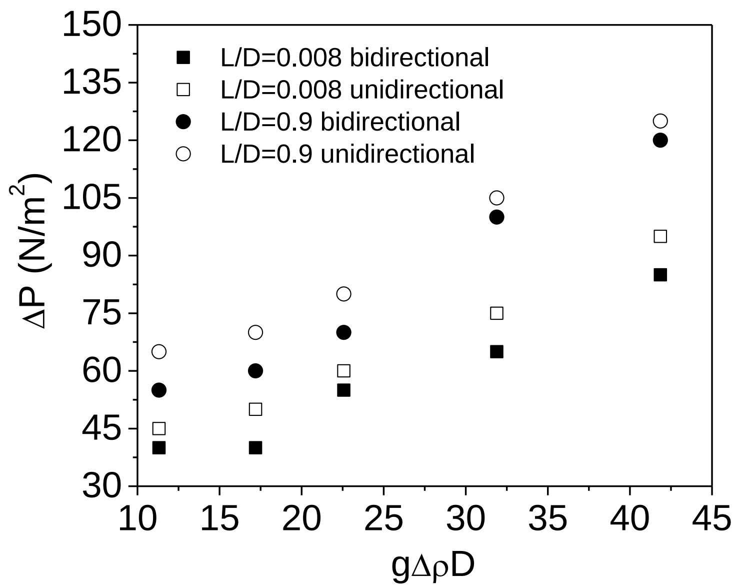

Figure 5.2: Flooding pressure as a function of gΔρD for D= 0.0254 m.

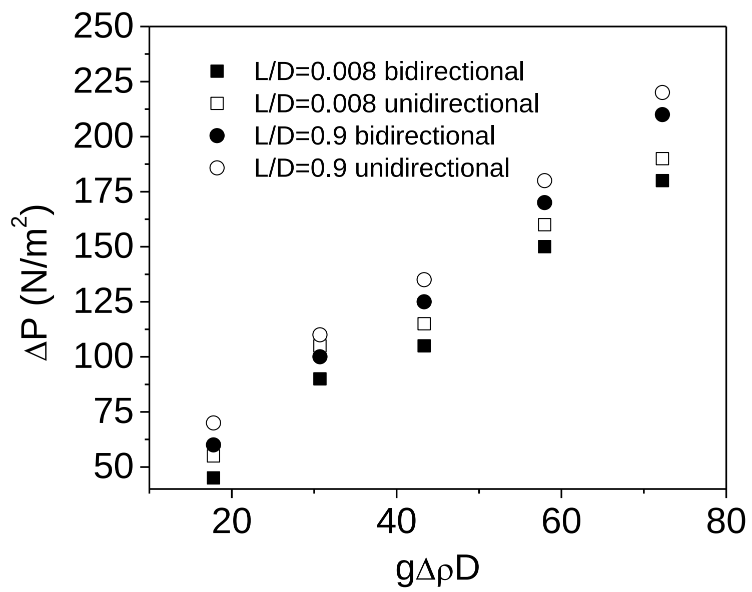

Figure 5.3: Flooding pressure as a function of gΔρD for D= 0.0508 m.

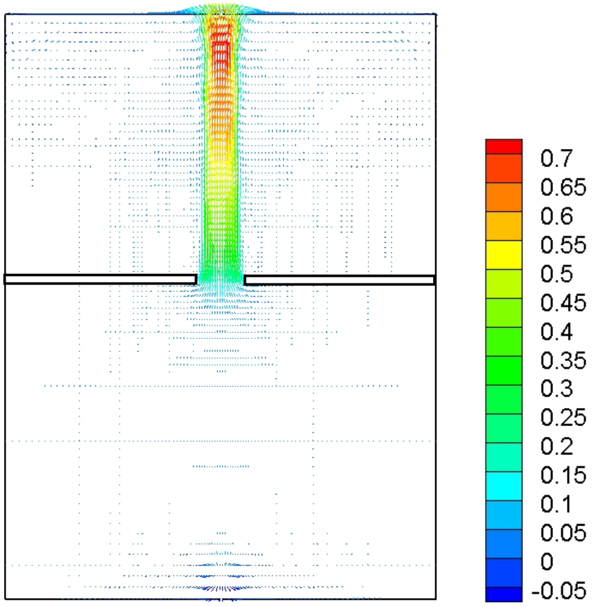

Figure 5.4: Instantaneous vectors at 10 s for L/D=0.1, Δρ=100 kg/m^3, ΔP=115 Pa

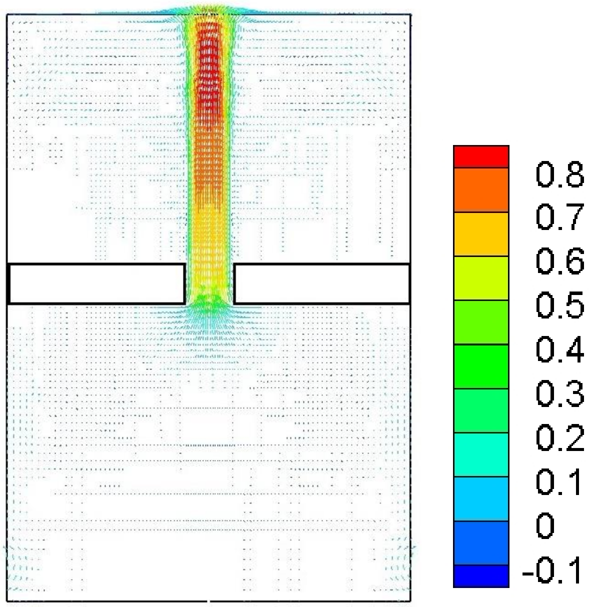

Figure 5.5: Instantaneous vectors at 10 s for L/D=0.9, Δρ=100 kg/m^3, ΔP=135 Pa

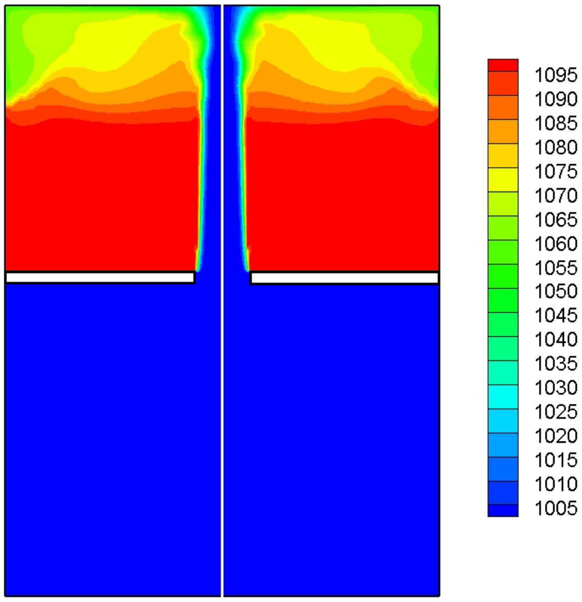

Figure 5.6: Density contour at 10 s for L/D=0.1, $\Delta\rho$=100 kg/m^3, ΔP=115 Pa

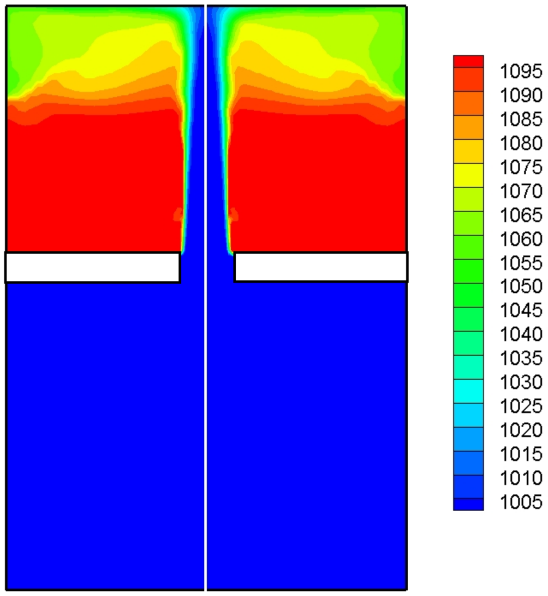

Figure 5.7: Density contour at 10 s for L/D=0.9, $\Delta\rho$=100 kg/m^3, ΔP=135 Pa

CHAPTER 6: STUDY OF HOT GAS FLOW IN A COMPARTMENT HAVING LARGE OPENING USING SALT WATER ANALOGY

6.1. Introduction

An interesting transport phenomenon is observed when light/hot gas is released in a compartment having opening connecting it to other compartments. It is essential to characterize such flow through large opening to determine the exchange from one compartment to another compartment accurately in presence of combined buoyancy and pressure driven force. Even if the area of opening is very large compared to injection area, the opening creates a flow resistance and mixing occurs in injection compartment, stratified layers are formed and a bi-directional flow through the opening is observed. Current zone based model calculates the flow using standard vent models based on pressure difference using flow coefficient that do not accurately take in to account the buoyancy component of the flow. In nuclear reactor containment resulting flow after an accidental condition, will be a function of the initial pressure difference, but in the long-term the flow field will be principally driven by density differences between the two compartments as long as the pressures have equalized. In accidental fires, the compartment below the partition contains lighter fluid (hot gases) compared to heavier fluid located in upper compartment (ambient air). In this scenario flow through a single opening in horizontal partition is oscillatory, bi-directional and follow irregular behaviour. During fire in an enclosure having opening in vertical partition, the smoke and hot gases get stratified in the top region of enclosure and leave from the upper portion (approximately half) of the opening while fresh air being heavier enters from the lower portion of the opening. The flow through opening in vertical partition is stable and bi-directional. If one of the compartments is at higher pressure, the pressure inside the room will also in addition govern the mixing in the compartment and flow through the opening. A large number of experimental and numerical studies have been performed to simulate such density driven flow using salt water -fresh water analogy. In salt water modelling, turbulent buoyant salt water moving in fresh water is used to substitute for turbulent buoyant hot gas moving in cold gas. The salt water flows have features consistent with fire-induced flows and provide an excellent test-bed for CFD turbulence. In the present work, experiments have been carried out for such type of flow and numerical computations with 3D LES approach have been performed for the experiments conducted to explain the observations and validation of the present CFD code.

6.2. Details of Experimental setup

Experimental setup has been fabricated to study buoyant jet, ceiling jet, flow through ceiling or vertical opening using salt-water analogy. The major dimensions of the test set up are shown in Figure 6.1. The compartment used for this investigation is 1:16th scale model of a (length X depth X height) 3.6 m X 2.4 m X 2.4 m room, which are standard ISO room dimensions. This gives the compartment dimensions of 0.225 m X 0.15 m X 0.15 m and outer large tank size is 0.625 m X 0.375 m X 0.375 m. The small tank has the provision to replace the bottom plate to accommodate different openings in the horizontal partition. The right side vertical wall of small tank is also replaceable to have different door and window openings at various locations. Initially both the tanks are filled with fresh water. Salt water is injected from top of the small tank creating buoyant jet/plume then forming buoyant ceiling jet. Stratification/mixing occur in small tank and fresh water from ambient room moves in small tank through horizontal and vertical openings. Separate experiments have been conducted for horizontal openings with closed vertical openings, and vertical openings with closed horizontal openings. 2D planar PIV and 2D PLIF measurement have been performed for twelve experiments. Four dye visualization experiments have also been performed. The geometries of window/door opening plates are shown in Figure 6.2.

An inner compartment (IC) is placed in a large compartment. Both the compartments are filled with fresh water initially and salt water is injected in the inner compartment from top wall (IC_T). A round/square hole of 8 mm is made in IC_T for salt water injection. The inner compartment is connected through outer compartment by opening in sidewall (IC_S) and/or opening in bottom wall (IC_B). The IC_S opening size can be varied from door (0.1 m X 0.05 m) and window (0.05 m X 0.05 m). The opening in IC_B is square shaped and of various sizes 30 and 50 mm.

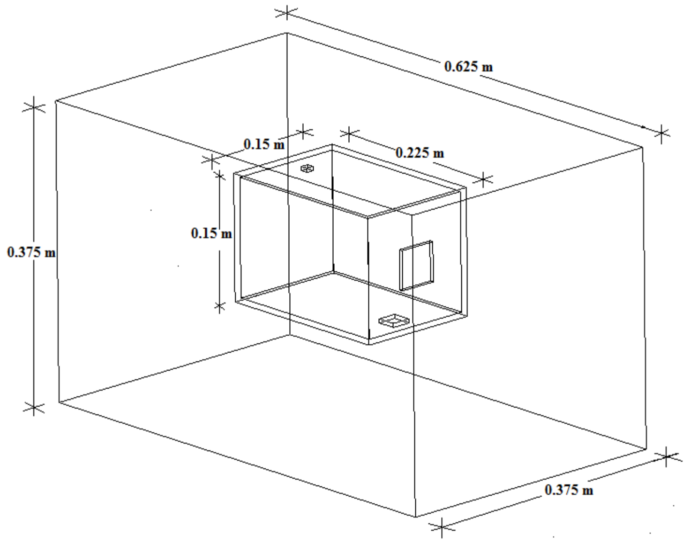

Figure 6.1: Setup to study effect of pressure and density difference on flow through opening in horizontal and vertical partition.

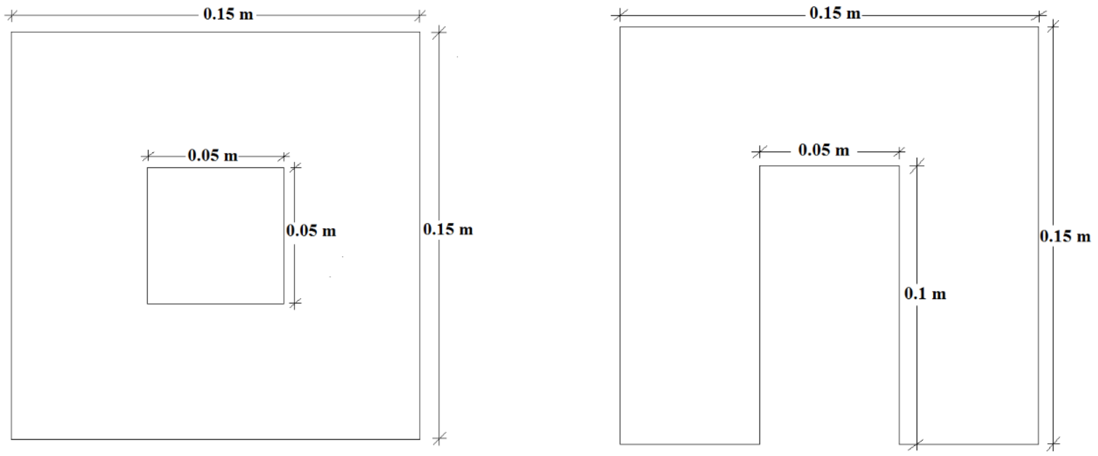

Figure 6.2: Geometry of different vertical opening.

Experiments were conducted at 20 °C in test setup comprising of two rectangular tanks with a smaller tank being placed inside a larger tank (Figure 6.3). The large tank has an open top and the small tank is a rectangular box with openings only at designated positions. The large tank has a capacity of 82 litres and the small tank has a capacity of 4.2 litres. The large tank is filled with 72 litres of water. Brine solution of required density difference with water is prepared and stored in an overhead tank. The small tank was suspended from the top with its top surface 3 cm below the free surface of water in the large tank. The small tank has two openings - one with 8 mm diameter on its top surface and another one of required size on its side face or bottom face. Denser fluid was allowed to flow from a constant head to the smaller tank through the top opening and allowed to interact with the ambient (fluid in the larger tank) through the side/bottom opening. The experiments were conducted for inlet flow in the turbulent flow regime. The corresponding inlet velocity/Reynolds number was maintained by changing the height of the overhead tank.

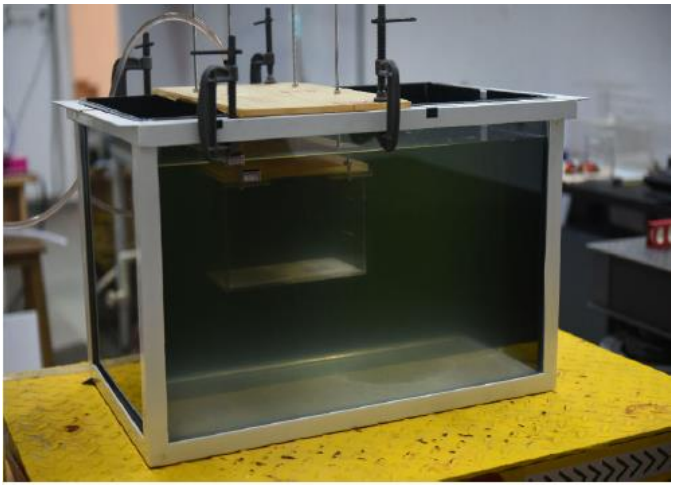

(a) Large tank filled with water

(b) Inner box with opening

Figure 6.3: Actual photo of experimental set up.

6.3. Arrangement to maintain a constant head salt water injection supply

An arrangement has been fabricated to maintain a constant head salt water injection supply. The source and supply tank are filled with salt water of required density as shown in Figure 6.4. The salt water to main setup is injected from supply tank; the level in supply tank is maintained constant by pumping the required salt water from the source tank. The pump flow rate is higher than the injected salt-water flow rate to ensure that the supply tank is always filled and excess salt water spills in source tank. The velocity of injection is varied by changing the elevation of supply tank while maintaining the fixed elevation of injection point.

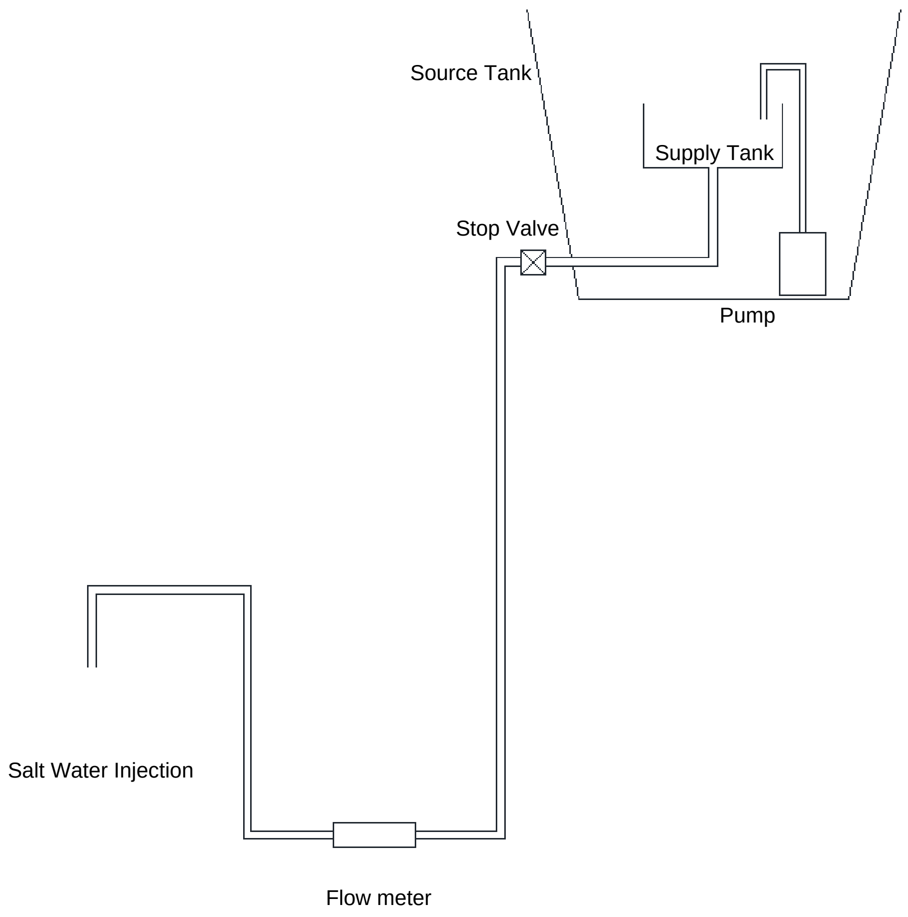

Figure 6.4: Arrangement to maintain a constant head salt-water injection supply.

6.4. Particle Image Velocimetry (PIV)

PIV is an established technique for measuring velocity components during an experiment in fluid mechanics research. It is non-intrusive and can be used for 2D planar and 3D volumetric measurement. In PIV small neutrally buoyant particles are seeded in the fluid and these particles are illuminated by laser light. A camera is used to record these seeded particle displacement over a time interval using a double pulse laser. Velocities are calculated by correlating two consecutive images over the interval between laser pulses. A schematic of PIV setup including laser, camera, light sheet and particles is depicted in Fig. 6.5. A filter is used to pass light scattered from the particles at 532 nm and block other wavelength.

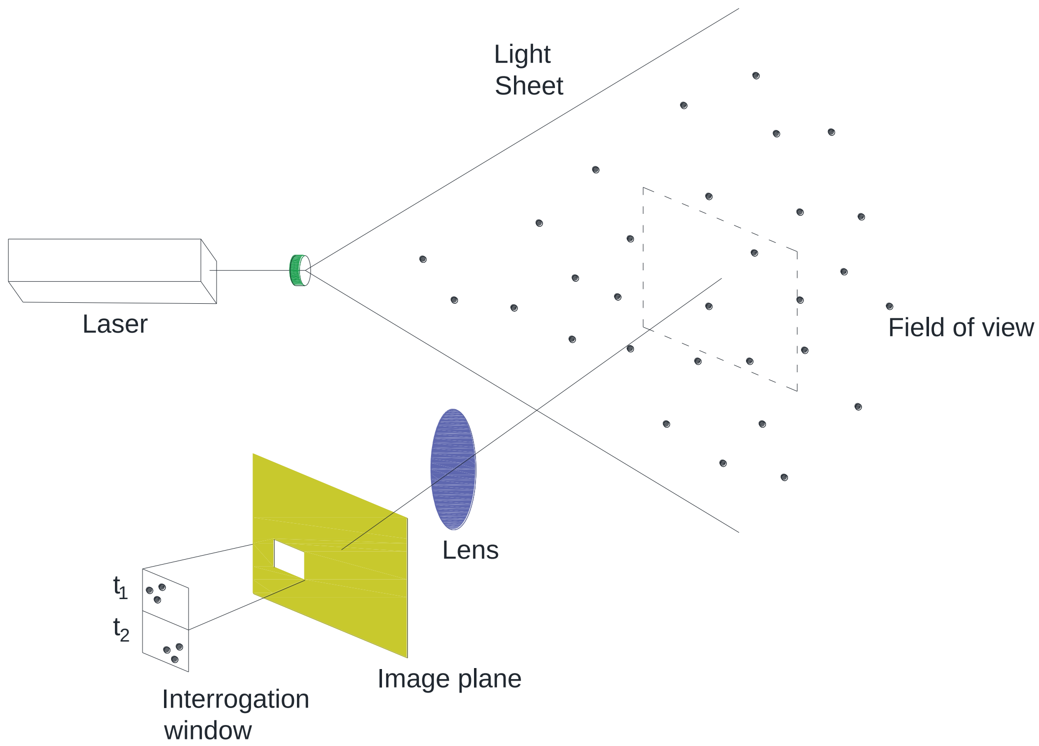

Figure 6.5: PIV set up Schematic.

For calculating velocities software supplied by Dantec Dynamics was used. The adaptive correlation method followed by universal outline detector and removal of spurious vectors is performed by the software to calculate the velocity field. The large interrogation window is divided in several small equal sized windows. The intensity of particle image is traced between two pair of images within small time and velocity is determined by measuring the displacement of particle and time between two images. (Fig 6.6). PIV experiments must be designed with the post-processing in mind and must satisfy a number of design rules to achieve accurate results (Adrian and Westerweel, 2011). Those rules are as follows:

(i) The number of particles in the interrogation region shall be greater than 10.

(ii) The particle image displacement shall be less than ¼ the width of the interrogation region.

(iii) The out-of-plane displacement shall be less than ¼ the thickness of the light sheet.

(iv) Local variation of displacements shall be less than 1/20th the size of the interrogation region.

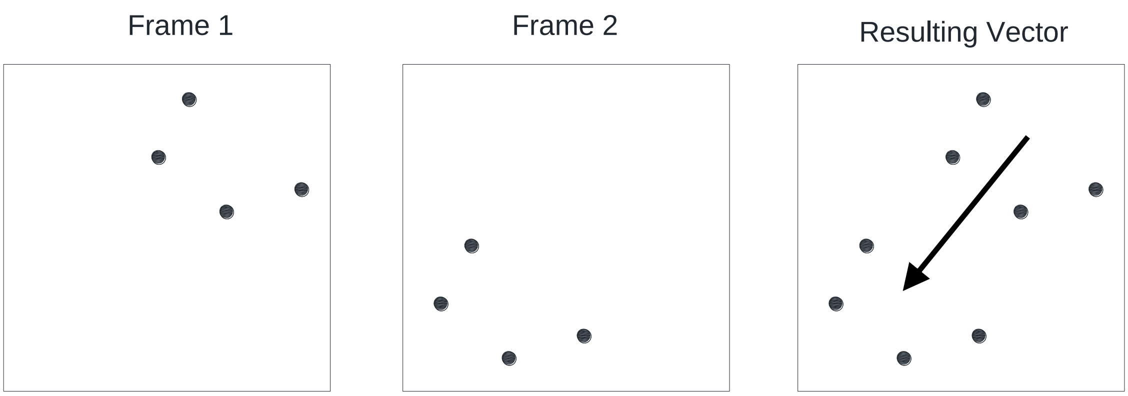

Figure 6.6: Vector calculation from PIV Data.

6.5. Planar Laser Induced Fluorescence (PLIF)

PLIF is non-intrusive technique to measure the density field spatially and temporally in a 2D plane. In PLIF a laser sheet is used to illuminate a dye tracer and a camera is used to record the light intensity emitted from the dye. The fluorescence dye used in PLIF technique has ability to absorb laser light and emit light of some wavelength specific to dye. The intensity is linearly proportional to the concentration of the dye in the liquid. Rhodamine 6G dye is the most popular choice for PLIF experiments based on salt water analogy. This dye has the peak absorption wavelength of 524 nm which is near the Nd: YAG laser wavelength i.e. 532 nm. Rhodamine 6G dye emits lights at around 565 nm, has resistance to photo bleaching and sensitivity to temperature is minimal. The emitted intensity from dye depends on the local concentration of the dye and the dye concentration represents the local fluid density (Shan et al., 2004).

6.6. Simultaneous PIV+PLIF Experiments

The combined PIV+PLIF experiments have also been performed. Combined PIV+PLIF experiments give useful knowledge about physics of these types of density-driven exchange-flows by “simultaneous” velocity and density measurements. The fluctuation velocity-density correlation can be calculated from PIV+PLIF measurements.

To determine velocity and density fields simultaneously at a given instance, the PIV must be used in conjunction with PLIF. This involves issues like (i) positioning of two cameras, (ii) focusing on the same plane, (iii) dewarping and image-correction, etc. This PIV+PLIF technique was successfully implemented and tested by carrying out simultaneous measurement. A schematic of combined PIV+PLIF experimental set up is depicted in Fig. 6.7.

A frequency doubled Nd-YAG, pulsed laser (λ = 532 nm, 200 mJ/pulse) was used to illuminate a plane in the flow shown in Figure 6.8. A combination of spherical and cylindrical lenses was used to make the laser sheet of 2 mm thickness. The intensity of the laser beam follows a Gaussian mode with respect to time. The laser was used to fire pulse pairs at a frequency of 10Hz.

55-micron polyamide particles were used as tracer particles. The relative density of these particles is 1.1 g/cc. Rhodamine 6G dye was used for PLIF measurement.

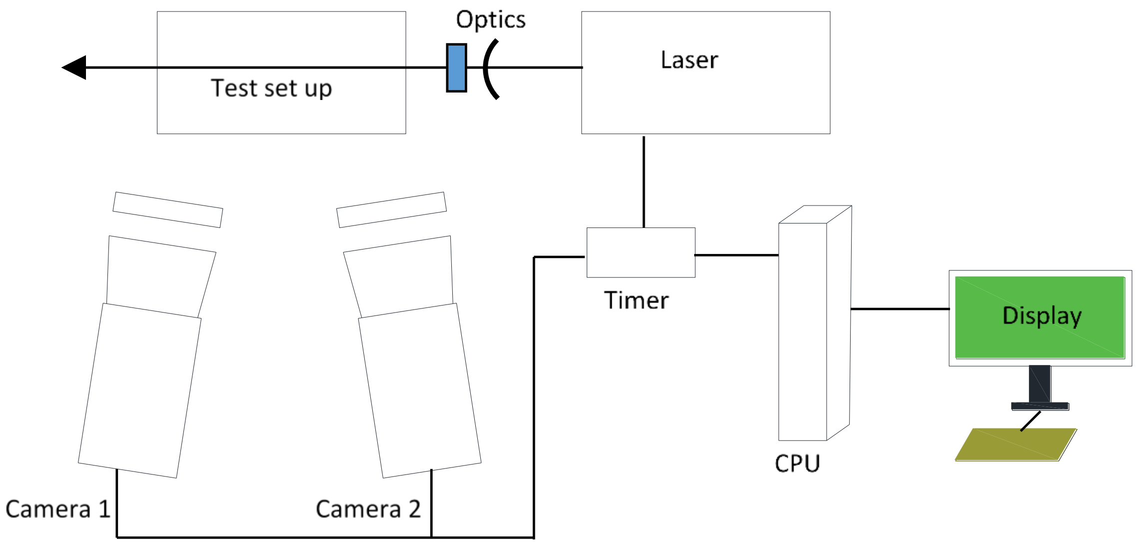

Figure 6.7: Schematic of combined PIV+PLIF experiment.

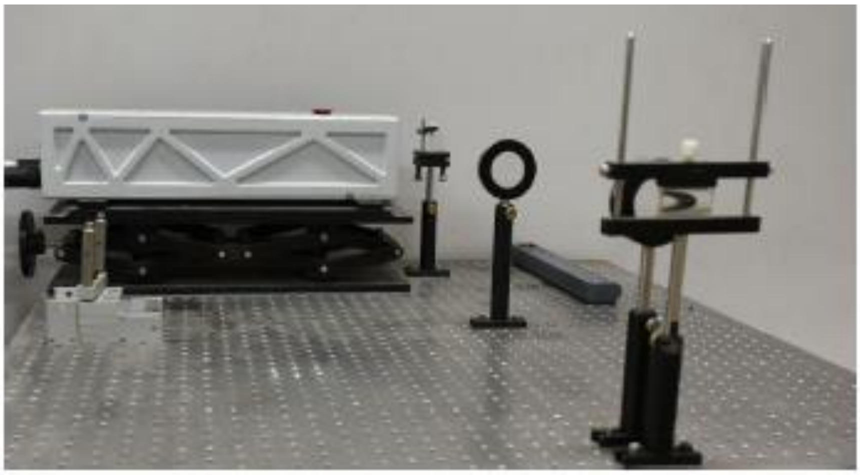

Figure 6.8: Laser and Optics used for generating laser sheet.

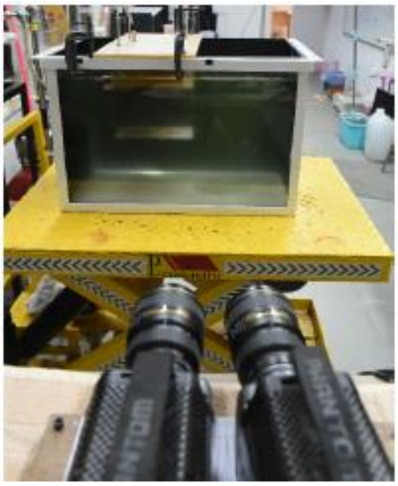

Figure 6.9: Position of cameras.

Two cameras were used for capturing images - one for PIV; with a 550 nm low pass filter to record images in scattered light and another for PLIF, with a 550 nm high pass filter to record images in fluorescence light shown in Figure 6.9. The light scattered by the particles have same wavelength that of laser i.e. 532 nm but light emitted by fluorescent dye used for PLIF emit light at 565 nm. Hence, corresponding filter at 550 nm was used to record separately PIV and PLIF data.

The laser and the camera are synchronized to fire and capture image pairs. The time between these image pairs or the time between pulses is an important parameter for PIV. This time should be sufficiently long to see the motion of the fluid but should be short enough that the tracer particles do not cross the interrogation window. Trials were conducted to find the optimum time for different flow rates.

Simultaneous capturing of images for PIV and PLIF requires two cameras synchronized with the laser. Since both cameras are looking at the same region, they need to be kept at an angle (5°) with each other. This causes warping of the captured images as shown in Figure 6.10.

Dewarping of images was done to reduce distortions and match them with the physical dimensions shown in Figure 6.11.

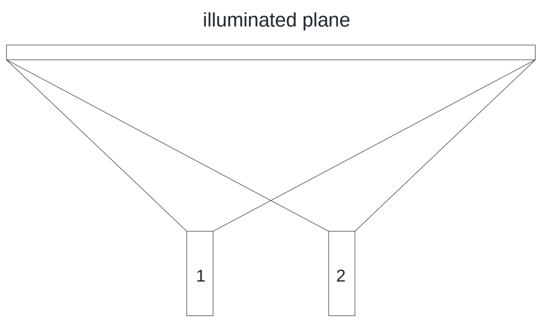

Figure 6.10: Field of view of cameras 1 and 2.

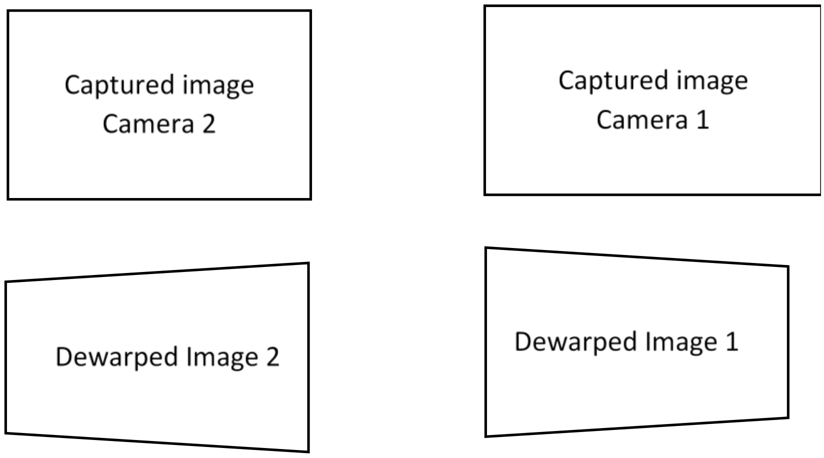

Figure 6.11: Warped images followed by dewarped images.

Optical recording methods like PIV and PLIF of a flow requires fluids of same refractive index interacting even though their densities are different. The refractive index of the incoming fluid will change due to the addition of salt. The refractive index of the ambient fluid (water) is adjusted to this value by adding ethanol to it. Addition of ethanol further reduces the density of the ambient fluid. Therefore, less salt is required for the incoming fluid to maintain the density difference. Various sample solutions were made covering the range of density difference for salt solution and ethanol solution and interpolations were done to find out the mass of salt and ethanol required to match refractive index for a specific density difference.

For Salt-water density

$$\rho_{SW} = 998.53 + 706.86 Y_{salt} + 124.22 Y_{salt}^2 + 238.07 Y_{salt}^3 \tag{6.1}$$

For Salt-water Refractive Index

$$RI_{SW} = 1.3336 + 0.1912 Y_{salt} - 0.5998 Y_{salt}^2 + 4.5744 Y_{salt}^3 \tag{6.2}$$

For Ethanol-water density

$$\rho_{EW} = 998.53 - 188.24 Y_{ethanol} + 274.66 Y_{ethanol}^2 - 71.205 Y_{ethanol}^3 \tag{6.3}$$

For Ethanol-water Refractive Index

$$RI_{EW} = 1.3336 + 0.0642 Y_{ethanol} - 0.059 Y_{ethanol}^2 + 0.7875 Y_{ethanol}^3 \tag{6.4}$$

Y represents the mass fraction. These equations are used to find the mass of salt and ethanol required to match refractive index of two fluids having a specified density difference. The density and refractive index were measured by a density meter and refractometer, respectively.

6.7. Dye Visualization Experiments

As it was difficult to conduct PIV measurement when density difference was high, i.e., 60 kg/m^3, dye visualization experiments were performed. For this blue dye (BLUE M3L Make ARTEK) was added in salt water. The experiment was recorded with a standard video recorder at 25 frames per seconds.

Table 6.1: List of Experiment Conducted

Exp. No.	Opening Location	Opening Size	Density Difference	Type of Experiment
1	Horizontal	30 mm Square	5 kg/m^3	PIV+PLIF
2	Horizontal	30 mm Square	15 kg/m^3	PIV+PLIF
3	Horizontal	30 mm Square	30 kg/m^3	PIV+PLIF
4	Horizontal	30 mm Square	60 kg/m^3	Dye Visualization
5	Horizontal	50 mm Square	5 kg/m^3	PIV+PLIF
6	Horizontal	50 mm Square	15 kg/m^3	PIV+PLIF
7	Horizontal	50 mm Square	30 kg/m^3	PIV+PLIF
8	Horizontal	50 mm Square	60 kg/m^3	Dye Visualization
9	Vertical	50 mm Square	5 kg/m^3	PIV+PLIF
10	Vertical	50 mm Square	15 kg/m^3	PIV+PLIF
11	Vertical	50 mm Square	30 kg/m^3	PIV+PLIF
12	Vertical	50 mm Square	60 kg/m^3	Dye Visualization
13	Vertical	50 mm X 100 mm	5 kg/m^3	PIV+PLIF
14	Vertical	50 mm X 100 mm	15 kg/m^3	PIV+PLIF
15	Vertical	50 mm X 100 mm	30 kg/m^3	PIV+PLIF
16	Vertical	50 mm X 100 mm	60 kg/m^3	Dye Visualization

6.8. Numerical Simulations

The numerical simulations were also performed using the in-house 3D CFD code based on LES approach. The governing conservation equations for mass, momentum, species transport, turbulent kinetic energy are already explained in Chapter 4. For convection terms third order QUICK scheme was used to interpolate the cell face values from cell centre values. For diffusion terms second order Central differencing scheme was employed. For temporal differencing second order scheme was employed. For initialisation of solution, the density of fluid in the entire computational domain was set as density of fresh water while density of the injected fluid was set as density of salt water. The velocity components were initialised to zero value as it was assumed that the fluid in computational domain is quiescent initially. The walls of the computational domain (side as well as partition wall) have been modelled as no-slip impermeable walls. At the inlet known velocity boundary condition was applied and instabilities were actuated. Random fluctuations of random duration with a maximum value of 0.1 and maximum duration of 200 time steps for each velocity component were applied. The mixture density was modelled using Eq. (3.8). The set of algebraic equations were solved iteratively using Gauss-Seidal method. The solution was assumed as converged in each time step if mass residual was below 10^{-5}. For a single simulation on a Xeon machine, the computational time was approximately 20 days for the 300 seconds of a problem run. Three different time steps, i.e., 0.001 s, 0.005 s and 0.01 s were used to perform time step independence study. It was observed that the smaller time step gives nearly similar results. Hence, time step of 0.005 s was used for final runs. To achieve the convergence maximum 50 internal iteration per time step were performed. For meshing a uniform grid with different size in different region was employed. Injection and opening region was resolved by fine mesh. The computational domain was divided in 110X80X109 grid points and injection region was resolved by 10X10 grids and opening region was resolved with 20X20 grids. The partition thickness was not modelled.

6.9. Experimental and Numerical Results

First the instantaneous flow visualisation images are discussed to explain the fluid motion during experiment. For this CFD results have been compared with dye visualisation experiments. In next section quantitative measurement using PIV and PLIF has been explained. Dye visualization experiments were necessary as it was difficult to conduct PIV measurement when density difference was high i.e. 60 kg/m^3. The movement of salt water plume in fresh water is demonstrated by Figs. 6.12-6.13. The salt water plume spreads as it enters in the small compartment. It impinges on the bottom wall of small compartment and further spreading occurs. The salt water moves towards opening and mixes with fresh water inside the small compartment. In case of opening in horizontal partition the salt water mixes with the entire fluid of small compartment, while in case of opening in vertical partition it mixes in lower half region. In case of opening in horizontal partition better mixing occurs inside small compartment.

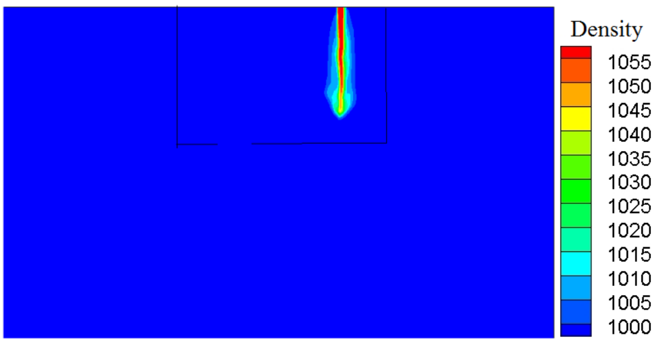

1 s

1 s

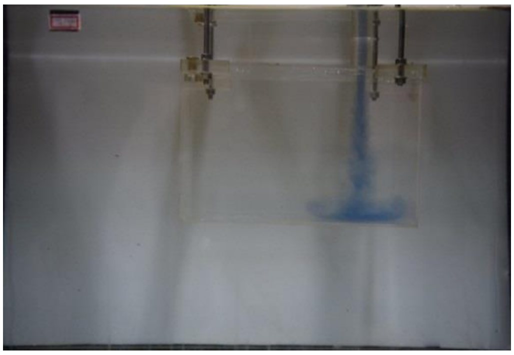

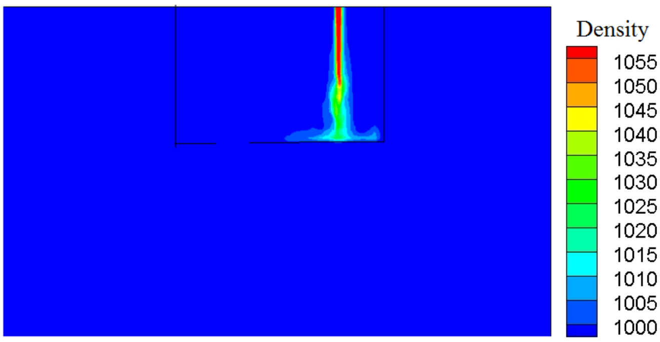

2 s

2 s

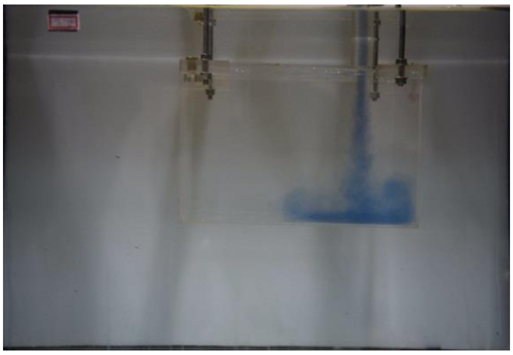

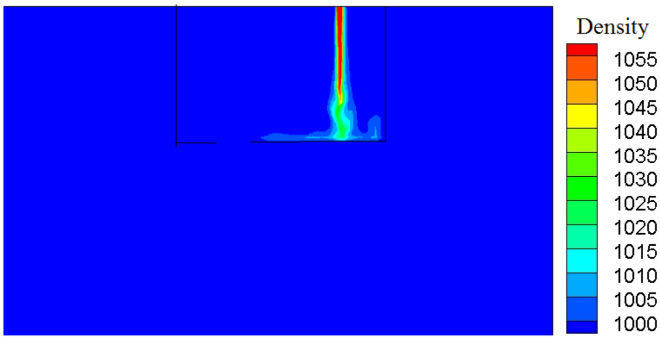

3 s

3 s

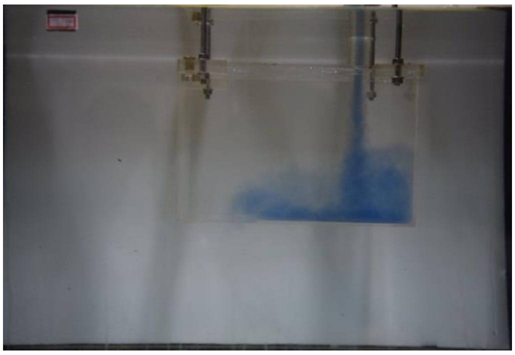

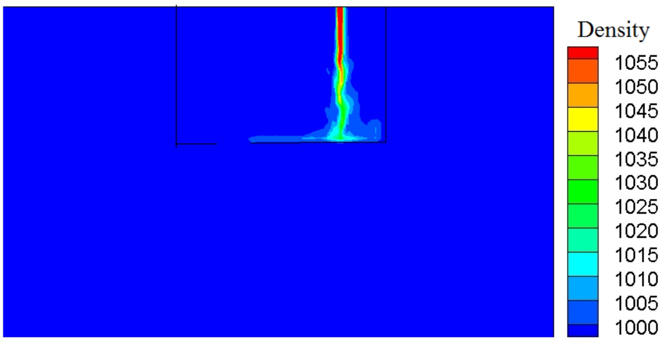

5 s

5 s

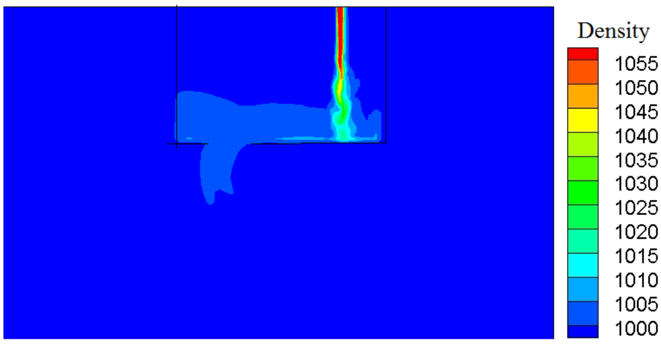

10 s 10 s

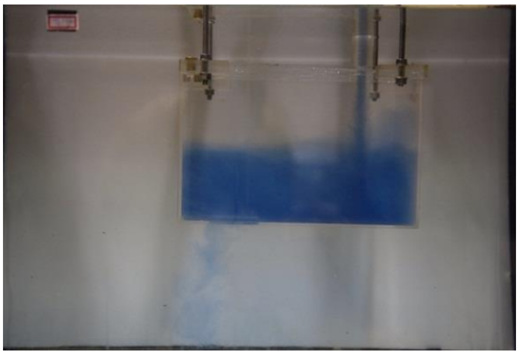

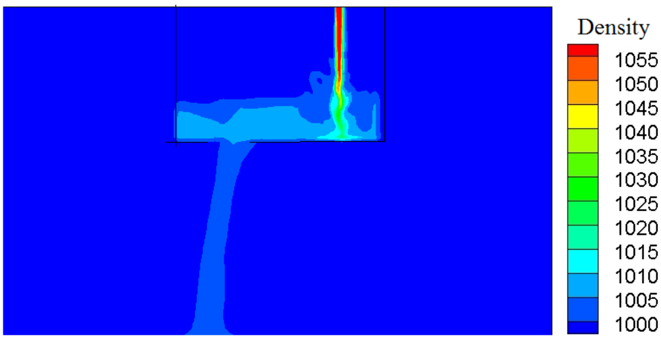

20 s 20 s

Figure 6.12: Qualitative Comparisons of numerical results with experiment (Exp. No. 8).

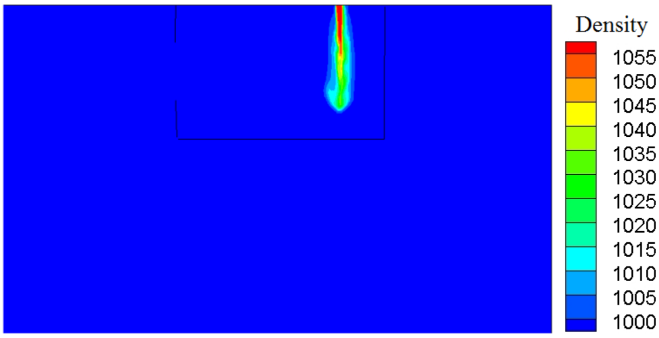

1 s

1 s

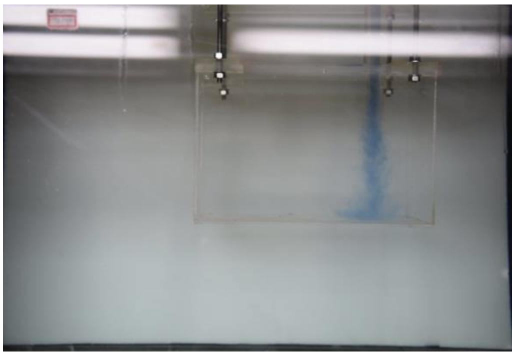

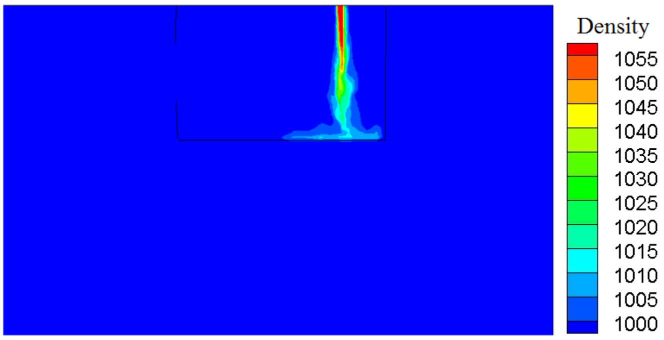

2 s

2 s

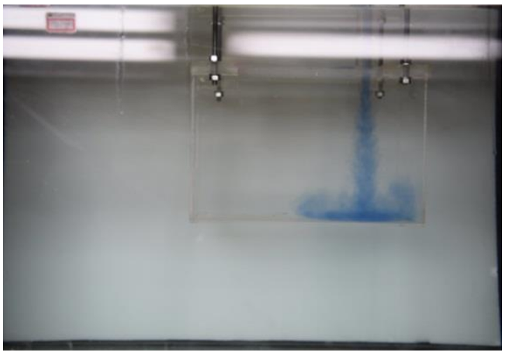

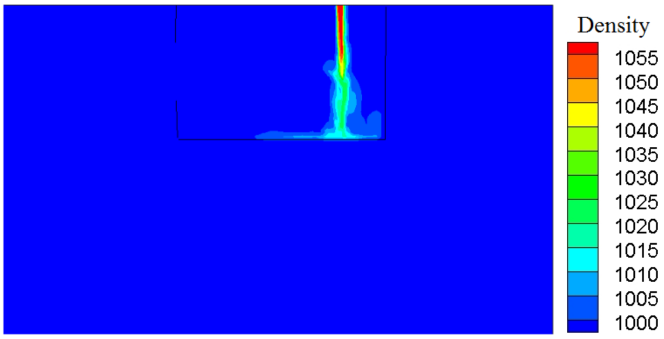

3 s

3 s

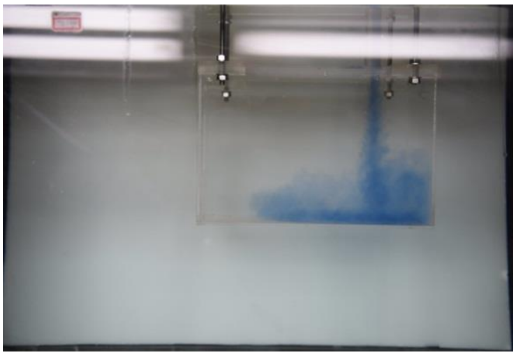

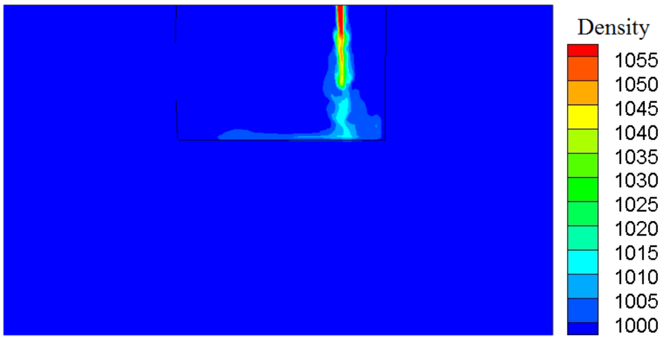

5 s

5 s

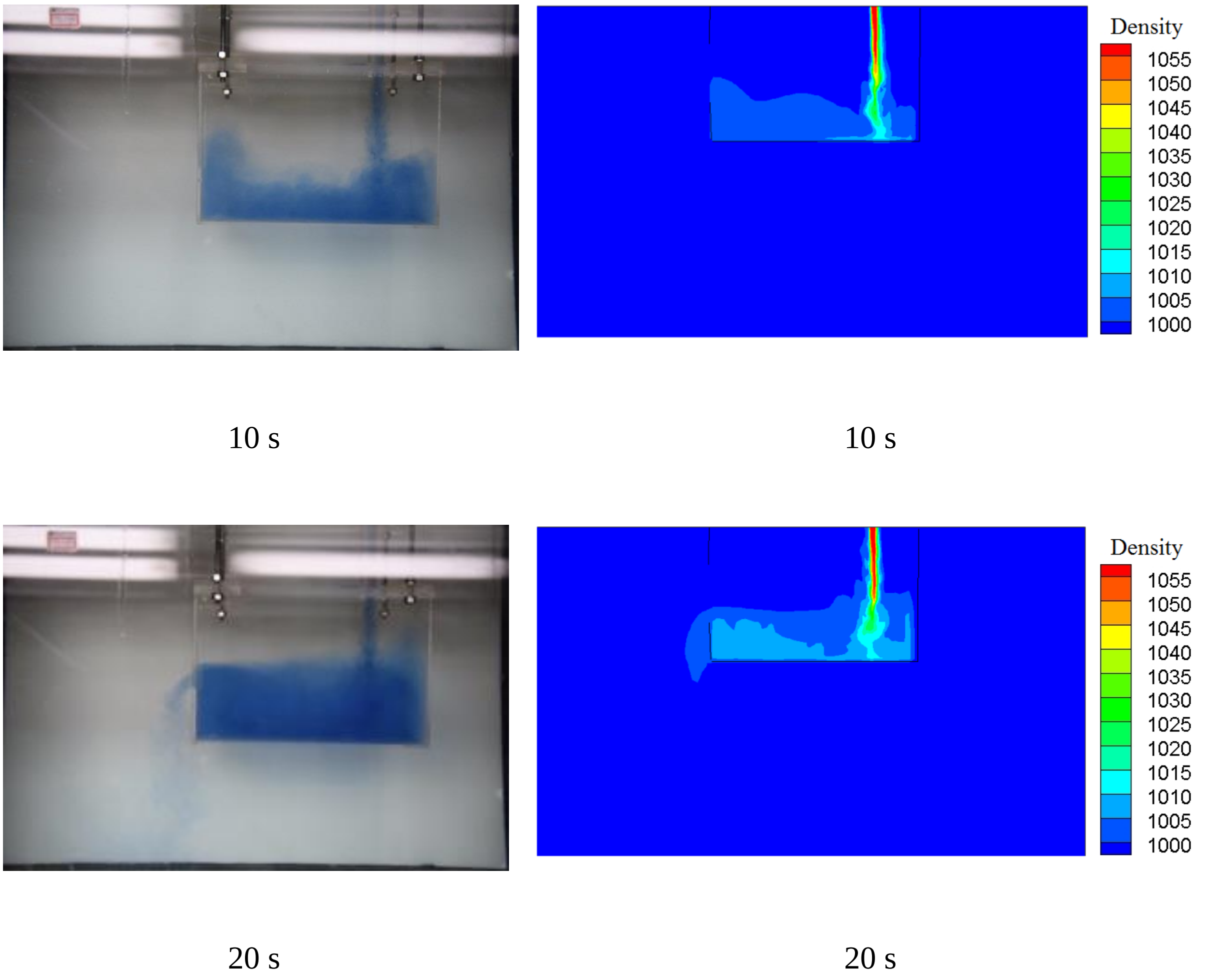

Figure 6.13: Qualitative Comparisons of numerical results with experiment (Exp. No. 12).

The LES based CFD computations were performed for all the conducted experiments. The CFD code was improved based on experimental data. The effect of buoyancy on turbulence generation was considered to predict the jet spread more accurately. Simulations were performed without buoyancy consideration in turbulent kinetic energy (TKE) equation; buoyancy consideration with SGDH and with GGDH schemes presented in Chapter 3 and further comparisons were conducted (Fig. 6.14-6.16). The spread is predicted very well when buoyancy modification with GGDH is considered. Comparison of velocity field by PIV data and CFD data are shown in Figs. 6.17-6.20. The time averaged horizontal velocity profile at 4D, 8D and 12 D distance from the injection obtained from PIV data is shown in Figs. 6.21-6.23. The injected jet was highly transient and it is not good to perform the averaging over entire 50 seconds. The averaging has been done over every 10 seconds; the initial profile (0-10 s) is different from other profile as PIV measurement started as soon as the experiment started. The time averaged horizontal density profile at 4D, 8D and 12 D distance from the injection obtained from PLIF data is shown in Figs. 6.24. The jet velocity profile obtained from CFD simulation compared with PIV data at 8D location for experiment 11 and 14 shown in Figs. 25-26. Various turbulent quantities are shown in Fig. 6.27-6.31. The cross-stream wise profiles of the fluctuation radial and axial velocities are shown in Figs. 6.27 and 6.28 respectively for experiment number 11 at 12D distance from injection. The turbulent shear stress and correlation quantity are depicted in Figs. 6.29 and 6.30 respectively for experiment number 11 at 12D distance from injection. The shear stress and correlation term has been used to compute eddy viscosity and turbulent diffusivity from general gradient hypothesis. Both these values have used to find turbulent Schmidt number which as shown in Fig. 6.31.

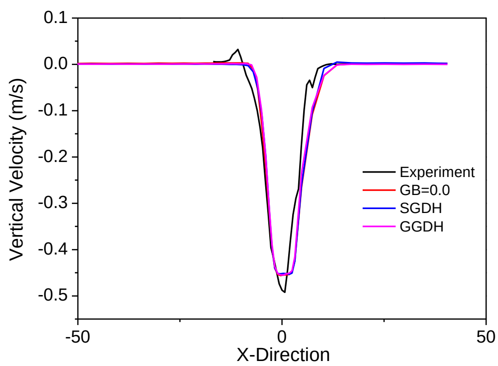

Figure 6.14: Jet velocity profile at 4D from injection (Exp. No. 6).

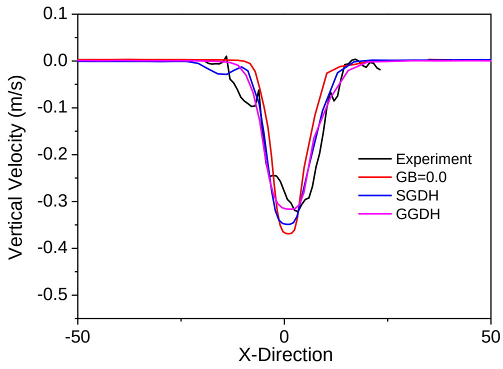

Figure 6.15: Jet velocity profile at 8D from injection (Exp. No. 6).

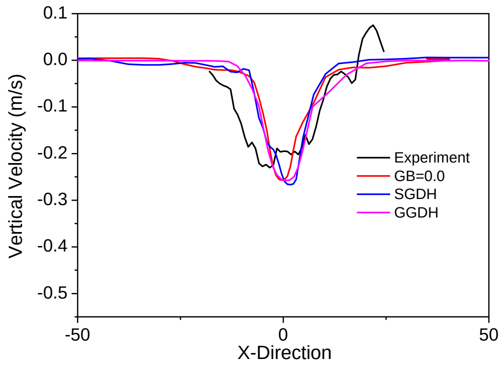

Figure 6.16: Jet velocity profile at 12D from injection (Exp. No. 6).

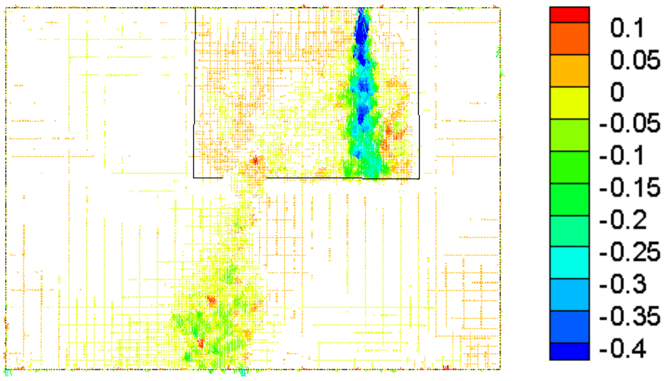

Figure 6.17: Instantaneous velocity vector at 50 s (PIV data, Exp. No. 6).

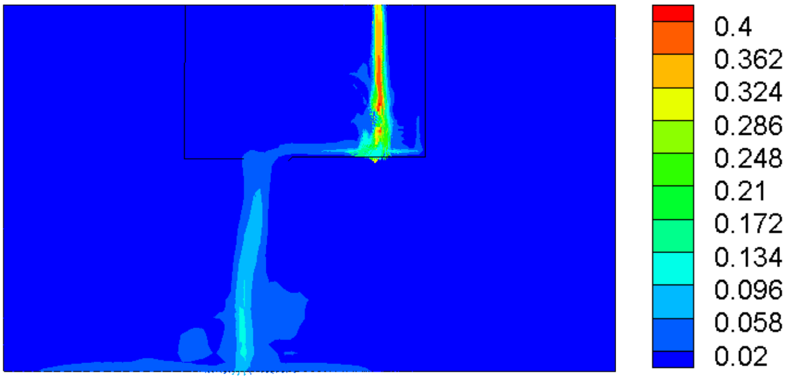

Figure 6.18: Instantaneous velocity vector at 50 s (CFD data, Exp. No. 6).

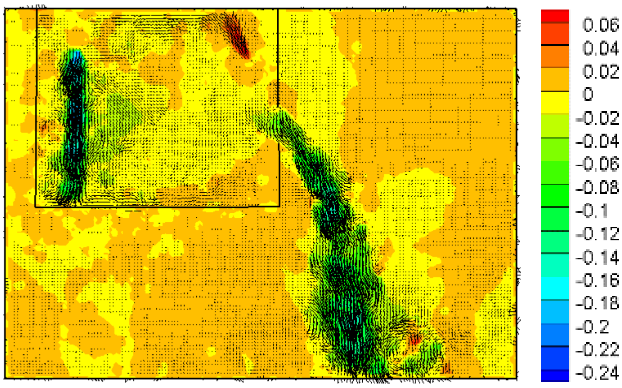

Figure 6.19: Instantaneous velocity vector at 50 s (PIV data, Exp. No. 10).

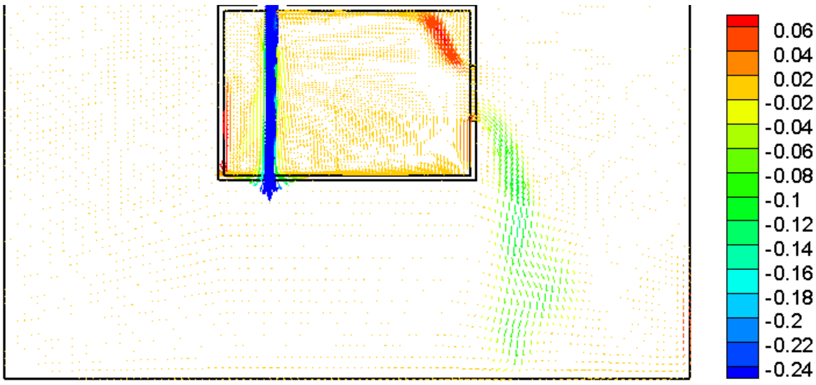

Figure 6.20: Instantaneous velocity vector at 50 s (CFD data, Exp. No. 10).

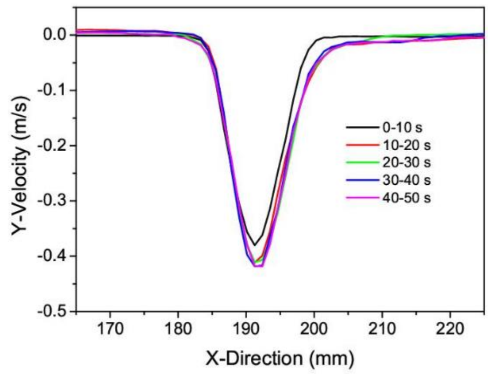

Figure 6.21: Time averaged horizontal velocity profile at 4D (PIV data, Exp. No. 6).

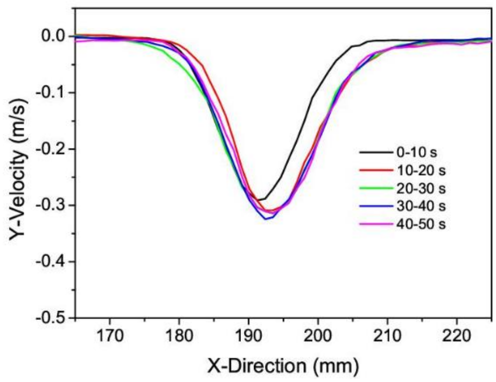

Figure 6.22: Time averaged horizontal velocity profile at 8D (PIV data, Exp. No. 6).

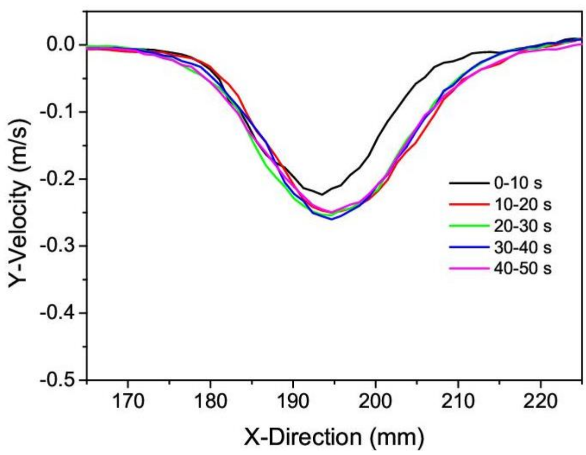

Figure 6.23: Time averaged horizontal velocity profile at 12D (PIV data, Exp. No. 6).

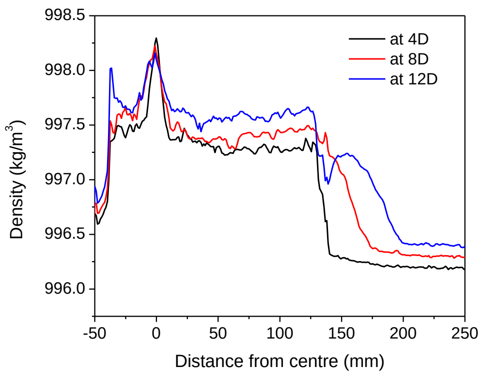

Figure 6.24: Time averaged horizontal density profile (PLIF data, Exp. No. 9).

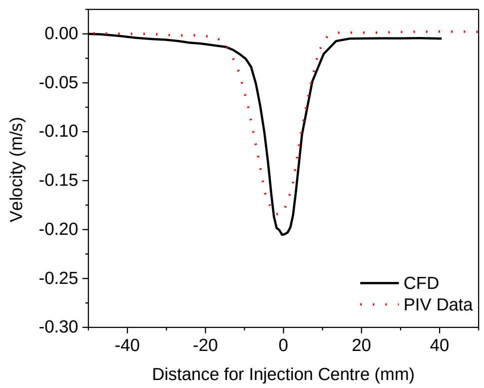

Figure 6.25: Jet velocity profile at 8D from injection (Exp. No. 11).

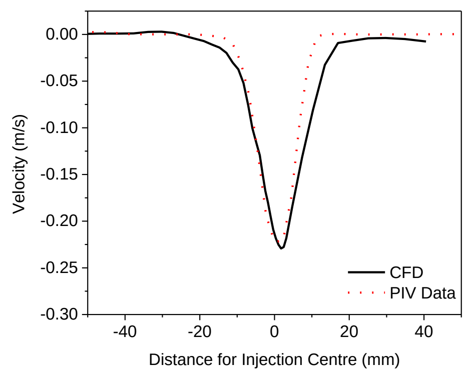

Figure 6.26: Jet velocity profile at 8D from injection (Exp. No. 14).

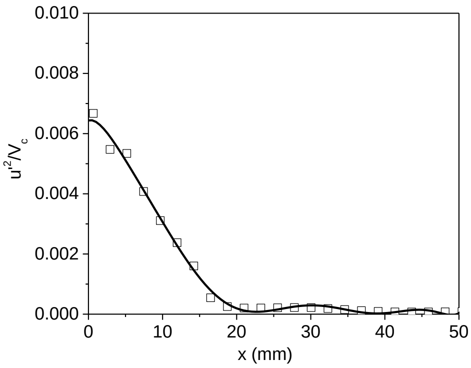

Figure 6.27: Fluctuating radial velocity (Exp. No. 11).

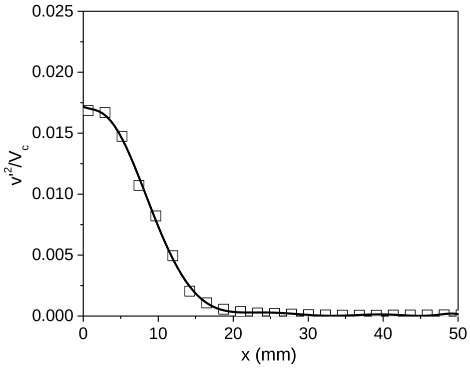

Figure 6.28: Fluctuating axial velocity (Exp. No. 11).

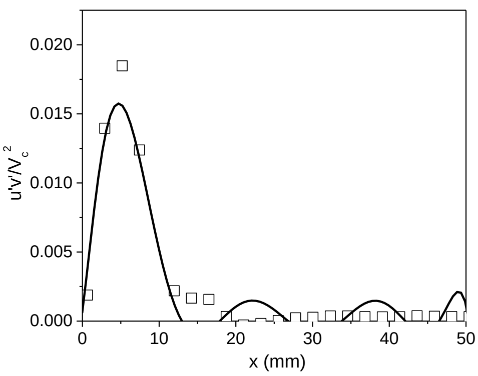

Figure 6.29: Shear stress (Exp. No. 11).

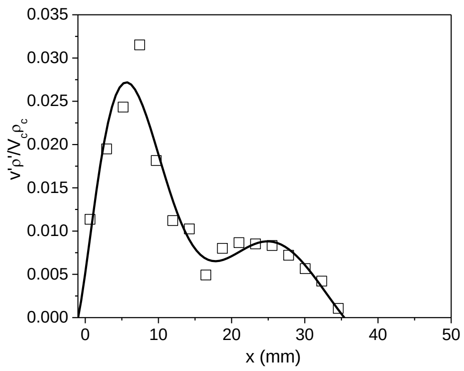

Figure 6.30: Turbulent correlation quantity (Exp. No. 11).

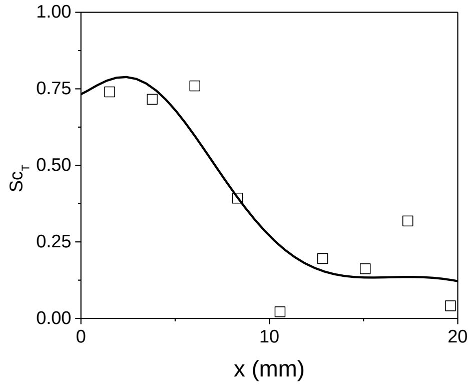

Figure 6.31: Turbulent Schmidt number (Exp. No. 11).

6.10. Closure

Combined PIV and PLIF data for flow field near opening flows was generated as it is not available in literature. PIV data was used to validate the hydrodynamic model of CFD code as different approaches were tested to quantify the effect of buoyancy induced turbulence and predict the velocity field. The CFD results are in very good agreement with experiments. The numerical model reasonably predicts the movement of salt water plume in fresh water and layers of salt water formed in inner compartment. PLIF data was used to improve the species transport model of CFD code. Stratified layer was formed in injection tank even when it had large ceiling opening. Oscillatory exchange flow occurs at ceiling opening and stable bi-directional flow occurs at vertical opening. These are captured by PIV measurement as well as numerically in a consistent manner.

CHAPTER 7: CONCLUSION AND FUTURE WORK

In the present work, salt water analogy has been used for simulation of buoyancy or combined buoyancy and pressure driven flows through opening in horizontal or vertical partition which is relevant for evaluating flow between compartments inside containment of nuclear power plants, in other installations in event of fire etc. CFD simulations have been performed for various scenarios and predicted results are shown to be in good agreement with the present and reported experiments. This chapter represents the summary and conclusions of the present research work. Recommendations for future work are also described in this chapter.

7.1. Summary and conclusions

2D axisymmetric CFD simulations for oscillatory exchange flow through opening in horizontal partition were carried out. The flow was turbulent for all the cases and oscillations in flow were observed in all the cases. Effect of density ratio on flow coefficient is less significant as normalised density and non-dimensional time for a given aspect ratio was approximately the same. The flow coefficient was maximum at L/D 0.6. Pulsation frequency increases with increase in $\Delta\rho_0 / \rho_{L,0}$. The effect of $\Delta\rho_0 / \rho_{L,0}$ is significant on axial velocity and pulsation frequency. Oscillatory frequency is proportional to square root of density ratio. The velocity magnitude also increases with increase in L/D but pulsation frequency decrease with increase in L/D.

3D transient LES of gravity currents related to backdraft for various compartment aspect ratios using salt water analogy have been carried out for opening in vertical partition. Six different opening configurations, five compartment aspect ratios and five density ratios were varied to characterise the gravity current under these scenarios. The time required for gravity current to reach the rear wall has been computed for all the cases and dimensionless Froude number is determined. The opening shape has strong influence on gravity current. As the compartment aspect ratio increases, the time required for gravity current to reach rear wall increases.

CFD analyses have also been carried to compute the flooding pressure corresponding to transition to unidirectional flow from bi-directional flow. As the density difference increases across the opening, high value of purging pressure is required to overcome the downward flow. The required value of purging pressure increases with increase in opening diameter. The required value of purging pressure also increases with increase in L/D to overcome the frictional resistance offered by opening length for the flow to remain unidirectional.

Combined PIV and PLIF data for flow field near opening flows was generated as it is not available in literature. PIV data was used to validate the hydrodynamic model of CFD code as different approaches were tested to quantify the effect of buoyancy induced turbulence and predict the velocity field. The CFD results are in very good agreement with experiments. The numerical model reasonably predicts the movement of salt-water plume in fresh water and layers of salt water formed in inner compartment. PLIF data was used to improve the species transport model of CFD code. Stratified layer was formed in injection tank even it has large ceiling opening. Oscillatory exchange flow occurs at ceiling opening and stable bi-directional flow occurs at vertical opening. These are captured by PIV measurement as well as numerically.

7.2. Recommendation for future work

In the present work most common location of salt injection has been chosen. However, in real case the salt water injection location can be anywhere i.e. corner, near wall, centre, etc. Experiments should be conducted for other locations of injection in future.

In the present work buoyancy modification has been incorporated in sub-grid kinetic energy equation. However, these formulations can be applied to turbulent scalar flux models which can give more accurate jet spread. This can be taken up in future.

Small scale fire test can be performed in future where fire strength is equivalent to salt water buoyancy strength and inter comparison can be made.

In the present work isothermal flows within Boussinesq have been investigated. However, during large temperature difference non-Boussinesq and heat transfer effects are important. Non-Boussinesq flow can be investigated in future.

SYNOPSIS

Study on buoyancy driven flows through large openings is important for evaluating inter compartmental flow inside nuclear power plants containment; in case of fire inside a building, heated structures natural cooling and in natural ventilation. In nuclear reactor containment, resulting flow after an accidental condition will be a function of the initial pressure difference; but in the long-term, the flow field will be principally driven by density differences between the compartments as long as the pressures have equalized. In accidental fires, the compartment below the partition contains lighter fluid (hot gases) compared to heavier fluid located in upper compartment (ambient air). A gravitational unstable system is created when fluid of higher density is placed in a compartment connected to a compartment filled with lighter density fluid having an opening in connecting horizontal partition. The nature of flow in this condition is turbulent, unstable and bi-directional. If one of the compartments is at high pressure, the pressure inside the room will also govern the flow through the opening in horizontal partition. Thus, the nature of flow through openings whether unidirectional or bidirectional, is governed by both pressure and density difference across the openings. The literature review suggests that the flow physics and characterization of such type of buoyancy or combined pressure and buoyancy driven flows through openings in horizontal partition is hardly undertaken in the past and hence, needs to be understood. The effect of opening aspect ratio on oscillating frequency has been studied in past but effect of initial density difference on pulsation frequency has not been understood.

Doors and windows are the most common openings in vertical partition, which provides passage for smoke to escape from the room in case of fire. The flow through openings in vertical partition is stable and bi-directional unlike the horizontal partition. If any large opening is suddenly exposed, backdraft is developed from an enclosure due to combustion of heated unburnt fuel (remaining due to oxygen starvation) with fresh air. Due to density difference across opening, shear flow occurs where heavier fluid from outside the compartment travels underneath the lighter fluid. This fluid flow is known as gravity current and is mainly responsible for mixing between high temperature unburnt fuel and fresh air. In numerous gravity current studies, the length of the floor over which gravity current travels is large (Baum et al., 1994, Mcgrattan et al., 1994, McBryde, 2008). In this scenario, the non-dimensional velocity of gravity current matches with the perfect fluid theory. However gravity current related to backdraft may not travel a long distance. While there are large number of studies on gravity currents for large aspect ratio systems, the influence of small compartment ratio on the gravity current flow has not been undertaken in the past and hence needs to be understood (Fleischmann et al., 1994, Weng et al., 2002).

In addition, when lower compartment is pressurised the flow through opening in horizontal partition convert into stable and unidirectional (Jaluria et al., 1998). However, the unidirectional flow may break down into bi-directional flow if the buoyancy dominates over the pressure driven flow. The condition under which this transition in the flow regime occurs is termed as purging or flooding. Limited studies have been undertaken in the past for this type of purging flow; especially the influence of L/D on the purging flow is not known and needs to be clarified, where, L is length of partition and D is opening diameter. The knowledge of smoke movement in enclosed space having opening is essential for building design. Improvement in this knowledge will lead to safer and economical design. The effect of various parameters on the entrainment of the confined plume and flow through openings needs to be studied in details. The confined plume behaviour is different as compared to free plume.

In view of the above, it is essential to accurately characterize such flows through large openings in presence of buoyancy or combined buoyancy and pressure driven forces. The flows in such openings are difficult to model mathematically because the counter current flows often occur simultaneously in opposite directions through different parts of the opening. Apart from these, buoyancy plays a major role on turbulence especially during unstable stratification, while during stable stratification buoyancy suppresses the turbulence. Current zone based model calculates the inter compartment flow using flow coefficient based on standard vent models that do not accurately take in to account the buoyancy component of the flow. Considering the complexity of flow physics inside such compartments, CFD treatment is a must. However, CFD codes must be validated before any treatment of gaseous flow exchanges between the compartments due to either buoyancy or combined buoyancy and pressure forces. In view of this, many researchers have adopted the salt water fresh water analogy which can be used to simulate such type of exchange flow, i.e., oscillatory exchange flow, gravity currents, etc. In this modelling approach for buoyancy driven flows, salt water (heavy fluid) and fresh water (light fluid) are used to create density difference across the opening, which is closed initially. While in combined buoyancy and pressure driven flows, salt water is injected in fresh water to create buoyant plumes which generates turbulent structure similar during fire plume and hot gas flows (Lequesne, 2010). There is a concern that the salt water model can only be used to simulate gas movement away from the source and heat transfer to the wall cannot be considered in salt water modelling. However, scaling laws to correlate salt water experiments with large size fire are already established and salt water measurements can be directly compared with fire experiment measurements (Steckler, 1986, Fleischmann, 1994, Lequesne, 2010, Yao & Marshall, 2006).

CFD simulations for such flows have been performed using salt water and fresh water as working fluids. For buoyancy driven flows through opening in horizontal or vertical partition, the code has been validated with available data in literature. For circular opening in horizontal partition, a FVM based CFD code has been developed to solve unsteady, axisymmetric Navier-Stokes equations along with RNG k-ε turbulence (Yakhot el al., 1992) model with standard wall function, buoyancy modification and species transport for salt mass fraction. For gravity currents simulations or combined buoyancy and pressure driven flows through square opening, 3D transient LES based code was developed. Combined PIV and PLIF based experiment has been performed for combined buoyancy and pressure driven flows through square opening for validation of CFD code. The turbulent Schmidt number has been derived from experimental data. The above mentioned scientific issues are resolved systematically in the thesis.

APPENDIX A Similarity of salt-water flows and hot gases flows

A-1. General similarity (Steckler et al., 1986)

The flow of saline fluid in a quiescent freshwater environment is driven by the density difference between the two fluids. Similarly, the flow of hot smoke in cool ambient air is driven by the density difference between the gases. The fact that the fluid movement in both cases is driven by the same phenomenon, a buoyancy force, means that there is similarity between the governing equations of motion for the two cases. The similarity of the governing equations is best illustrated when the equations are non-dimensionalised.

Distance
$$x^* = \frac{x}{H} \tag{A.1}$$

Time
$$t^* = \frac{t}{H}U \tag{A.2}$$

Velocity
$$u^* = \frac{u}{U} \tag{A.3}$$

Pressure Perturbation
$$P^* = \frac{P}{\rho_\infty U^2} \tag{A.4}$$

Fire Buoyancy
$$\theta^* = \left(\frac{T - T_\infty}{T_\infty}\right)\frac{1}{\xi} \tag{A.5}$$

Saltwater Buoyancy

$$Y_S^* = \frac{Y_S}{\xi}, \; \xi = U^2 / gH \tag{A.6}$$

Velocity Scale

$$U = \left(\frac{\dot{Q}_{fire} g}{\rho_\infty C_p T H} \right)^{1/3} = \left(\frac{\dot{m}_{salt} g}{\rho_\infty H} \right)^{1/3} \tag{A.7}$$

Following equations show a non-dimensional form of the governing equations for both fire induced smoke flow and buoyant salt water flows. In this non-dimensional form, the conservation of mass equation is the same for both the saline flow and the smoke flow. Similarly, the conservation of momentum equation has exactly the same form in both cases; the third conservation equation for fire induced thermal gas flows is the conservation of thermal energy. For buoyant salt-water flows, the third conservation equation is the conservation of salt mass in solution.

Continuity

$$\nabla^* . u^* = 0 \tag{A.8}$$

Momentum

$$\frac{\partial u^*}{\partial t} + \left(u^* . \nabla^* \right) u^* + \nabla^* P^* - \theta^* \hat{k} = \left(\frac{1}{\mathrm{Re}} \right) \nabla^{*2} u^* \tag{A.9}$$

Energy (for hot gases)

$$\frac{\partial \theta^*}{\partial t} + \left(u^* . \nabla^* \right) \theta^* = \left(\frac{1}{\mathrm{Re}\,\mathrm{Pr}} \right) \nabla^{*2} \theta^* \tag{A.10}$$

Species (for salt water)

$$\frac{\partial Y_S^*}{\partial t} + \left(u^* . \nabla^* \right) Y_S^* = \left(\frac{1}{\mathrm{Re}\, Sc} \right) \nabla^{*2} Y_S^* \tag{A.11}$$

The conservation of energy equation has exactly the same form as the conservation of salt mass equation for saline flows. The similarity in form of the three governing equations means that the same solution procedure can be used to solve the equations from each flow case. This similarity of the non-dimensional governing equations is used in salt water modelling theory to derive the scaling laws that will achieve dynamic similarity between the two flows.

A-2. Similarity for flow only due to density difference (gravity current) (McBryde, 2008)

$$\beta_{initial} = \frac{\Delta\rho}{\rho}$$

(A.12)

$$Fr = \frac{u}{\sqrt{\beta_{initial} gH}}$$

(A.13)

$$t^* = \frac{t\sqrt{\beta_{initial} gH}}{H}$$

(A.14)

$$x^* = \frac{x}{H}$$

(A.15)

$$U = \sqrt{\beta_{initial} gH}$$

(A.16)

$$\nabla^* = H\nabla$$

(A.17)

$$t^* = tU / H$$

(A.18)

$$u^* = u / U \tag{A.19}$$

$$\rho^* = \rho / \Delta\rho \tag{A.20}$$

$$P^* = \frac{P}{\Delta\rho U^2} \tag{A.21}$$

$$T^* = T / T_\infty \tag{A.22}$$

Following equations show a non-dimensional form of the governing equations for both fire induced smoke flow and buoyant salt water flows. In this non-dimensional form, the conservation of mass equation is the same for both the saline flow and the smoke flow. Similarly, the conservation of momentum equation has exactly the same form in both cases; the third conservation equation for fire induced thermal gas flows is the conservation of thermal energy. For buoyant salt-water flows, the third conservation equation is the conservation of salt mass in solution

Continuity
$$\nabla^*.u^* = 0 \tag{A.23}$$

Momentum
$$\frac{\partial u^*}{\partial t^*} + \left(\nabla^*.u^*\right)u^* + \frac{1}{\rho^*}\nabla^* P^* - 1 = \frac{Fr}{\mathrm{Re}}\nabla^{*2}u^* \tag{A.24}$$

Energy (for hot gases)
$$\frac{\partial T^*}{\partial t^*} + \left(u^*.\nabla^*\right)T^* = \left(\frac{Fr}{\mathrm{Re}\,\mathrm{Pr}}\right)\nabla^{*2}T^* \tag{A.25}$$

Species (for salt
$$\frac{\partial Y}{\partial t^*} + \left(u^*.\nabla^*\right)Y = \left(\frac{Fr}{\mathrm{Re}\,Sc}\right)\nabla^{*2}Y \tag{A.26}$$

water)

A.3 Similarity between fire and salt-water plume (Siang, C.C., 2010)

Table A.1: Similarity between fire and salt water plume (Arcoumanis et al., 1997).

Sr. No.	Dimensionless Variable	Full Scale Fire	Salt Water Model
1	Source strength parameter	$Q^*_{fire} = \beta_T Q_{fire}\left(\rho_\infty C_p g^{1/2} L_f^{5/2}\right)^{-1}$ $\beta_T = 1/T_\infty$	$m^*_{SW} = \beta_{SW} m_{salt}\left(\rho_\infty g^{1/2} L_f^{5/2}\right)^{-1}$ $\beta_{SW} = 0.76$
2	Velocity	$u^* = u\left(gL_f\right)^{-1/2}\left(Q^*_{fire}\right)^{-1/3}$	$u^* = u\left(gL_{SW}\right)^{-1/2}\left(m^*_{SW}\right)^{-1/3}$
3	Position	$x^* = x / L_f$	$x^* = x / L_{SW}$
4	Time	$t^* = t_{fire}\left(g / L_f\right)^{1/2}\left(Q^*_{fire}\right)^{1/3}$	$t^* = t_{SW}\left(g / L_{SW}\right)^{1/2}\left(m^*_{SW}\right)^{1/3}$
5	Density difference	$\theta^*_T = \beta_T\left(T - T_\infty\right)\left(Q^*_{fire}\right)^{-2/3}$ $\theta^*_{smoke} = \dfrac{\beta_T Y_{smoke}\Delta H_C}{y_{smoke} C_p\left(Q^*_{fire}\right)^{2/3}}$	$\theta^*_{SW} = \beta_{SW} Y_{salt}\left(m^*_{SW}\right)^{-2/3}$
6`	Pressure	$p^* = p / \left(Q^*_{fire}\right)^{2/3}\rho_\infty g L_f$	$p^* = (p - p_\infty) / p_\infty$

Following the above similarity, the dimensionless equations for fire/Salt water analogy are

Momentum equation for fire flow

$$\frac{\partial u_j^*}{\partial t^*} + u_i^* \frac{\partial u_j^*}{\partial x_i^*} = -\frac{\partial p^*}{\partial x_i^*} + \frac{\nu}{\left(Q^*_{fire}\right)^{1/3}\left(gL_f\right)^{1/2} L_f}\frac{\partial^2 u_j^*}{\partial x_i^* \partial x_i^*} + \theta_T^* . f_j^*$$

(A.27)

Or $$\frac{\partial u_j^*}{\partial t^*}+u_i^*\frac{\partial u_j^*}{\partial x_i^*}=-\frac{\partial p^*}{\partial x_i^*}+\frac{1}{\left(Gr_{source}^{fire}\right)^{1/3}}\frac{\partial^2 u_j^*}{\partial x_i^*\partial x_i^*}+\theta_T^*.f_j^*$$

Where $f_1^*=0;\ f_2^*=-1;\ f_3^*=0$ and $Gr_{source}^{fire}=\dfrac{\beta_T g Q_{fire} L_f^2}{\rho_\infty C_p \nu^3}=\dfrac{g Q_{fire} L_f^2}{\rho_\infty C_p T_\infty \nu^3}$

(A.28)

Energy equation for fire flow

$$\frac{\partial \theta_T^*}{\partial t^*}+u_i^*\frac{\partial \theta_T^*}{\partial x_i^*}=\left(\frac{1}{\left(Gr_{source}^{fire}\right)^{1/3}}\right)\left(\frac{1}{\mathrm{Pr}}\right)\frac{\partial^2 \theta_T^*}{\partial x_i^*\partial x_i^*}+\dot{q}^*$$

(A.29)

Smoke mass species equation

$$\frac{\partial \theta_{smoke}^*}{\partial t^*}+u_i^*\frac{\partial \theta_{smoke}^*}{\partial x_i^*}=\left(\frac{1}{\left(Gr_{source}^{fire}\right)^{1/3}}\right)\left(\frac{1}{Sc}\right)\frac{\partial^2 \theta_{smoke}^*}{\partial x_i^*\partial x_i^*}+w_{smoke}^*$$

(A.30)

Momentum equation for salt-water flow

$$\frac{\partial u_j^*}{\partial t^*}+u_i^*\frac{\partial u_j^*}{\partial x_i^*}=-\frac{\partial p^*}{\partial x_i^*}+\frac{\nu}{\left(\dot{m}_{SW}^*\right)^{1/3}\left(gL_{SW}\right)^{1/2}L_{SW}}\frac{\partial^2 u_j^*}{\partial x_i^*\partial x_i^*}+\theta_{SW}^*\cdot f_j^*$$

(A.31)

Or $$\frac{\partial u_j^*}{\partial t^*}+u_i^*\frac{\partial u_j^*}{\partial x_i^*}=-\frac{\partial p^*}{\partial x_i^*}+\frac{1}{\left(Gr_{source}^{SW}\right)^{1/3}}\frac{\partial^2 u_j^*}{\partial x_i^*\partial x_i^*}+\theta_{SW}^*\cdot f_j^*$$

Where $f_1^*=0;\ f_2^*=-1;\ f_3^*=0$ and $Gr_{source}^{SW}=\dfrac{\beta_{SW} g \dot{m}_{salt} L_{SW}^2}{\rho_\infty \nu^3}$

(A.32)

Salt mass species equation

$$\frac{\partial \theta_{SW}^{*}}{\partial t^{*}} + u_i^{*} \frac{\partial \theta_{SW}^{*}}{\partial x_i^{*}} = \left(\frac{1}{\left(Gr_{source}^{SW} \right)^{1/3}} \right) \left(\frac{1}{Sc} \right) \frac{\partial^2 \theta_{SW}^{*}}{\partial x_i^{*} \partial x_i^{*}} + w_B^{*}$$

(A.33)

REFERENCES

Adrian, R.J. and Westerweel, J., Particle Image velocimetry, Cambridge University Press, 2011.

Baum, H.R., Ezekoye, O.A., McGrattan, K.B., Rehm, R.G., Mathematical modelling and computer simulation of fire phenomena, Theoretical and Computational Fluid Dynamics, vol. 6, pp. 125-139, 1994.

Blomqvist, C. and Sandberg, M., A Note on Air Movements through Horizontal Openings in Buildings, Natural Ventilation, University of Gavle, Centre for building Environment, 2000.

Brown, W.G. and Salvason, K.R., Natural convection through rectangular openings in partitions-1 vertical openings. International Journal of Heat and Mass Transfer, 5, 859-867, 1962a

Brown, W.G. and Salvason, K.R., Natural Convection through Rectangular Openings in Partitions-2 Horizontal Openings, Int. J. Heat Mass Transfer, vol. 5, pp. 869-880, 1962b.

Cholemari, M.R. and Arakeri, J.H., Experiments and a model of turbulent exchange flow in a vertical pipe. International Journal of Heat and Mass Transfer, vol. 48, pp. 4467–4473, 2005.

Chow, W.K. and Gao, Y., Oscillating Behaviour of Fire-induced Air Flow through a Ceiling Vent, Appl. Therm. Eng., vol. 29, pp. 3289–3298, 2009.

Christensen, J. and Peterson, P.F., A 1-D Langrangian model for large volume mixing. Nuclear Engineering and Design, vol. 204, pp. 299-320, 2001.

Clement, J.M., Experimental verification of the fire dynamics simulator (FDS) hydrodynamic model. PhD Thesis, University of Canterbury, Christchurch, New Zealand, 2000.

Clement, J.M. and Fleischmann, C.M., Experimental verification of the fire dynamics simulator hydrodynamic model. Fire Safety Science–Proceedings of the Seventh International Symposium, pp. 839-851, 2003.

Conover, T.A., Kumar, R. and Kapat, J.S., Buoyant Pulsating Exchange flow through a Vent, J. Heat Transfer, vol. 117, pp. 641-648, 1995.

Cooper, L.Y., Calculating Combined Buoyancy and Pressure Driven Flow through a Shallow, Horizontal, Circular Vent, Fire Saf. J., vol. 27, pp. 23-35, 1996.

Daly, B. J., Harlow, F. H., Transport equations in turbulence,Phys. Fluids, vol. 13, pp.2634-2649, 1970.

Epstein, M., Buoyancy driven Exchange Flow through Small Opening in Horizontal Partitions, J. Heat Transfer, vol. 110, pp. 885-893, 1988.

Epstein, M. and Kenton, M.A., Combined Natural Convection and Forced Flow through Small Opening in Horizontal Partitions, with Special References to Flow in Multi Compartment Enclosures, J. Heat Transfer, vol. 111, pp. 980-987, 1989.

Fleischmann, C.M., Pagni, P.J. and Williamson, R.B., Salt Water Modelling of Fire Compartment Gravity Currents. In: Fire Safety Science –Proceedings of the Fourth International symposium, Ottawa, International Association for Fire Safety Science, Gaithersburg, pp. 253–264, 1994.

Fleischmann, C.M. Backdraft phenomena, NIST-GCR-94-646. University of California, Berkeley, 1994.

Fleischmann, C.M., McGrattan, K.B., Numerical and experimental gravity currents related to backdrafts, Fire Safety Journal, vol. 33, pp. 21–34, 1999.

Gera, B., Investigation of Bi-directional Flow through Large Opening, M. Tech. Thesis, Indian Institute of Technology, Delhi, New Delhi, 2005.

Gera, B., Sharma, P.K., Singh, R.K. and Vaze, K.K., Numerical Simulation of Buoyant Pulsating Exchange Flow through Circular Opening in Horizontal Partition, CFD Lett., vol. 4, pp. 20-32, 2012.

Harrison, R.P. and Spall, R.E., The Effect of Partition Thickness on Buoyant Exchange Flow through a Horizontal Opening, Numer. Heat Transfer Part A, vol. 44, pp. 451-462, 2003.

Hayase, T., Humphrey, J.A.C. and Grief, R.A., Consistently Formulated QUICK Scheme for Fast and Stable Convergence using Finite Volume Iterative Calculation Procedures, J. Comp. Phys., vol. 98, pp. 108–118, 1992.

Hunt, G.R. and Linden, P.F., Steady-state flows in an enclosure ventilated by buoyancy forces assisted by wind. Journal of Fluid Mechanics, vol. 426, pp. 355-386, 2001.

Jaluria, Y., Lee, S.H.K., Mercier, G.P. and Tan, Q., Transport Processes across a Horizontal Vent due to Density and Pressure Differences, Exp. Therm. Fluid Sci., vol. 16, pp. 260-273, 1998.

Jankiewicz, S.P., Predicting smoke detector response using a quantitative salt-water modeling technique. MS Thesis, University of Maryland, College Park, 2004.

Jankiewicz, S.P., Siang, C.C., Yao, X., Santangelo, P.E., Marshall, A.W., Roby, R.J., Analyzing fire induced dispersion and detector response incomplex enclosure using salt-water modeling, Fire Saf. J., vol. 65, pp. 19-29, 2014.

Kerrison, L., Galea, E.R. and Patel M. K., A Two-dimensional Numerical Investigation of the Oscillatory Flow behaviour in Rectangular Fire Compartments with a Single Horizontal Ceiling Vent, Fire Saf. J., vol. 30, pp. 357-382, 1998.

Kuhn, S.Z., Bernardis, R.D., Lee, C.H., Peterson, P.F., Density stratification from buoyancy driven exchange flow through horizontal partition in a liquid tank. Nuclear Engineering and Design, vol. 204, pp. 337-345, 2001.

Lequesne, M.A., Salt water modelling of fire gas flow through a horizontal ceiling opening, ME Thesis University of Canterbury, Christchurch, New Zealand., 2010

Li, Z., Heiselberg, P. and Nielsen, P.V., Characteristics of Buoyancy Driven Single-Sided Natural Ventilation through Horizontal Openings, Proc. of Built Environment and Public Health, Shantou, China, 2004.

Linden, P.F., LawSerff, G.F., Smeed, D.A., Emptying filling boxes: the fluid mechanics of natural ventilation. Journal of Fluid Mechanics, vol. 212, pp. 309-335, 1990.

Markatos, N.C., Malin, M.R. and Cox, G., Mathematical Modelling of Buoyancy-Induced Smoke Flow in Enclosures, Int. J. Heat Mass Transfer, vol. 25, pp. 63–75, 1982.

McBryde, J.D., Experimental and Numerical Modelling of Gravity Currents preceding Backdrafts, M.E. Thesis, University of Canterbury, Christchurch, New Zealand, 2008.

Mcgrattan, K.B., Rehm, R.G., Baum, H.R., Fire-driven flows in enclosures, Journal of Computational Physics, vol. 110, pp. 285-291, 1994.

Menon, S. and Rizk, M., Large Eddy Simulations of Three-Dimensional Impinging Jets, Int. J. Comp. Fl. Dyn., Vol. 7, pp. 275, 1996.

Mishra, A.A., Hasan, N., Sanghi, S. and Kumar, R., Two-dimensional Buoyancy Driven Thermal Mixing in a Horizontally Partitioned Adiabatic Enclosure, Phys. Fluids, vol. 20, pp. 063601, 2008.

Patankar, S.V., Numerical Heat Transfer and Fluid Flow, Hemisphere Pub. Co., Washington DC, 1980.

Rehm, R.G., Mcgrattan, K.B., Baum, H.R., Cassel, K.W., Transport by gravity currents in building fires, Proceedings of Fourth International Symposium on Fire Safety Science, International Association of Fire Safety Scientist, Ottawa, Ontario, Canada, 1994.

Shan, J.W., lang, D.B., Dimotakis, P.E., Scalar concentration measurements in liquid-phase flows with pulsed lasers, Experiments in Fluids, vol. 36, pp. 268-273, 2004.

Shin, J.O., Dalziel, S.B., Linden, P.F., Gravity currents produced by lock exchange, Journal of Fluid Mechanics vol. 521, pp. 1-34, 2004.

Siang, C.C., Characterizing Smoke Dispersion along Beamed Ceilings using Saltwater Modeling, MS Thesis, University of Maryland, College Park, 2010.

Singhal, M. and Kumar, R., Unsteady Buoyant Exchange Flow through a Horizontal Partition, J. Heat Transfer, vol. 117, pp. 515–520, 1995.

Sleiti, A.K., Effect of Vent Aspect Ratio on Unsteady Laminar Buoyant Flow through Rectangular Vents in Large Enclosures, Int. J. Heat Mass Transfer, vol. 51, pp. 4850–4861, 2008.

Spall, R.E. and Anderson, E.A., A Numerical Study of Buoyant, Pulsating Exchange Flows through a Vent in a Thin Horizontal Partition, Numer. Heat Transfer Part A, vol. 36, pp. 263–272, 1999.

Steckler, K.D., Baum, H.R., Quintiere, J.G. , Salt water modeling of fire induced flows in multi compartment enclosures, Twenty-first Symposiums (International) on Combustion, The Combustion Institute pp. 143-149, 1986.

Tan, Q. and Jaluria, Y., Mass Flow through a Horizontal Vent in an Enclosure due to Pressure and Density Differences, Int. J. Heat Mass Transfer, vol. 44, pp. 1543-1553, 2001.

Tovar, R., Garrido, C.A.C., Linden, P.F., Thomas, L.P., Buoyancy-driven flow in two interconnected rooms: effects of the exterior vent location and size. Journal of Solar Energy Engineering, vol. 131, 021005, 2009.

Viollet, P.L., The Modelling of Turbulent Recirculating Flows for the Purpose of Reactor Thermal-hydraulic Analysis, Nucl. Eng. Des., vol. 99, pp. 365–377, 1987.

Weng, W.G., Fan, W.C., Qin, J. and Yang, L.Z., Study on Salt Water Modelling of Gravity Currents Prior to Backdrafts using Flow Visualization and Digital Particle Image Velocimetry, Exp. Fluids, vol. 33, pp. 398–404, 2002.

Weng, W.G., Fan, W.C., Hasemi, Y., Prediction of the formation of backdraft in a compartment based on large eddy simulation, International Journal for Computer Aided Engineering and Software, vol. 22, pp. 376–392, 2005.

Yakhot, V., Orszag, S.A., Thangam, S., Gatski,T.B. and Speziale, C.G., Development of Turbulence Models for Shear Flows by a Double Expansion Technique, Phys. Fluids A, vol. 4, pp. 1510–1520, 1992.

Yao, X., Characterization of fire induced flow transport along ceilings using salt-water modeling. PhD Thesis, University of Maryland, College Park, 2006.

Yao, X. and Marshall, A.W., Characterizing turbulent ceiling jet dynamics with salt-water modeling. Fire Safety Science–Proceedings of the Eighth International Symposium, IAFSS, Beijing, China, pp. 927–938, 2005.

Yao, X. and Marshall, A.W., Quantitative Salt-water Modelling of Fire-induced Flow, Fire Saf. J., vol. 41, pp. 497–508, 2006.

Yao, X. and Marshall, A.W., Quantitative salt-water modeling of fire-induced flows for convective heat transfer model development, Journal of Heat Transfer, vol. 129, pp. 1373-1383, 2007.

Yii, E.H., Exploratory salt-water experiments of balcony spill plume using laser induced fluorescence technique. ME Thesis, University of Canterbury, Christchurch, New Zealand, 1998.

Zhigang, L., Characteristics of buoyancy driven natural ventilation through horizontal openings. PhD Thesis, Aalborg University, 2007.